IMAGE PROCESSING OF THE RADIOISOTOPE ANGIOCARDIOGRAMS

KOZABURO HACHIMURA

FEBRUARY 1979

IMAGE PROCESSING OF THE RADIOISOTOPE ANGIOCARDIOGRAMS

KOZABURO HACHIMURA

FEBRUARY 1979

CONTENTS

Chapter 1 Introduction

In recent years there has been an increaseing interest in the field of image processing or picture processing by digital computer. Application of the digital image processing concepts dates from the middle 1960's. Studies concerning the processing of pictorial data had been done before that time. Those were, however, mainly on the optical, electro-optical or analog basis. In the middle 1960's, the third generation digital computers came into the world and they offered the means for the digital processing of pictorial data. That is, they furnished the storage and speed capabilities required for the practical application of the image processing. Since then, this field has been grown exponentially, encouraged by the needs from wide variety of application fields. The most significant of them is the space program supported by NASA. Most of the restoration and enhancement techniques have been developed more or less in conjunction with this program, and the usefulness of the digital image processing was proved by many of the examples, the luner or Mars images.

Applications of the image processing technique to medical science has also been an outstanding problem for a long preiod. In medicine, since wide variety of pictorial information has been routinely produced and manipulated, there have been implicit but urgent desires, even before the developement of digital computers, to handle the pictorial information quantiatively and to automate the measurement process.

Applications of the image processing technique to the field of medicine are desired mainly from the following reasons. (1) Reduction of labour: Inspections via pictorial image data have been routinely made and vast amount of data has been produced and treated daily, especially in a mass screening, a large set of data must be processed in a short time. The image processing technique will do much for reducing the labour of the physicians. (2) Quantification of inspections: Being obtained under limited conditions, images of this field are usually of poor quality. Therefore, the inspections based on images are apt to be made empirically and qualitatively. The image processing technique will

be helpful for recovering the image quality and for establishing the quantative and objective inspections. (3) Visualization of the invisible information: Physicians want to visualize and measure objects, which they cannot see under usual conditions in any way. Current technology and information processing technique may answer their desires.

Let us, next, consider the problems involved in the medical image processing. First of all, since medical images are not always obtained under favorable conditions for imaging, quality of images is inferior to images treated in other scientific fields. Rapid development of modern technologies has brought a tolerable improvement on the quality of medical images. However, since the object of the measurement is a living human body and information is obtained by exposing a kind of energy to the body, it must be considered, by reason of subject's safety, to be an inevitable consequence that the quality of the image may be limited.

Secondly, this being the most serious problem, the object image of the processing is not originally two-dimensional but obtained by projecting or intersectioning the three-dimensional entity onto the two-dimensional plane. The processing of the originally two-dimensional figure or image can be done, at least principally, just like the processing of the one-dimensional data or signal. This can be understood by the fairly fruitful results in the processing and recognition of the typed or hand printed letters. On the other hand, "images", especially the medical images are two-dimensional projections of the three-dimensional scenes and much of the information contained in the originals might be lost during the process. Of course, this problem is not restricted only in the scope of medical image processing. However, the situaltion is more serious in this field, since, as previously stated, the object of the study is living organs and the range of the methods and means to be applied for imaging is inevitably limited. Hence, in processing or analyzing the medical images, we have to employ much of a priori knowledge about the three-dimensional structure of the objects and the background.

These may be the causes for that the automatic processing of medical images has not yet given fruitful results although the introduction of this technique has been urgently desired.

1.1 Image processing in cardiology

When looking into the information processing in medicine, many research efforts are concentrated into the field of cardiology. Reasons for this fact may be as follows: (1) The cardiovascular system is a basic system and it plays quite an important role in maintaining the whole system of living body, so the diseases happened in the cardiovascular system are very serious and may sometimes cause deaths. (2) Since the cardiovascular system is a dynamical system, data obtained from the system involove many kinds of information about the heart and the vascular system. Clarification of the information is the first step of clinical diagnosis. The extraction and the analysis of information by human investigators are usually very troublesome and tedious, and may sometimes be inaccurate. Therefore, the information processing technique by computer has been expected to become a powerful tool for clarifying the function of the cardiovascular system.

In the cardiovascular system, the left ventricle plays the most important role. The left ventricle repeats the cycle of contraction and relaxation and pumps out the blood into the whole body. Therefore, it bears the most prominent part of the dynamical function of the system and the defect in it may cause a fatal damage of the whole body. Since the change of shape and dimensions of the left ventricle against time serves important information to describe the dynamical function of the left ventricle, various techniques for imaging the left ventricle have been developed and used in the clinical inspection.

Imaging techniques used in the cardiology are largely classified into three categories. They are radiographic, scintigraphic and ultrasonic techniques.

The radiographs, usually also referred to as X-ray images or roentgenographs, are most common in medicine, and have been applied to a wide variety of object organs. Radiography has been established in a technical and applicational point of view, and it offers us the most accurate and reliable images of human organs to date.

Radiographic angiocardiography is an established technique for

imaging a selected heart chamber, especially the left ventricle, by injecting the radiographic opaque contrast medium into the chamber. This radiograph is usually photographed on a cine film so that we may observe and analyze the motion of the left ventricular chamber. From this cine angiocardiography, we are able to obtain clear and accurate images due to the improvement of the performance of the radiographic imaging devices. However, many problems are also involved in this technique: It requires surgical operation to insert a catheter, which is used to inject contrast medium, into the chamber of the heart through arteries or veins. It is, therefore, invasive, and it requires hospitalization. Moreover, the dynamics of the ventricle is greately affected by the injection of the contrast medium. Consequently, it is not applicable to the out patients or the seriously ill patients, and it cannot be applied repeatedly.

On the other hand, scintigraphic and ultrasonic imaging techniques are non-invasive and can be performed easily. Because the ultrasonic technique is least invasive to living human body and tomographic image can be easily obtained by this technique, it is expected to be the most principal technique for inspection.

Radioisotope images, frequently referred to as scintigrams, are obtained by detecting the radioactive rays which are emitted from the radionuclides contained in the object organ, and by depicting the spatial distribution of the detected radioactive counts. By choosing radionuclide and/or chemical compound to be labelled by radionuclide which are matched to the metabolic and physical characteristics of the specific organ, one can depict the organ selectively. Besides, using the radionuclides as tracers, one can observe the dynamic metabolic characteristics of the object organs. Also, this method can usually be done in a noninvasive manner, and total radiation dose may probably be lower than usual fluoroscopy.

By these reasons, a radioisotope scintigraphy is very useful in cardiology to obtain the information about the dynamical characteristics and to reduce the influence of irrelevant surrounding organs. However, since the radioisotope images are formed by the disintegration of radionuclides, they are very much corrupted by statistical noise. Besides, since the resolution of the scintillation imaging devices are limited in

principle, the fine structures of the object cannot be visualized. Consequently, the images obtained are of low quality, and objects depicted are usually ill-defined and hard to be recognized. These are the main objections of the scintigraphy.

In the case of imaging scintigrams of static organs which do not move so rapidly in a short time, we can reduce the effect of the statistical disturbance by a simple temporal integration operation. For the dynamic organ like heart, however, the inconsistent application of this simple integration over a long period must be avoided, because the image obtained by the operation may be blurred by the dynamical movement of the organ. However, since without this integration we can hardly get the image of the heart, we cannot do completely without it. Therefore some means for the integration without losing the dynamical information of heart have been desired. A technique to fulfill this contradictory requirement, to a certain extent, has been established, which uses the electrocardiogram (ECG) of the subject as the synchronizing signal for measuring the radioactive counts. This technique is usually called ECG-gated RI-angiocardiography. An RI-image of the left ventricle at any phase of the cardiac contraction-relaxation cycle can be easily obtained by this technique, but it is inevitable that the image obtained is yet ill-defined. Since the images obtained by the method is so obsecure and ill-defined, the measurements or inspections by human observers are apt to be objective, and in order to obtain quantitative information from the image, automated processings of the image have been desired. However, the inferiority in image quality may prevent success of the automated processing.

1.2 Organization of this thesis

This thesis is devoted to the digital processing of radioisotope images of the left ventricle, namely the ECG-gated RI-angiocardiograms. Principal subjects of this thesis are as follows.

(1) Methods of data handling in RI-angiocardiography: In Chapter 2 the techniques to obtain radioisotope images of the left ventricle at any phase of the contraction/relaxation cycle of the heart will be described.

(2) Filtering techniques for radioisotope images: Problems in recovering the quality of the RI-images will be reviewed and a new filtering technique, which will be helpful for improving the quality of the RI-angiocardiography, will be introduced in Chapter 4.
(3) Methods of extracting the left ventricular contour and computing its volume: Simple but hopeful system for extacting the left ventricular boundary from such a ill-defined image as RI-angiocardiogram is presented in Chapter 3. In Chapter 5, more sophisticated and consistent processing system for extracting the left ventricular contour and for computing the left ventricular volume is described.
(4) Analysis of the left ventricular wall motion: In Chapter 6, left ventricular wall motion pattern is analyzed by the pattern recognition technique. This will be helpful for diagnosing a kind of ischemic heart failures such as myocardial infarction.

1.3 Related works

In this section we will briefly review some research activities concerning the topics treated in this thesis, namely some image processing techniques in cardiology and nuclear medicine.

Many research efforts on the processing of heart images have been concentrated in X-ray cine-angiocardiograms. The main aim of the processing is the boundary extraction of the left ventricle for the calculation of its volume. Chow and Kaneko [1-1] proposed the "dynamic thresholding method" in which the threshold gray level value for region extraction was varied according to the local gray level distribution of the image. Although this method have given a solution for the extraction of objects from the image which may involve strong shading, and it have come to be frequently referred, results of its applications to the actual cine-angiocardiograms were not necessarily satisfactory. In fact, the left ventricular boundaries extracted by the method could not be readily used for volume calculation. Beckenbach and Desilets [1-2] proposed the method to detect the left ventricular boundary by referencing the information of the boundary obtained in the previous frame of the cine film. Namely, considering

the fact that the shape of the left ventricle is not so changing between the consequtive two frames of the cine-angiocardiogram, they introduce the method to look for the left ventricular boundary in the vicinity of the boundary obtained in the previous frame. In their method, the boundary in the first frame is given manually. Tasto [1-3,4] also utilized the boundary information of the previous frame, but he determined the estimate of boundary in the first frame by the "motion extraction method". It extracts the region where the boundary is considered to be present by detecting the temporal change of the gray level value, since the change at the nearby area of the left ventricular boundary is usually very great compared to the inner region of the ventricle. Instead of analyzing photographic cine film, Clayton et al. [1-5] processed the television video signal to determine the boundary of the left ventricle. Arranging the orientation of the scan line so that the major axis of the ventricle crosses perpendicularly to the scan lines, the boundary points are located on each of the scan lines. The positions and the gray levels of the boundary points on the previous scan line and the positions of the boundary points in a previous frame were used to determine consistent boundary points. Heintzen et al. [1-6] have developed the system for the processing of cine and video angiocardiograms, which has been used in the routine work of the hospital. However, the extraction of the left ventricular boundary are made mainly by manual tracing. Their research efforts seem to be directed to the representation of the three dimensional motion of the ventricle from the figures of the boundaries obtained from several projections. Thus, the processings of the cine and video angiocardiograms are concentrated to the idea of utilizing the correlation between consequtive frames.

On the other hand, less research efforts have been devoted to the processing of radioisotope image. Budinger et al. [1-7] developed a computer system for acquisition, manupulation and display of two-dimensional images in nuclear medicine. A minicomputer is connected to the scintillation camera and is used for the image formation. Douglas et al. [1-8] established the method of computerized ECG-gated redioisotope angiocardiography. In either methods, however, measurements are mainly made interactively using a light pen.

Next, let us direct our attention to the topic of the restoration

and enhancement of the RI images. Iinuma [1-12] described the linear spatial filters that had spatial frequency characteristics suitable for recovering blur and reducing noise of the static RI images. However, since the RI images are formed by the radioactive counts and they have somewhat different nature from usual photographic images, restoration by this inverse filtering gives not always remarkable results, especially for images of low count rate. Pizer and Vetter [1-9] named the low count RI-images as "quantum limited" images, and pointed out that non-linear adaptive filters suitablly designed were more powerful than usual linear techniques for the restoration and enhancement of these quantum limited images. They proposed the "variable averaging filtering", in which the averaging size are varied according to the local gray level characteristic, and also the "dot shifting" scheme, in which dots are shifted toward the points where the dots are considered to be found originally. Varoutas et al. [1-10] applied the E-transformation technique originally developed by Moore and Parker [4-3] in order to preserve the gray level changes of greater magnitude while eliminating the noisy ripple components. Although it was a complex and time consuming filtering, no marked improvement has been observed in the filtered image. Wahl et al. [1-11] organized the optimum (Wiener) filter of which weighting coefficients, namely the transfer function, were varied according to the local statistical characteristics of the input image such as average local gray level.

Finally, some research efforts are observed on the measurement and recognition of the heart shape. Sezaki and Ukena [1-13] developed the system for extracting the region of the heart shadow from anterior-posterior chest radiographs and determining the cardiothoracic ratio. This system was implemented by a television camera and a minicomputer and was used for the mass screening. Roellinger et al. [1-14] and Ueyama et al. [1-15] extracted the contour of the heart shadow from a chest radiograph, and by paramenterizing the shape of the whole heart they tried to detect and classify the valvular and septal defect of the heart. Thus they developed the way for automatic inspection of the heart diseases using the overall shape of the heart.

Thus, many investigations have been made on image processing in cardiology. However, we cannot find the hardware and/or software system

to handle and process the RI-angiocardiographic images consistently.

Chapter 2 Radioisotope Angiocardiography

2.1 Introduction

RI-images or scintigrams of the human organs can be obtained by RI-imaging devices, such as a scintillation camera, by detecting radioactive rays which are emitted by the radionuclide contained in the object organs. Figure 2-1 shows the schematic diagram of the Anger type scintillation camera which is commonly used in the clinical field.

Radioactive ray passing through the hole of the collimator incidents on the scintillation crystal and, consequently, scintillation is occurred at the point of incidence. Light radiated by the scintillation is caught by the several, e.g.19, photomultiplier tubes arranged two-dimensionally behind the crystal.

Since the proportion of light intensities caught by each of the photomultiplier tubes varies according to the position of the scintillation, the position of the scintillation can be derived from the magnitude of output pulses of each photomultiplier tube. Thus, X and Y coordinate components of the scintillation position are determined by the analog weighting matrix.

Intensity of the scintillation, which is proportional to the energy level of the incident radioactive ray and is given as a Z-axis component of the scintillation camera signal, is obtained by summing all the outputs of photomultiplier tubes. Energy of radioactive ray is lowered by the scattering caused by the tissues or the edges of the collimator holes, and a path of ray is bent by the scattering. Therefore, the scattered rays should not be used to form the RI-image. By using the pulse height analyzer, and windowing the Z signal, only the scintillation signals corresponding to the energy level inherent to the radionuclide used are detected. X, Y and Z signals thus obtained are, then, applied to the deflection circuits and intensity control circuit of cathode-ray-tube (CRT), respectively. Consequently the bright spot is displayed at the position corresponding to the position of original scintillation. The image of the organ is formed by taking a photograph of these spots displayed on the CRT screen. The shutter of the photo-

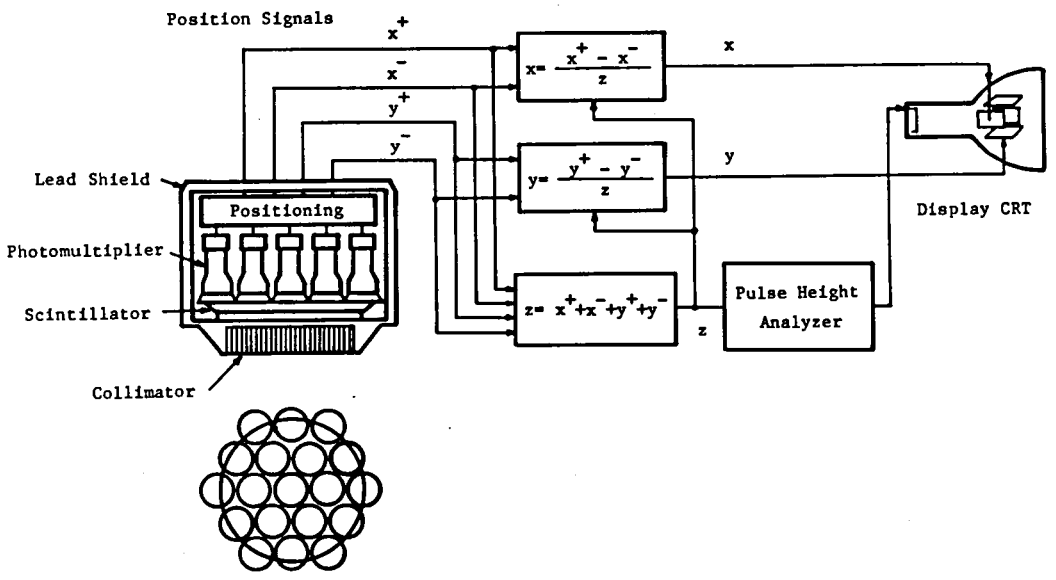

Fig. 2-1 Schematic diagram of the Anger type scintillation camera

graphic camera should be opened during a period necessary to accumulate sufficient number of spots on the photo film.

As stated earlier, if we are going to depict the image of the heart, the accumulation of spots over a long period will cause the image to lose the dynamical information about the motion of the heart. Therefore, we cannot obtain accurate image showing the real state of the heart by the scintillation camera alone.

Since the motion of the heart is periodical, and, in the resting condition, the pattern of motion is not so largely changed cycle by cycle, the extraction of one average cycle of motion from some consecutive cycles will suffice. Also, since a close and constant relation exists between electrical and mechanical events in the heart, an electrocardiogram (ECG) may be used as synchronizing signal for obtaining the image of the left ventricle [2-1].

The electrocardiogram is obtained by measuring, from the surface of the body, the action potential of the myocardium which is generated by the contraction of the heart, that is,the excitation of the myocardium. In the common measuring method, the ECG signal exhibits the waveform shown in Fig.2-2 and the significant parts of the signal are named P,Q,R,S and T waves as shown in the figure. The P wave is considered to indicate the excitation corresponding to the atrial contraction,and it is known that the R wave, which exhibits the most prominent peak, is the indication of the action potential by the ventricular contraction. The T wave appears at the end of the ventricular contraction period.

In the consequence, we use two methods to depict the image of the heart at any specified phase of the cycle. One of them is a method using the actual electrical circuit and obtaining the image photographically. Another is a method using the computer data processing system connected on-line to the scintillation camera, and in the method the image is formed by the computer software.

These methods to obtain RI-images of the heart using subject's ECG signal are generally referred to as ECG-gated RI-angiocardiography.

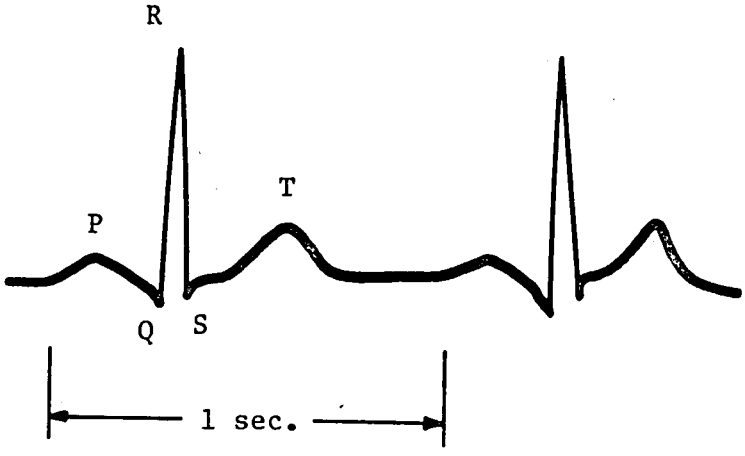

Fig. 2-2 ECG waveform

2.2 ECG-gated RI-angiocardiography

As shown in Fig.2-3, a gating circuit, which acts synchronously with the subject's ECG signal, is attatched to the scintillation camera previously described, in order to obtain the heart image at a specific phase of a cardiac cycle. A magnetic tape recording device, which is a standard optional device of the scintillation camera system and is actually a video tape recorder, is used to facilitate the data storage and the repeated operation for forming images at several different cardiac phases. Usually, only the scintillation positional signals are recorded on this magnetic tape. We have attatched the ECG recording circuit to this standard recording facility. Slicing and shaping the ECG signal, we obtain a series of rectangular pulses which indicate the R-wave of the original ECG. This pulse signal is then frequency modulated and recorded in the audio track of the magnetic tape simultaneously with the recording of the scintillation positional signal.

When we replay the tape after the recording, position coordinate signals are fed to a display section through a gating circuit, which is controlled by the pulse signal demodulated from the audio track signal. As shown in Fig.2-4, gating pulse is generated by the retrieved pulse after some delay from the rise of the retrieved pulse, and the gate is opened for the duration of the gating pulse so that only scintillations recieved in this duration are displayed on the CRT screen. The delay time and the duration of the gating pulse can be varied independently. The delay time is a parameter to determine the phase of the imaging and the duration of the pulse determines the temporal resolution.

Since the gated scintillations in one cardiac cycle are usually insufficient to produce a significant heart image, gated scintillations over several consecutive cardiac cycles are multiply photographed on a single photographic film.

Though the principle of the RI-angiocardiography is just as described above, there are many variations according to radioactive pharmaceuticals used and whether the image formation is done before or after the radionuclides distribute uniformly throughout the body. As for these variations of the method we will consider later on and here we will restrict ourselves to showing some of examples in Fig.2-5.

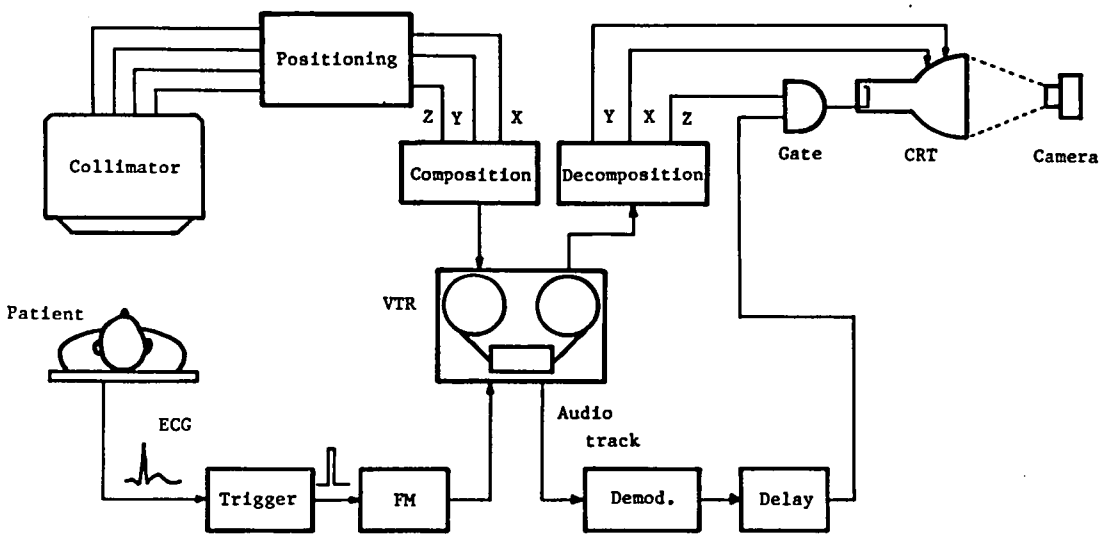

Fig. 2-3 Block diagram of the instrumentation for ECG-gated RI-angiocardiography

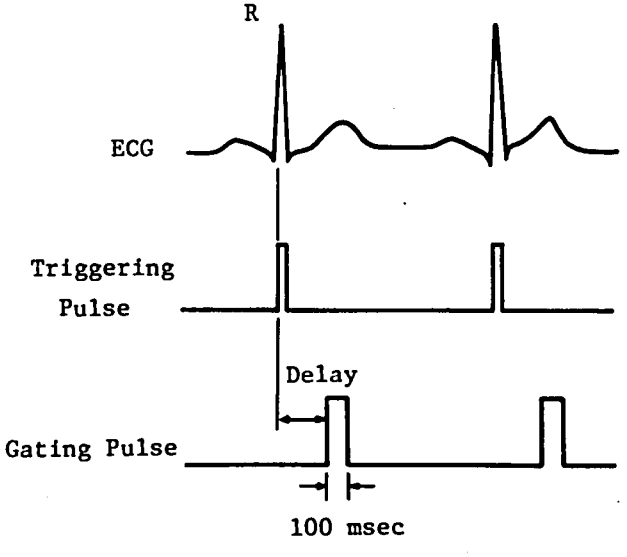

Fig. 2-4 ECG gating

The image of Fig.2-5a is the one obtained at the phase of end-diastole (relaxation) setting the delay time to open the gate to zero, and Fig.2-5b at the phase of end-systole (contraction) adjusting the delay time so that the gate is opened at the onset of T-wave, usually about 0.3 second after R-wave. These images are, as is seen, very ambiguous or in other words noisy.

2.3 Computerized ECG-gated RI-angiocardiography

Since RI images are, basically, formed by the discrete count of radioactive rays and are digital in nature, the digital computing facility has come to be used for measurement and data processing, connected with the scintillation camera system. The position signals obtained from the coordinate calculating circuit of the scintillation camera are converted to digital signal and fed into the computer. Electrocardiogram measured from the subject is also converted to digital and is simultaneously accessible from the computer. Such system as described above are now commercially available and are widely used in the routine works of hospitals.

In this section we will briefly mention about the digital data acquisition and processing system for obtaining the ECG-gated image of the heart. The simplified schematic diagram of the system for digital data acquisition is shown in Fig.2-6. In order to follow the rate of occurence of scintillation, the direct memory access channel is usually used for the data acquisition. The system can be operated in two distinct modes according to the way for sorting scintillation events into the computer memory. One of them is the mode to arrange the coordinate values of scintillation in the order of their occurence, and it is called the list mode. The other is the mode to form the image sorting the scintillation events according to their coordinate values simultaneously with the measurement. This is called a frame mode or a histogram mode. The frame mode is convenient for the quick looking of the image. However, as is understood without difficulty, it requires a large memory space. Usually, dimension of the image matrix in the frame

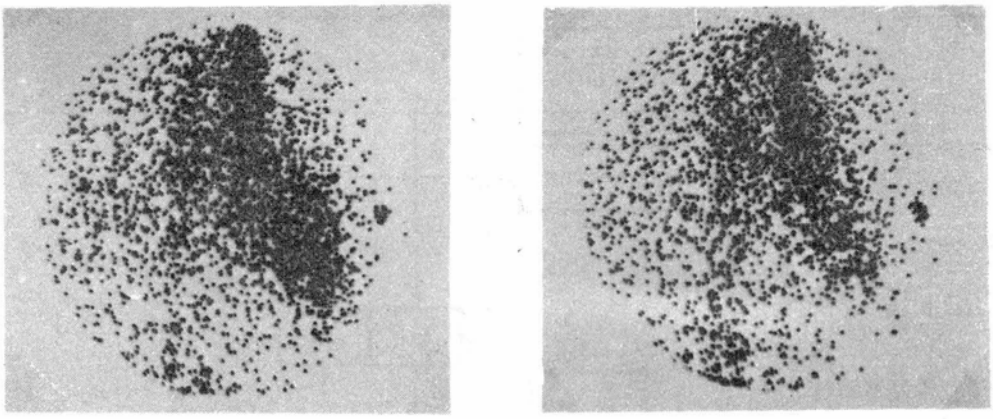

(a) End-diastole (b) End-systole

Fig. 2-5 Example of ECG-gated RI-angiocardiogram

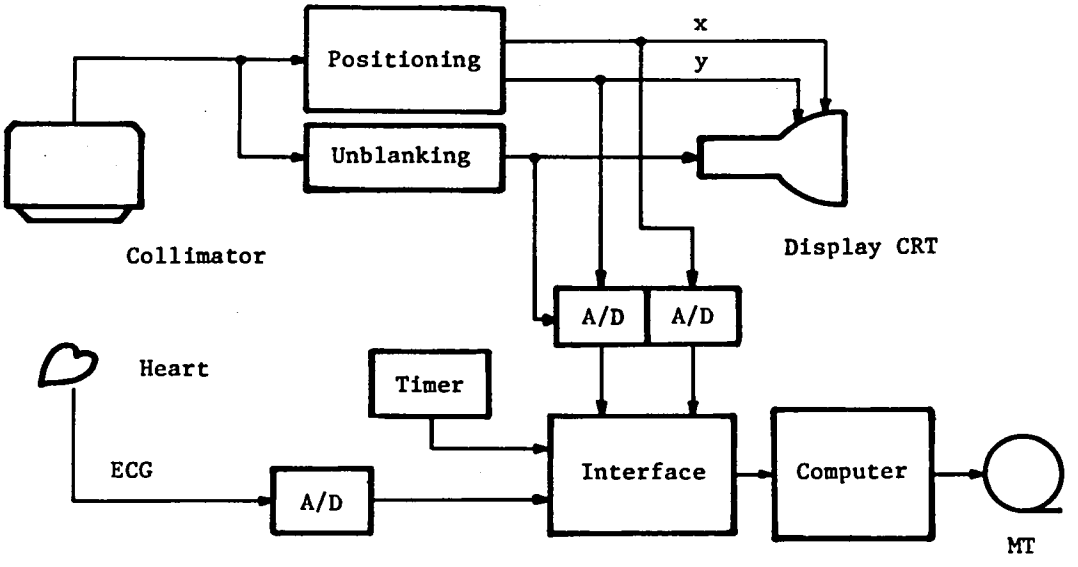

Fig. 2-6 Schematic diagram of a system for digital acquisition of scintillation data

mode is limited up to 64 x 64 due to the storage capacity of the computer. On the other hand, a list mode is used for sorting the data for later investigation, since the list mode data reserve raw information. It is usual to use magnetic tape for data storage and for data exchange, in which the data are recorded in a form of the list mode togather with a physiological signal such as electrocardiogram.

The magnetic tape recording format is illustrated in Fig.2-7. Successive scintillation coordinate values are recorded and ECG-signal, which is sampled and digitized at the interval of 10 msec, intervenes in the series of the coordinate values. Therefore, the scintillation coordinate values lying between two consecutive samples of ECG-signal correspond to the scintillation events occurred in this 10 msec interval.

Figure 2-8 shows a processing flow of the image formation from the magnetic tape recorded data. First, the time activity curve, which is a time course of the number of counts measured in a short unit interval, is formed so that we may observe the flow of the radionuclide injected and determine the period which can be used for the image formation. Then, the R-waves of ECG-signal are detected and a frequency histogram of the time duration between two consecutive R-waves, namely R-R interval, is obtained. Since the ECG-gated RI-angiocardiography is based upon the assumption that the beat of the heart is steady and with sinus rhythm, it is undesirable to use the scintillation data occurred in the cycle possessing the interval too different from the interval of the average. Hence, observing the distribution of R-R intervals, one should set the bound of the R-R interval and discard the scintillation data in the unusual heart cycle. Lastly, using the parameters established above and specifying the delay time from the rise of the R-waves and the gate duration, we can sort the scintillation events during each of the gate periods in the image buffer according to their coordinate values. As was done in the technique in the previous section, scintillations during gate period are summed for some consecutive heart cycles on this image buffer rather than on the photo film.

Position of the R-wave is detected by the thresholding operation. Since the drift of the base line caused by patient's movement may cause the erroneous detection, the retrieved ECG-signal is high pass filtered

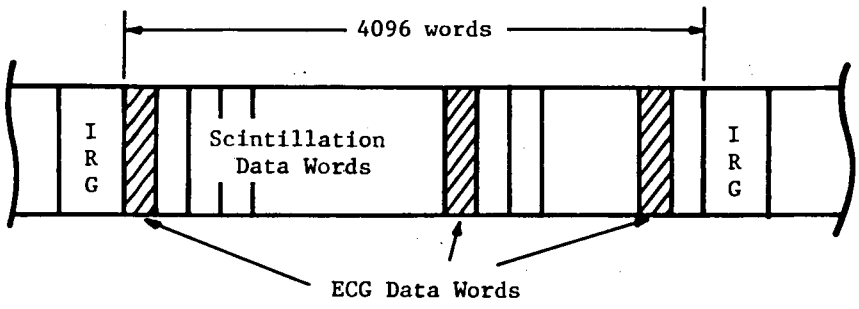

(a) Format of the tape

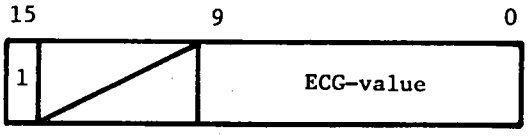

(b) ECG data word

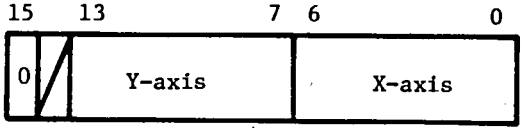

(c) Scintillation data word

Fig. 2-7 Magnetic tape recording format of the list mode data

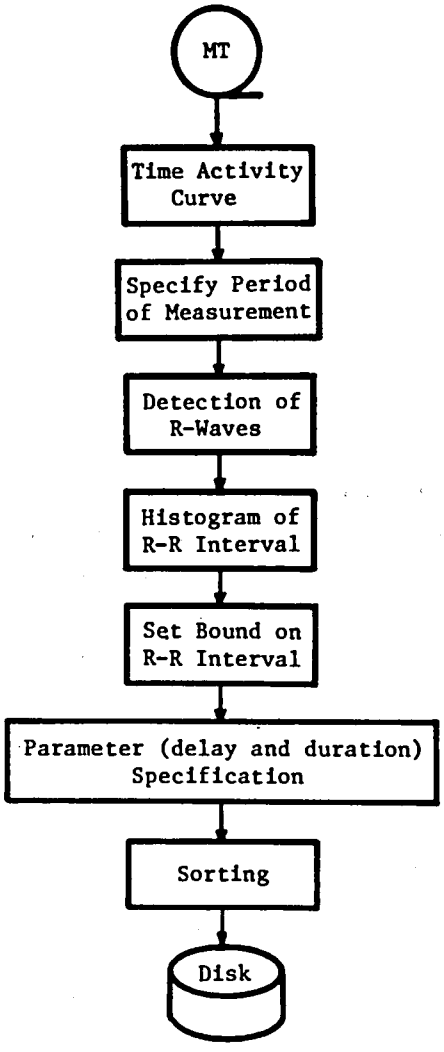

Fig. 2-8 Processing flow of the image formation

and the drift component is removed from the signal. Figure 2-9 shows an example of detection of R-waves from ECG-signal, and an example of the histogram of the R-R intervals is shown in Fig.2-10.

The coordinate values of the scintillation position are quantized into 7 bits. Two dimensional buffer area of 128 x 128 pixels is taken in the minicomputer's main memory and is used for image formation. Obtained images are stored in the magnetic disk. Image display is made on the storage type graphic display device. Details of the minicomputer system used for this image formation are shown in the Appendix B.

Examples of images obtained by the method described in this section are demonstrated in Fig.2-11 and Fig.2-12. Figure 2-11 shows the sequence of the heart images obtained by accumulating the scintillation counts occurred during each of the consecutive heart cycles after injecting radionuclides into the vein of the subject's arm. Hence, actually, the gating by the R-wave of ECG is not applied in this case. Numbers attached to each of the images indicate the number of beats (cycles) after the injection. The flow of radionuclides is clearly observable from this sequence of images. The collimation was made in a left anterior oblique (LAO) view (cf. Fig.2-15). Figure 2-12 shows the series of the heart images in one average cardiac cycle, which are obtained by ECG gating. Numbers attached to each of the images indicate delay times from the R-wave, in the unit of millisecond. From this figure, we can observe the movement of the left ventricle.

2.4 Varieties of images obtained by RI-angiocardiography

Using the ECG gating technique described in the preceding two sections as fundamental techniques, we can obtain several kinds of image according to the purposes of the diagnosis and inspection.

As for the state of the radionuclides' distribution at the time when imaging is started, there are two different approaches. One of them is a method in which the radionuclides injected intravenously are allowed to become uniformly distributed throughout the blood volume. This method is sometimes called the "pool imaging". The another is the

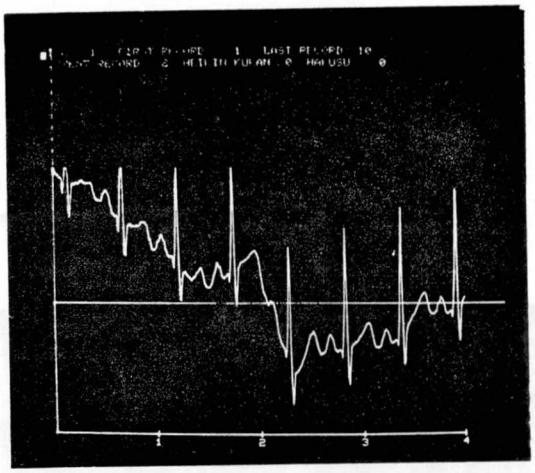

(a) Original

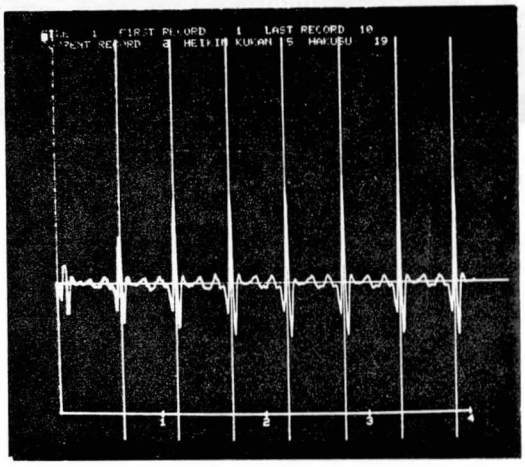

(b) Processed

Fig.2-9 Elimination of drift in ECG waveform and detection of R-waves

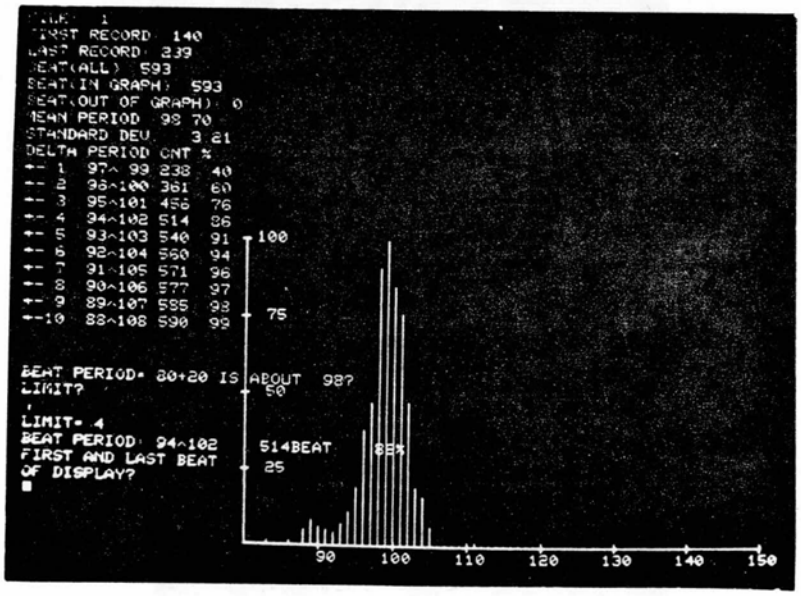

Fig. 2-10 Histogram of R-R intervals

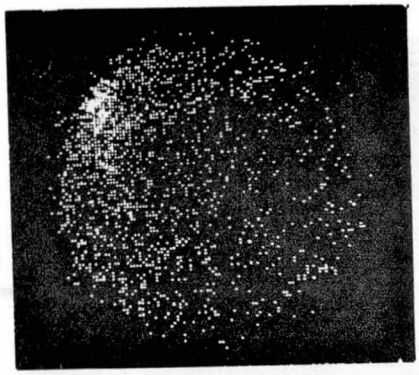

(a) 1 - 5

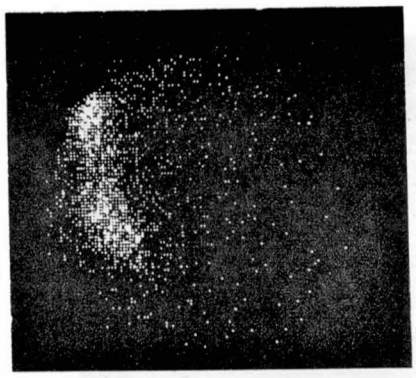

(b) 6

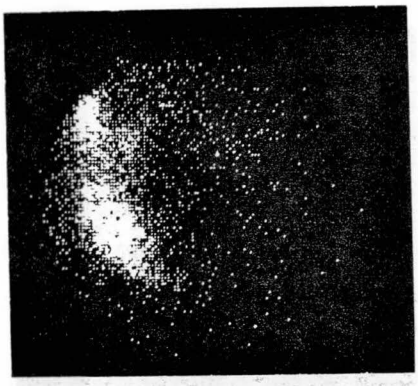

(c) 7

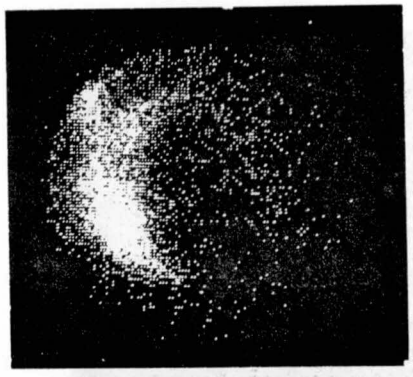

(d) 8

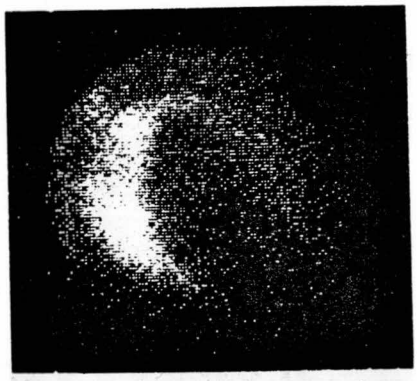

(e) 9

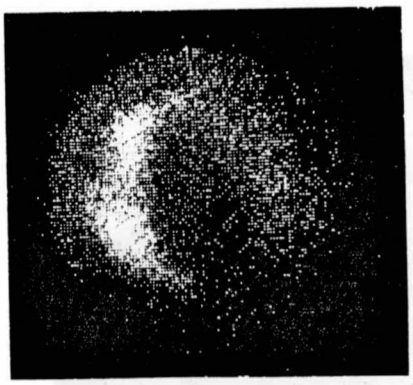

(f) 10

Fig. 2-11 Example of digitally acquired RI-angiocardiogram; images obtained sequentially immediately after the injection of radionuclide without ECG-gaing

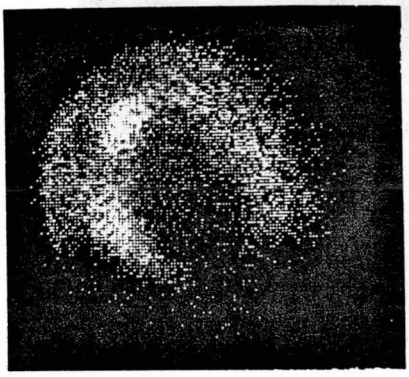

(g) 11

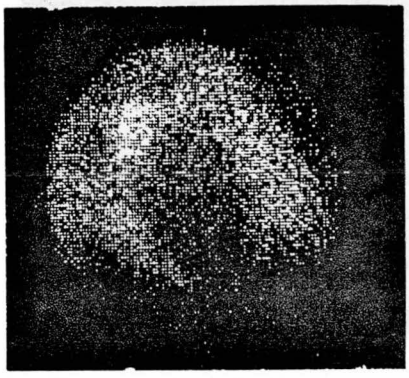

(h) 12

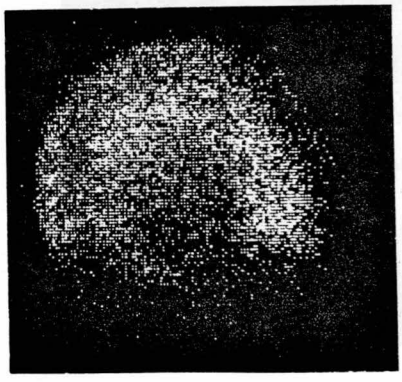

(i) 13

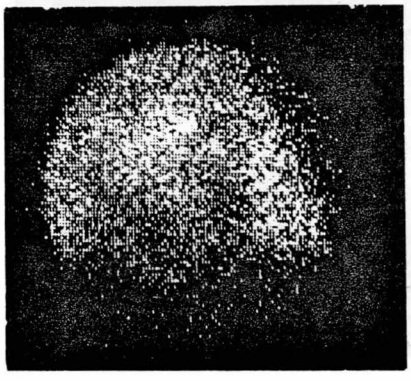

(j) 14

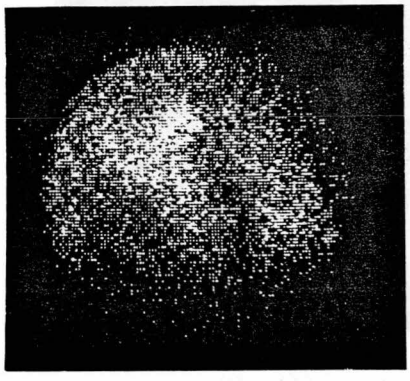

(k) 15

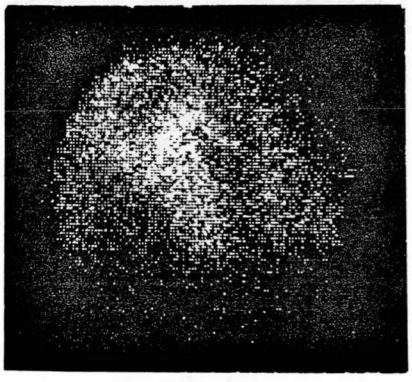

(l) 16

Fig. 2-11 (continued)

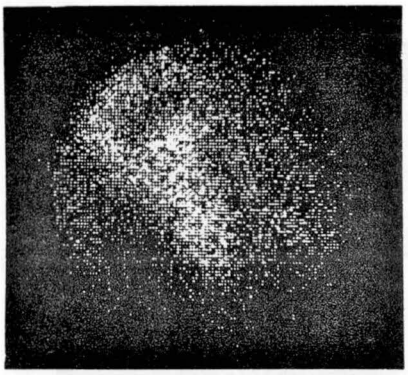

(m) 17

(n) 18

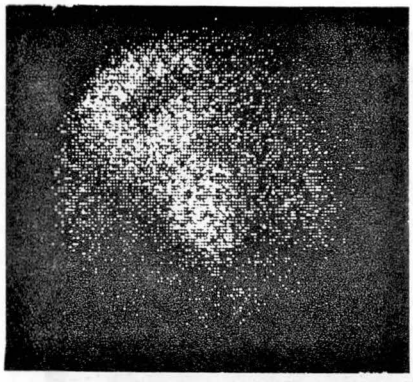

(o) 19

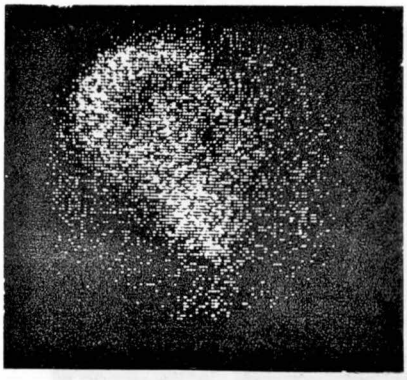

(p) 20

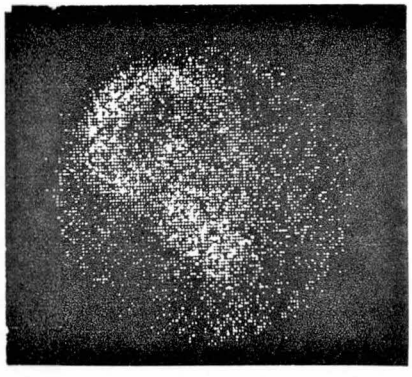

(q) 21

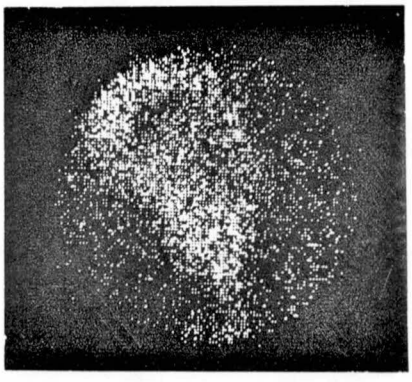

(r) 22

Fig. 2-11 (continued)

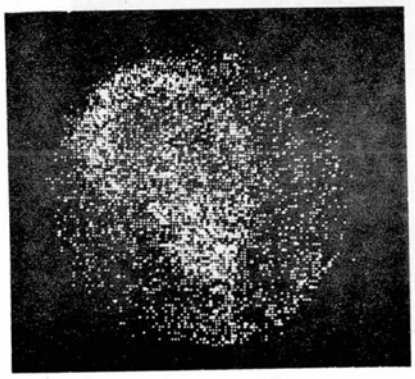

(s) 23

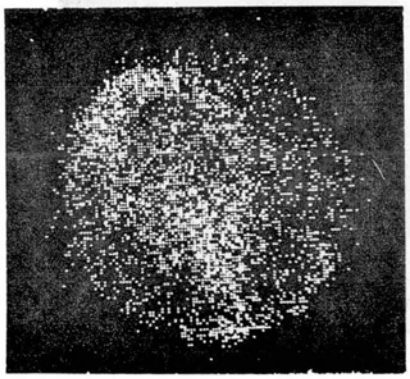

(t) 25

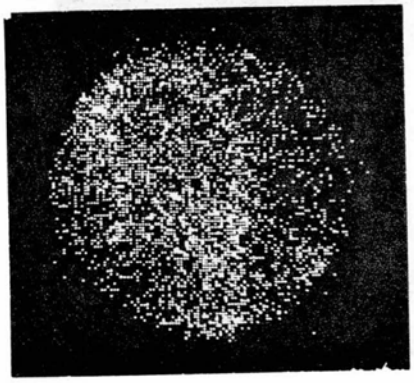

(u) 27

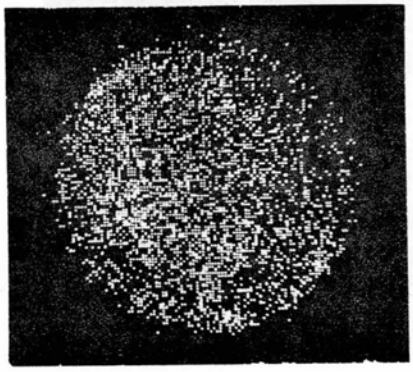

(v) 30

Fig. 2-11 (continued)

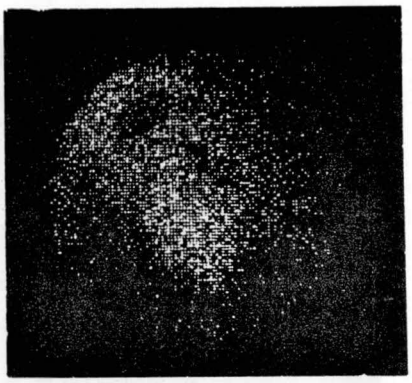

(a) 0

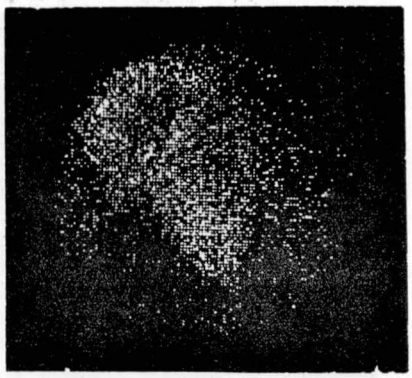

(b) 100

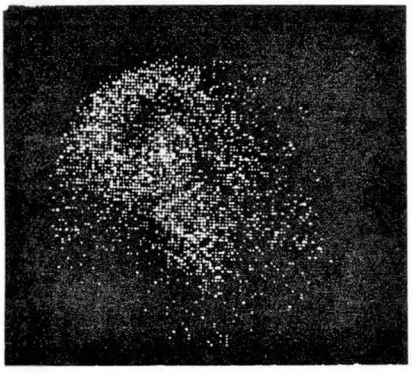

(c) 200

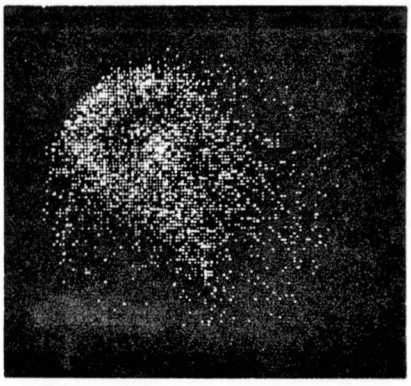

(d) 300

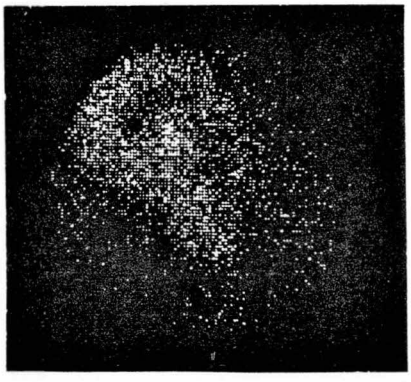

(e) 400

(f) 500

Fig. 2-12 Example of digitally acquired RI-angiocardiogram; images obtained in one average heart cycle with ECG-gating

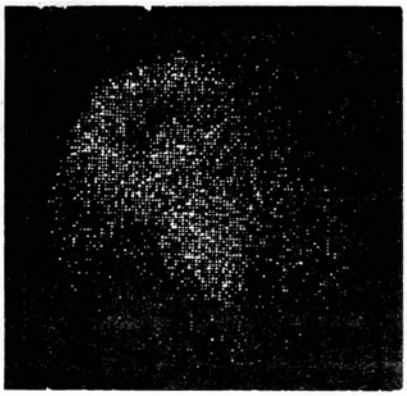

(g) 600

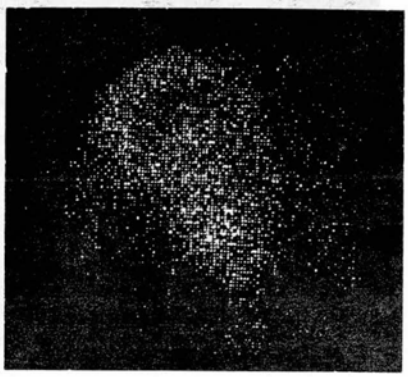

(h) 700

Fig. 2-12 (continued)

methods in which radionuclides are injected as a bolus into the peripheral vein, and the gated scintillation image is obtained during the first transit of the radionuclides through the heart chamber. We will call this method the "first transit imaging".

In the former method, since the state of the distribution of radionuclides is steady for a while, one can accumulate the gated scintillation for a considerably long series of heart cycles, say, several hundreds of cycles, so that one may reduce the noise component of the image by accumulating as many counts as possible. However, since the radionuclides are distributed throughout the body, there remain high activities of radionuclides in the surrounding organs, e.g., lungs, livers and so on. This will cause the irrelevant background and make the relevant object less identifiable. Moreover, one cannot depict the selected heart chamber alone. On the other hand, in the latter method, by carefully observing the time activity curve obtained within the region of interest established to cover the area of heart, one can determine the period during which the bolus injected radionuclides remain in the left or right heart. Hence, one can obtain the image less affected by the background activity. Figure 2-13 shows an example of time curve depicting the time course of the count rate from the injection of radionuclide into the peripheral vein. The first peak corresponds to passage of radionuclides through the right heart and the second to the left heart. From this, we can determine the period during which the radionuclide passes through the left ventricle. However, since the period in which the radionuclides remain in the left heart chamber is short, one can accumulate the gated scintillation only for several heart cycles. For this reason, the image is generated by relative small amount of counts, and it is quite noisy and ambiguous. The images shown in Figs.2-5 and 2-12 are the first transit images and those in Fig.2-14 are obtained by the pool imaging.

Various radio pharmaceuticals are used according to the object and the problem. The pharmaceutical can be concentrated in the area of interest, when matched to specific metabolic and physical function of the object organs. ^{99m}Tc-HSA (Human serum albumin) is a compound which is made by labelling the serum protein by the radioisotope of

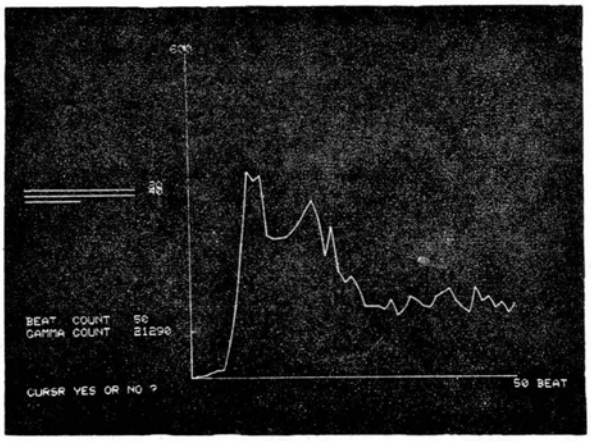

Fig. 2-13 Time activity curve

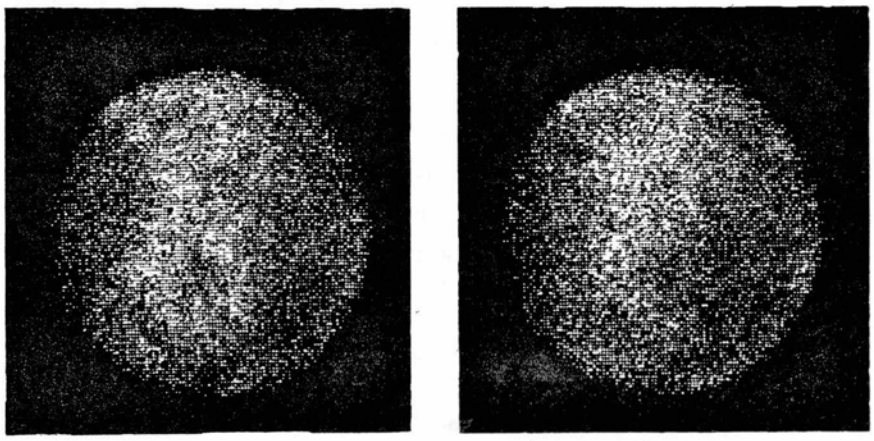

(a) End-diastole (b) End-systole

Fig. 2-14 Heart image obtained by ECG-gated pool imaging

technetium. This agent behaves like the usual plasma in the blood, and it is only slowly removed from circulation by the liver and spleen. Hence, it is suitable for blood pool imaging, after complete equilibration of the agent in the blood volume. ^{99m}Tc-pertechnetate ($^{99m}TcO_4^-$) is used as the agent for the first transit imaging because pertechnetate is removed from circulation by the thyroid.

It is a matter of course that the pattern of the heart image obtained will vary when the orientation of view is changed. According to the purpose of the inspection, there are several methods of orientation (Fig.2-15). When we use the right anterior oblique (RAO) view, we can best understand the shape of the left ventricle spatially separated from the left atrium. However, the region of right heart overlaps the left heart in this veiw. So, it cannot be used in the pool imaging, and is used in the first transit imaging. On the other hand, since the left anterior oblique (LAO) view can separate the left heart and the right heart, the pool imaging is performed in this view. However, the left atrium overlaps, in part, the left ventricle. The images in Fig.2-5 are obtained in RAO view and those in Figs.2-12 and 2-14 are in LAO view.

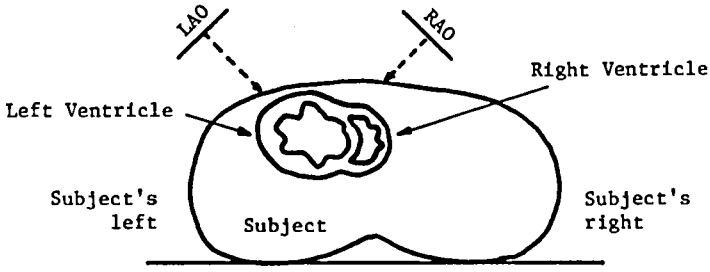

Fig. 2-15 Two typical orientations for heart imaging

Chapter 3 Left Ventricular Boundary Detection by the On-Line FSS System

3.1 Introduction

In this chapter, the methods of detecting the left ventricular boundary from the RAO ^{99m}Tc left ventriculogram by a prototype image processing system are described. The system consists of a flying-spot-scanner built in the authour's laboratory and connected on-line to the standard minicomputer system.

It has been said that it is impractical to process images by a minicomputer system since the large storage capacity and the flexibility in data handling are required in image processing. It is true in a sence, but if we can utilize image input device with random scanning capability coupled with the minicomputer, we can regard the device as an external mass storage device of image data, and consequently we will be able to treat image data by a minicomputer. The image data is considered to be stored in an original image in a form of photographic film or printed photograph, and we can access image data of any point randomly by the aid of random access capability of the device. On the other hand, since the precise image output device is hard to obtain and, even if it is available, the information is lost and modified in the photographic process, it is not practical to apply successive processing by feeding the image obtained by the first processing to the second processing as an input. Therefore, a processing is likely limited to rather simple one. However, since, in this concept, it does not need vast amount of data storage, implementation on the minicomputer with a small-sized memory is possible. Moreover, in the every-day routine work of handling a good deal of images, it is usual that there is no room or capacity to store the image in a digital form together with the original photos. Hence, it is quite natural to process images directly accessing the original photos by the random accessible input devices.

Among the image input devices with random access capabilities, a flying-spot-scanner (FSS) is most commonly used. This device can scan

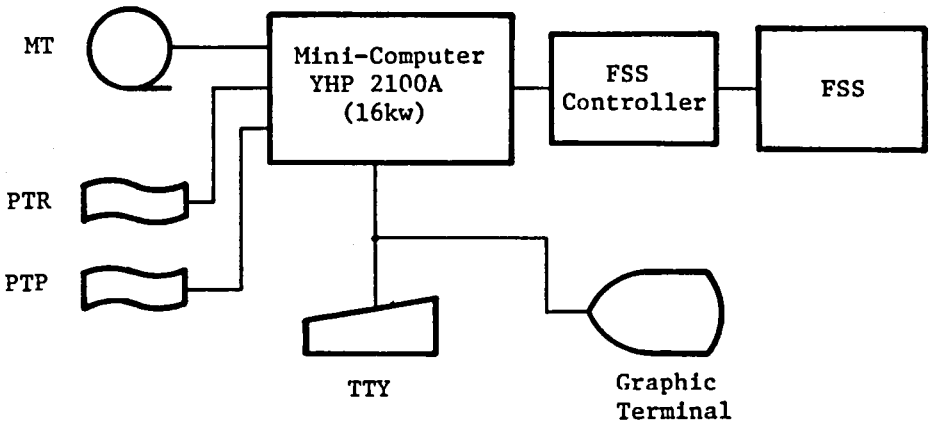

Fig. 3-1 Prototype image processing system used in Chapter 3

the object image in a fairly high scanning rate and with high accuracy in positions and gray levels. Since scanning is made addressing the x and y coordinates of the point to be read, it is not hard to control the scanning of FSS by computer. Hence, FSS can be used as a random access image input device.

A simplified block diagram of the on-line FSS system used for the image processing described in this chapter is shown in Fig.3-1. The FSS is designed for reading 35-mm transparencies, and is connected to the minicomputer through the FSS controller circuit. In a monitor mode, scanning is made in the standard television raster and the object image is displayed on the conventional television monitor. When a scanning mode is activated, monitoring scan raster is replaced by the computer programmed scan. After the beam of the CRT moved to the specified point, the gray level value of the point is measured and transferred to the computer. Detailed description of this FSS will be found in Appendix A. The minicomputer is furnished with the standard set of peripherals, and a storage type graphic terminal is used as a display device as well as a console keyboard. The main memory of the computer was 16 kwords at the time when the methods in this chapter were first developed.

The subject of this chapter is to detect the left ventricular boundary from the RAO ventriculogram by this FSS system.

3.2 Boundary detection by a radial scan method

In general, we can assume that in the RAO ventriculogram the left ventricular region exhibits a convex shape like an ellipse and also has a greater dot density, i.e., the number of dots per unit area, than the background. Then, in the case where the scan is made radially from a central point of the left ventricular region (Fig.3-2), every scan line crosses the left ventricular boundary almost perpendicularly, and we can detect the difference in dot density between the left ventricular region and the background. This scanning manner will be referred to as radial scan.

Since the original image is formed by clusters of dots, very rugged

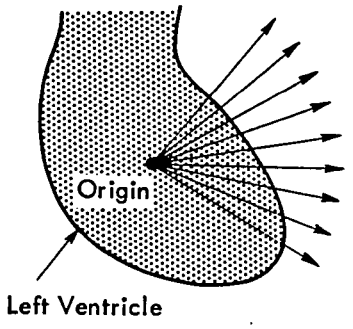

Fig. 3-2 Radial scan

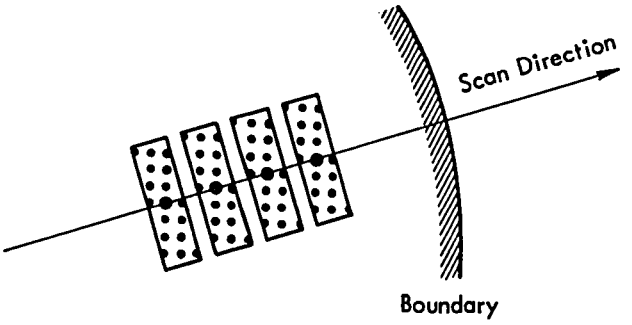

Fig. 3-3 Simulated rectangular spot

gray level distribution is obtained if the scan is made by a small spot. Hence, we make use of a larger rectangular spot to smooth out the noise component caused by the dot structured image as much as possible. This rectangular spot is simulated by a computer program which averages the gray level values within the rectangle. In scanning, the spot is aligned so that its longer side lies normally to the scan direction (Fig.3-3). By scanning in this manner, we can prevent the obtained gray level distribution from being greately affected by slight variation in a scanning direction, while suppressing the increase of blur due to the averaging (smoothing) operation.

The array data of gray levels thus obtained exhibit, on the average, higher value in the range corresponding to the left ventricular region and lower value in the background. Figure 3-4 shows one of the examples. However, there are still involved a great deal of variations of gray levels in the array, and, hence, it seems scarecely feasible to decide the point corresponding to the boundary between the left ventricular region and the background by simply thresholding or differentiating the gray level data. We have to, therefore, detect the difference of gray levels in a more global sense. A fitting method is employed for this purpose, in which the model of gray level distribution is fitted to the actual data. The model represents the ideal gray level distribution of the data which will be obtained by the radial scan. The gray level distribution of the model is formulated as Fig.3-5 so that it has constant gray level values d_1 and d_2 within and outside the left ventricular region respectively, and it has a step-like transition in gray levels at the point corresponding to the boundary. This ideal model is fitted to the array of raw data to minimize the fitting error which is defined as the sum of absolute value of deviation at every point as follows:

$$E(n) = \sum_{i=1}^{n} |f(i)-d_1| + \sum_{i=n+1}^{N} |f(i)-d_2| \qquad (3\text{-}1)$$

where

$$d_1 = \frac{1}{n} \sum_{i=1}^{n} f(i),$$

and

$$d_2 = \frac{1}{N-n} \sum_{i=n+1}^{N} f(i).$$

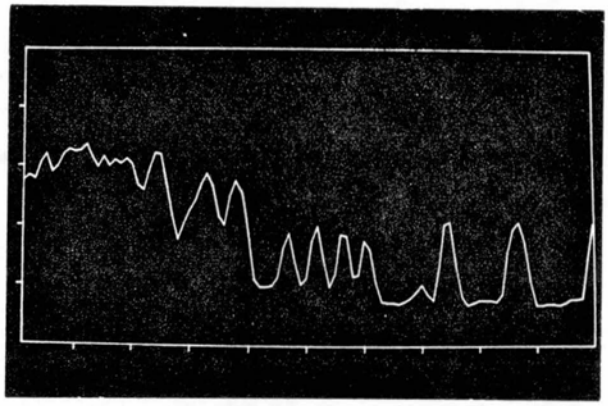

Fig. 3-4 Gray level profile obtained by the radial scan

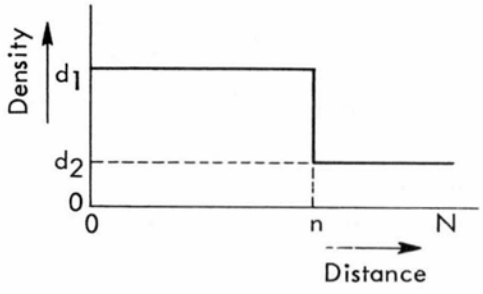

Fig. 3-5 Idalized gray level distribution

and N is a number of sampling points. The sum of absolute value of deviation is used instead of the sum of squares only from the viewpoint of the processing time.

The quantity $E(n)$ is to be minimized with respect to n, the position of the boundary. This minimization procedure of $E(n)$ cannot be performed analytically because n does not appear explicitly as a variable in $E(n)$. The minimization is done by calculating $E(n)$ for all possible values of n and picking out that n giving the minimum. The value of n thus obtained represents the position of discontinuity of the best-fit model, and this point given by n is the boundary which discriminates the left ventricle and the background. An example of fitting is shown in Fig.3-6.

The procedure described above is repeated for every scan line at a proper angular interval and the boundary points determined are successively connected so as to depict the left ventricular boundary curve.

In actual RI-angiocardiography of the first transit obtained by the right anterior oblique view, it is difficult to image the left ventricle alone. In fact, the ascending aorta is usually imaged connected with the upper part of the left ventricle, and the descending aorta and the left atrium overlap the upper left part of the left ventricle. Therefore, if the scan line enters the region of the aorta or the overlapping area above described, the determination of the boundary points by the model fitting may not work well, since the difference in gray levels between the left ventricular rigion and other regions are quite little and sometimes there is no difference between them. To avoid these complications, the region of interest, that is, the window, is set up so as to include the left ventricle and exclude the region of the aorta and the left atrial region. Further, the range of the angle of scan is limited so that the scan line does not enter the region of the aorta.

Experimental results of the left ventricular boundary detection are shown in Fig.3-7. In this figure the detected boundaries are superimposed on the original images, and the regions of interest are depicted by the rectangular frame. Except for the fact that the boundary points cannot be determined around the upper part of the left ventricle, the method works well for determining a contour in a dot-structured low-quality image.

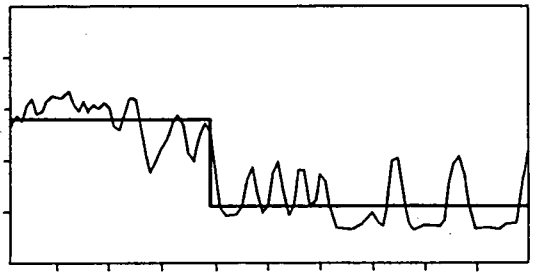

Fig. 3-6 Example of fitting

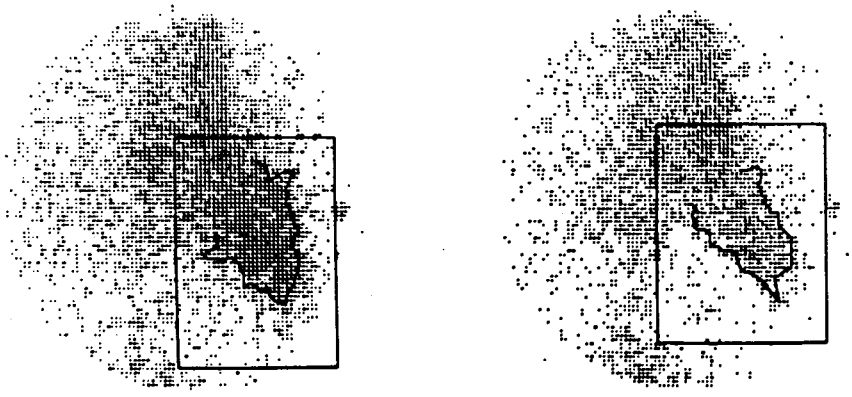

(a) End-diastole (b) End-systole

Fig. 3-7 Result of boundary detection by radial scan method

3.3 Boundary tracing by a nonlinear edge detection technique

Though the radial scan method described in the previous section is very simple, it seems to be difficult to construct a model which can be applied to the entire angular range of radial scan. An alternative which will be described is to use a boundary tracing method as a local processing technique in a sense that only local image property within the neighbourhood of the contour is examined. The boundary points are detected by a local edge detector which is constructed using the nonlinear edge detection technique originally developed by Rosenfeld [3-1]. The tracing of contour is controlled by the information about the direction of contour so far obtained.

In the noisy or highly textured image, much of irrelevant noisy gray level transition is involved in addition to the releveant ones which correspond to the region boundaries or major edges. The standard edge detection techniques which involve derivative operation cannot be directly applied to detect this major edge, for they are highly sensitive to noise. Adding the smoothing operation to the derivative operation, we can reduce the influence of noisy gray level distribution. However, excessive smoothing will, in turn, make the position of edge ambiguous. Rosenfeld found that a product of differences of averages taken over different pairs of adjacent neighbourhoods would tend to yield sharply localized edges [3-1]. This edge detection or enhancement technique is called the nonlinear edge detection technique.

The local edge detector is constructed by making use of this nonlinear edge detection technique. As shown in Fig.3-8, the detector measures the running differences of the averaged gray level between two adjacent k x k neighbours for some different k's, and, then, takes their product. The x-direction specifies the direction of the detector that is the direction of neighbour's running and x = 0 specifies the origin of the detector. Setting the origin and the direction of the detector properly, running difference $d_k(x)$ is calculated as

$$d_k(x) = \frac{1}{k^2} \left| \sum_{(i,j)\in R_k(x)} f(i,j) - \sum_{(i,j)\in S_k(x)} f(i,j) \right| \qquad (3\text{-}2)$$

where $x \varepsilon [-N,N]$, and $f(i,j)$ represents the gray level value at the point (i,j) and N specifies the range of search. The product of $d_k(x)$'s are caluculated by the following;

$$p(x) = \prod_k d_k(x) \qquad (3\text{-}3)$$

$$x \in [-N, N]$$

The point where $p(x)$ has the maximum value is decided as the location of the edge.

Setting of the origin and the direction of the detector is controlled by a tracing procedure. Suppose that we can locate a point P near the region boundary by some appropriate means. We, then, determine the the direction D nearly normal to the boundary from the point P now located. We can use this point P as the origin of the edge detector and this direction D as the direction for the edge detector. The determination of the direction is done as follows: The absolute differences of the average denstiy levels in two neighbouring areas laid on either side of the point P as shown in Fig.3-9 are calculated varing the direction of neighbouring areas around the point P. We may decide the direction giving the maximum absolute difference as the direction D nearly normal to the boundary from the point P. In practice, four quantized orientations; horizontal, vertical and two diagonals are used for simplification. The edge detector above described is applied to the image, aligning its origin to the point P and its direction to D. Once the location of the boundary point is decided by the edge detector, next point near the boundary, which may be called estimated boundary point, is determined from the boundary point now decided and the direction to which the detector is applied, i.e., one may locate the point in a certain distance apart from the boundary point in the direction perpendicular to the detector's direction as shown in Fig.3-10.

A new direction to which the detector should be applied is now determined on this new estimated point, and the tracing operation will be continued repeating the procedure above described.

The point which will be used as the starting estimated boundary point is determined near the apex of the left ventricle by using the

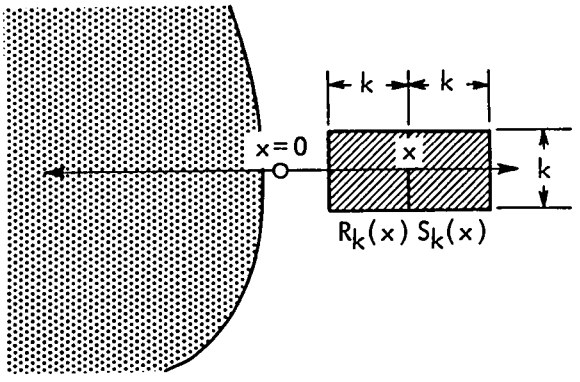

Fig. 3-8 Nonlinear edge detector

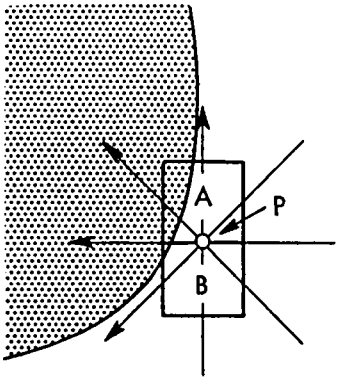

Fig. 3-9 Determination of the detector's direction

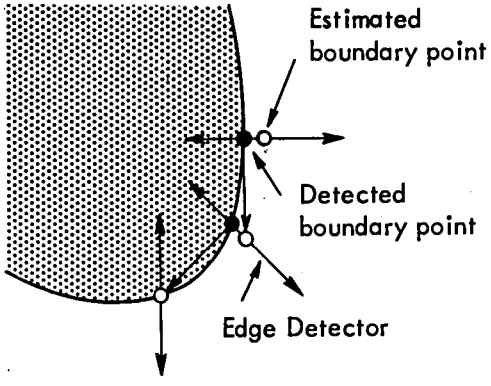

Fig. 3-10 Location of the next estimated point

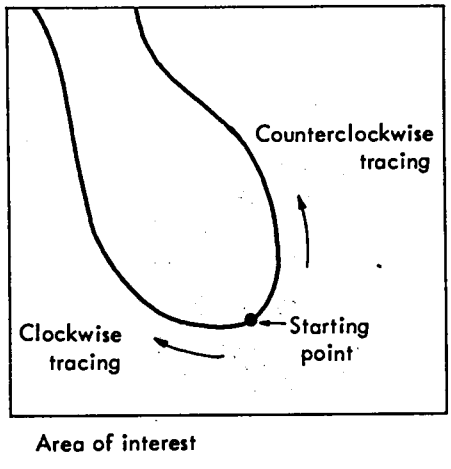

Fig. 3-11 Boundary detection

method mentioned in the previous section. Namely, this is done by applying the radial scan method in a limited angular range covering the apical area of the left ventricle and picking out the furthest boundary point from the origin of the scan. The tracing is made along the clockwise and counter-clockwise directions from this point as shown in Fig.3-11. The region of interest is manually specified to terminate the tracing.

Consequently, the procedure for tracing the left ventricular boundary can be summarized as follows:

1) Specify the region of interest.
2) Determine the first estimated boundary point.
3) Determine the direction to which the edge detector should be applied.
4) Apply edge detector from the estimated point in the direction determined in the step 3), and decide the edge point.
5) Locate the next estimated boundary point.
6) If the estimated point is out of the region of interest terminate the procedure. Otherwise go to 3).

Sample experimental results are presented in Fig.3-12. The digitization of the image was done in a 1024 x 1024 grid resolution, but the image was displayed in a 128 x 128 array of pixels in this figure. The boundary curve obtained by connecting the successively detected boundary points is drawn over the image displayed.

3.4 Conclusions

In this chapter two methods to determine the left ventricular boundary from RI-angiocardiogram by using the on-line FSS system were described. Although the system and methods are simple, one can obtain fairly satisfactory results, considering that the object images are quite noisy and ambiguous. However, some problems are left unsolved and the methods may not be readily applied to actual clinical sites.

The boundary of the area where the left ventricle and the left atrium are overlapping could not be determined satisfactorily by either methods. It is difficult to locate exact boundary even by human eyes in

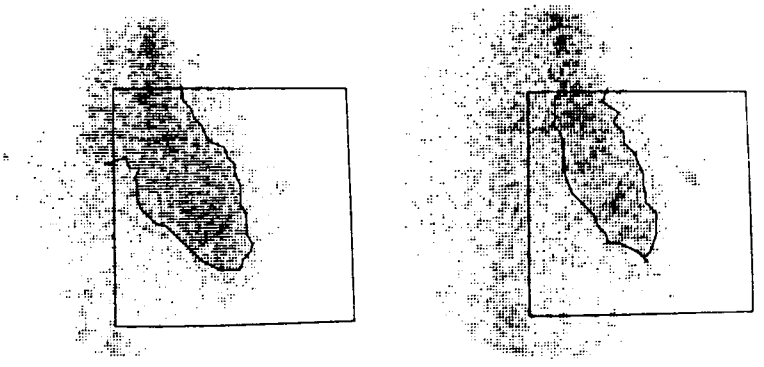

(a) End-diastole (b) End-systole

Fig. 3-12 Results obtained by the nonlinear tracing method

this area, if we are allowed only to utilize the local gray level information. Hence, some methods employing the knowledge about the global shape of the left ventricle will be desired. The tracing method will be always in danger of straying. So it will be desirable to control the tracing process by the plan which is made from the knowledge and information of the left ventricular shape obtained beforehand.

Chapter 4 Image Enhancement by the Nonlinear Filtering Technique

4.1 Introduction

Although the quality of RI-images have been considerably improved by the progress of RI-imaging techniques, these images are still quite noisy and ambiguous compared with usual medical X-ray images. This is mainly due to the inherent statistical characteristics of radionuclide disintegration and the limited resolution characteristics of RI-imaging devices. Recently, as discussed earlier, RI-imaging techniques have come to be applied to dynamic studies like angiocardiography. In this condition, images obtained are usually low-count and contain much noise and blur. This inferior image quality has prevented us to successfully employ automated approach of image processing.

In this chapter, we will discuss the method to improve the image quality or to transform the raw indistinct images into distinct images, images from which some features can be extracted. This aspect of image processing is usually referred to as image enhancement or recovery.

Many types of filters have been devised and used for the enhancement of RI-images. One of them is a class of linear filters, whose output value of a pixel in observation is determined by weighted sum (linear combination) of gray level values of several pixels in a neighbour of the pixel in observation. Its application to the RI-image processing had been studied by many researchers. However, this linear filtering cannot fulfill our requirements to enhance RI-images of low-count, like RI-angiocardiograms, which are considered to contain excessive amount of noise as well as blur, because the noise reduction and the sharpening of the blurred image are essentially contradictory in this linear filtering approach.

On the other hand, there is a class of nonlinear filters whose outputs cannot be expressed in terms of linear combinations of gray level values of neighbouring pixels. Nonlinear filters may be classified into three categories, which are (1) filters based on some non-

linear statistics, (2) homomorphic filters and (3) adaptive filters. One of the filters involved in the first category is the median filter [4-1]. Homomorphic filters are introduced by Oppenheim et al. [4-2], and similar techniques are given by Moore et al. [4-3]. The last category comprises many varieties. Newman et al. [4-4] examined the smoothing filter which used gradient information to maintain sharp edges. Pizer et al. [1-9] introduced nonlinear techniques called variable spatial averaging and dot shifting into the medical RI-image processing. Tomita et al. proposed the filter which can be used to extract the textured region by investigating the properties of the local area surrounding the pixel in observation [4-5].

In this chapter, a nonlinear filter is proposed which will be used to enhance medical RI-images, especially low-count ones. This filter belongs to the third catergory of the above classification. Although this filter is based on rather simple idea and calculation, it has a powerful function both to remove the quantum noise and to sharpen the blurred boundaries of the objects.

4.2 RI-imaging process and enhancement of RI-images

Detecting a radioactive ray at a certain point of the image plane, the number of count at this point is incremented by one. This may be a conceptual interpretation of the RI-imaging process. In order to clarify the inherent nature of RI-images and the reason why the linear filtering technique does not suffice, let us investigate the process by which RI-images are formed.

Establishing the coordinate axes of the space containing the object and the image plane as shown in Fig.4-1, we will lead the formula of RI-image formation. Let $m(x,y,z,t)$ be the distribution of radioactive disintegration in the object at time t, and $p(x,y,z)$ be the probability of detecting, at the point (x,y,z), radioactive ray originated from the origin of the space. Then the number of counts in the time interval $[t,\ t+T]$ at the point (x,y,z), $n(x,y,z,t)$ can be expressed as;

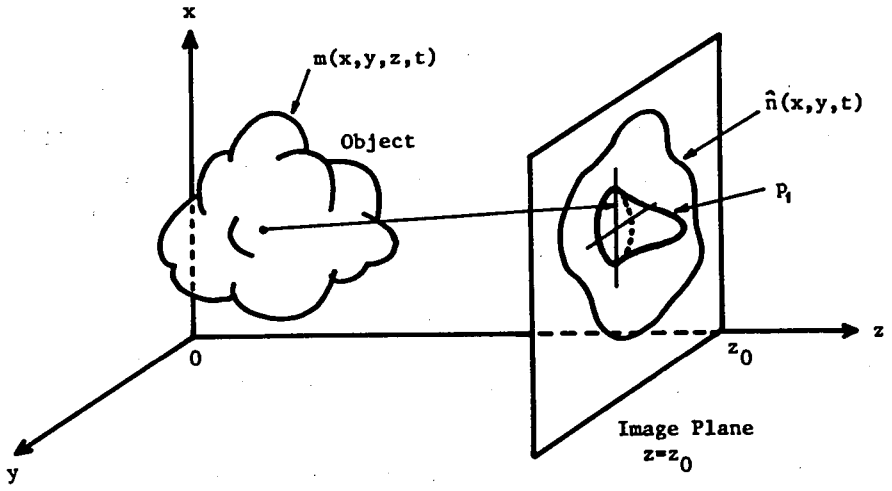

Fig. 4-1 Object and image plane of RI-imaging process

$$n(x,y,z,t) = \int_{t}^{t+T} \iiint_{-\infty}^{\infty} m(\xi,\eta,\zeta,\tau)p(x-\xi,y-\eta,z-\zeta)d\xi d\eta d\zeta d\tau \qquad (4\text{-}1)$$

As we are concerned to the two-dimensional RI-image observed at the image plane, say $z = z_0$, we can obtain the count distribution on the image plane substituting $z = z_0$ in eq. (4-1) as;

$$\hat{n}(x,y,t) = n(x,y,z_0,t)$$

$$= \int_{t}^{t+T} \iiint_{-\infty}^{\infty} m(\xi,\eta,\zeta,\tau)p(x-\xi,y-\eta,z_0-\zeta)d\xi d\eta d\zeta d\tau \qquad (4\text{-}2)$$

This equation is a fundamental formula describing the RI-imaging process.

Assuming that the probability distribution $p(x,y,z)$ is separable as $p(x,y,z) = p_1(x,y)p_2(z)$, we can modify the equation (4-2) as;

$$\hat{n}(x,y,t) = \int_{t}^{t+T} \iiint_{-\infty}^{\infty} m(\xi,\eta,\zeta,\tau)p_1(x-\xi,y-\eta)p_2(z_0-\zeta)d\xi d\eta d\zeta d\tau$$

$$= \iint_{-\infty}^{\infty} \left\{ \int_{-\infty}^{\infty} \int_{t}^{t+T} m(\xi,\eta,\zeta,\tau)p_2(z_0-\zeta)d\tau d\zeta \right\} p_1(x-\xi,y-\eta)d\xi d\eta$$

$$= \iint_{-\infty}^{\infty} \tilde{m}(\xi,\eta)p_1(x-\xi,y-\eta)d\xi d\eta \qquad (4\text{-}3)$$

where

$$\tilde{m}(\xi,\eta) = \int_{-\infty}^{\infty} \int_{t}^{t+T} m(\xi,\eta,\zeta,\tau)p_2(z_0-\zeta)d\tau d\zeta \qquad (4\text{-}4)$$

We can regard $\tilde{m}(\xi,\eta)$ as the original two dimensional image describing the raw object projected onto the plane $z = z_0$ in the observation time interval $[t, t+T]$, and p_1 as the degradation by the imaging process.

Number of occurences of radioisotope disintegration $m(x,y,z,t)$ is known to be the random variable obeying the Poisson distribution and this is considered to be a source of the noise of the RI-image. If the object is stationary, we are able to reduce noise by prolonging the

interval T of temporal integration in eq. (4-4). However, in the case where the object is always moving, it is not permitted to integrate the counts over so long time interval. Consequently we have to use spatial averaging, but this in turn induces spatial blur.

On the other hand, the probability distribution $p(x,y,z)$ is characterized by the scattering of radioactive rays, and is prescribed mainly by the characteristics of the collimator used. This scattering process is considered to be the source of spatial blur in RI-image. The right hand side of equation (4-3) looks like the convolution formula used to express the image degradation process in a linear (deterministic) system. It seems to be easily deconvolved and the original image expressing the raw object seems to be recovered. This will be a ground for using the linear filtering technique to recover the quality of RI-images, regarding the scattering characteristics as the point spread function of the system [1-12]. However, it must be noted that the image is degraded (blurred) rather statistically than deterministically; $p(x,y,z)$ is a theoretical probability distribution function, and $\hat{n}(x,y,t)$, therefore, a theoretical distribution of counts. These theoretical distributions are usually quite different from empirical distributions, namely, the actual count distributions of the image. When the number of total counts is large enough, the empirical distribution becomes to a good approximation to the theoretical distribution. However, if the number of total counts is not so large, the shape of the empirical distribution is quite different from that of the theoretical distribution. Consequently, the deconvolution based on the above consideration cannot give satisfactory results but rather emphasizes the noise component of the image. Thus, except the case where the number of counts is large enough, it is not desirable to apply the linear deconvolution technique to the statistically blurred image.

As described above, for the restoration of low-count RI-images, linear filtering technique will not work satisfactory and some powerful nonlinear adaptive filtering techniques have to be investigated.

4.3 V-filtering

In this section a new type of nonlinear filter named V-filter is introduced.

4.3.1 Sample variance as a measure for edge existence

As mentioned in the previous section, it is inevitable that noise reduction or smoothing operation on an image employing spatial average may blur the image. However, if one can smooth the image without blurring edges in the image, the contrast of the image is increased, and consequently the image is apparently deblurred. Practically, we can do this by detecting the existence of edges by some appropriate means and by smoothing so as not to average over dominant edges. Adequate smoothing is applied within the area where no edge is inferred to be present.

What type of measure should we use for detecting the presence of edge? Newman et al. used gradient information. However, in a quite noisy or highly textured image, the simple gradient information will not reflect the presence of edge any more. We will show that the sample variance value of image gray level values within a certain local area serves a simple but good index for edge existence.

Now let us consider an image made from two neighbouring regions with different gray level distributions. One region, say region A, is assumed to have a gray level distribution $f_A(x)$ with mean μ_A and variance σ_A^2, and the other region, B to have $f_B(x)$ with μ_B and σ_B^2. We will, next, consider a local area in the image. If this local area is occupied by the regions A and B with ratios p_A and p_B respectively (where $0 \le p_A, p_B \le 1$ and $p_A + p_B = 1$) as in Fig.4-2a, the mixed gray level distribution in this local area will be

$$f(x) = p_A f_A(x) + p_B f_B(x) \tag{4-5}$$

Mean and variance of $f(x)$ are

$$\mu = \int x f(x) dx = p_A \mu_A + p_B \mu_B \tag{4-6}$$

$$\sigma^2 = \int x^2 f(x) dx = p_A \sigma_A^2 + p_B \sigma_B^2 + p_A p_B (\mu_A - \mu_B)^2 \tag{4-7}$$

Assuming $\mu_A \neq \mu_B$ and substituting the relation $p_A + p_B = 1$ into eq. (4-7), we get

$$\sigma^2 = -(\mu_A-\mu_B)^2 \left[p_A - \frac{1}{2} \left\{ 1 + \frac{\sigma_A^2-\sigma_B^2}{(\mu_A-\mu_B)^2} \right\} \right]^2 + \frac{1}{4} (\mu_A-\mu_B)^2 \left\{ 1 + \frac{\sigma_A^2-\sigma_B^2}{(\mu_A-\mu_B)^2} \right\} + \sigma_B^2 \qquad (4\text{-}8)$$

This equation shows how the variance value varies according to the change of p_A. That is, the variance σ^2 varies quadratically as shown in Fig. 4-2b according to the change of p_A from zero to unity, namely the change of relative positional relationship between the region boundary and the local area.

A necessary and sufficient condition to have the extremum of σ^2 within the interval [0,1] of p_A is

$$(\mu_A-\mu_B)^2 > | \sigma_A^2 - \sigma_B^2 | \qquad (4\text{-}9)$$

Namely, if the condition (4-9) holds, the sample variance in a local area shows the largest value when this local area lies on the boundary (edge) of the two regions. Presence of edge can be suggested from this. We call this sample variance in a small local area a local variance, and we make use of the value of local variance as an index for presence of edge.

Now, let us breifly examine a physical interpretation of measuring the local variance. First of all, a signal to noise ratio of an edge is defined. Since we can regard the difference of mean gray level values between either sides of an edge as a signal component of the edge and a sum of standard deviations of either side of the edge as a noise component, we can define a SN ratio of the edge as

$$S/N \equiv | \mu_A - \mu_B | / (\sigma_A + \sigma_B) \qquad (4\text{-}10)$$

Generally, since $\sigma_A > 0$ and $\sigma_B > 0$, the following inequality holds.

$$(\sigma_A - \sigma_B)^2 > | \sigma_A^2 - \sigma_B^2 | \qquad (4\text{-}11)$$

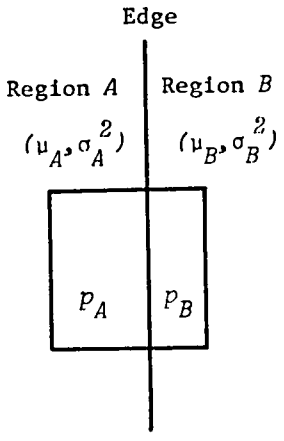

(a) Region boundary and local mask

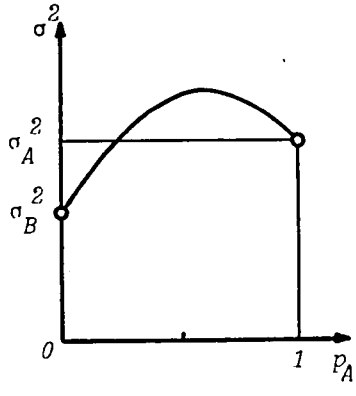

(b) Relationship between fraction of regions and local variance

Fig. 4-2 Local variance as a measure of edge existance

Therefore, if the SN ratio of the edge is greater than unity, namely, if

$$| \mu_A - \mu_B | > \sigma_A + \sigma_B \tag{4-12}$$

holds, then it leads by using eqs. (4-11) and (4-12) to

$$(\mu_A - \mu_B)^2 > (\sigma_A + \sigma_B)^2 > | \sigma_A^2 - \sigma_B^2 |$$

Thus we have obtained the condition (4-9) for local variance to exhibit the maximum on the edge. Consequently, we may conclude that the presence of the edge can be detected by the local variance if the edge possesses sufficiently high SN ratio.

4.3.2 V-Filter

In 4.3.1 we showed that the presence of edge was inferred by the local variance value of the image. We will build a filter which smooths noisy gray level distribution but does not blur edges of the object image.

As illustrated in Fig.4-3, around a pixel (i,j) in consideration we take four k x k rectangular neighbours R_l (l = 1,..,4) and construct filters of the type whose output values at the pixel (i,j) is determined according to the mean gray levels μ_l and the sample variances σ_l^2 within each R_l. Letting $\{a_{ij}\}$ and $\{b_{ij}\}$ be input and output images, respectively, we can formulate the input-output relationship of this type of filters as

$$b_{ij} = \frac{\sum_{l=1}^{4} \mu_l w_l}{\sum_{l=1}^{4} w_l} \tag{4-13}$$

Where w_l is a weighting factor determined from the variance value σ_l^2 in neighbour R_l. Mean μ_l and variance σ_l^2 are determined by

$$\mu_l = \frac{1}{k^2} \sum_{(i',j') \in R_l} a_{i'j'} \tag{4-14}$$

and

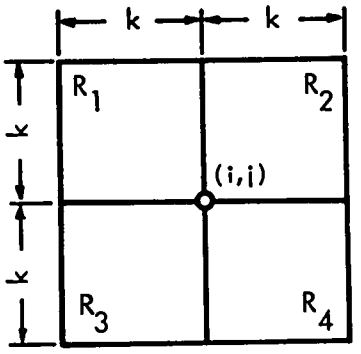

Fig. 4-3 Filter mask of the V-filter

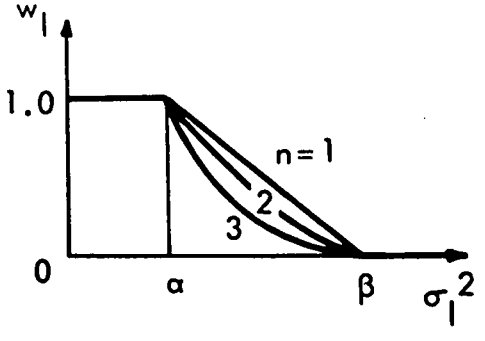

Fig. 4-4 Weighting in V-filter type II

$$\sigma_l^2 = \frac{1}{k^2} \sum_{(i',j') \in R_l} (a_{i'j'} - \mu_l)^2 \qquad (4\text{-}15)$$

Filter of this type does not have the property of linearity, so it may be termed nonlinear filter. We will name this type of nonlinear filter *V-filter*, since its operation is dependent on the variance of the local area.

As for the weighting in eq. (4-13), two ways are proposed. One of them is

$$w_l = \begin{cases} 1 \ ; \ \sigma_l^2 \leq \sigma_m^2 \ , \text{ for all } m \neq l \\ 0 \ ; \ \text{otherwise} \end{cases} \qquad (4\text{-}16)$$

This weighting forms the filter whose output is the mean gray level value of the neighbour with the minimum local variance. This is based on the concept that among the four neighbours there is at least one neighbour which is entirely covered by one region of the image rather than laid across the boundary. From this, we pick out, for every pixel, one neighbour by the criteria of minimum variance and take the average gray level within this neighbour as the output value at this pixel. Hence, we can avoid to take average over the region boundaries and to blur boundaries. This type of V-filter will be referred to as a type I, hereafter.

The other way of weighting is

$$w_l = \begin{cases} 1 & ; \ \sigma_l^2 \leq \alpha \\ (\sigma_l^2 - \beta)^n / (\alpha - \beta)^n & ; \ \alpha < \sigma_l^2 < \beta \\ 0 & ; \ \sigma_l^2 \geq \beta \end{cases} \qquad (4\text{-}17)$$

where n is a positive integer. The change of weight w_l versus σ_l^2 is depicted in Fig.4-4. This type of V-filter will be called a type II. Constants α and β which determine the break point of the curve of weighting is decided by investigating the histogram of local variance values over the whole object image. Namely, for example, the value of variance which gives the left-most peak of the histogram is taken for α, and,

say, 95 percentile of the distribution of the variance values for β. On the other hand, since for increasing the order n, the acuity of the edge increases, n is determined according to the acuity desired. However, n is usually fixed to three and this gives good results.

Idea of this filter is to take average over as wide area as possible, as long as no edge is contained in the neighbours. This processing can be interpreted as a variable sized smoothing which varies the effective size of averaging neighbour according to the local property of the object image, in this case according to the SN ratio of the edges.

In type I, since neighbours are selected according to the minimum variance criterion, switching of the neighbours takes place definetely when the filter mask traverses the region boundary of the image, and consequently quite sharp edges can be obtained by this filtering. However, since even slight difference in variance may cause the switching of neighbours, the spike-like noise is liable to be generated around the boundary. This may be the by-product of the edge sharpening function of the filter. Furthermore, while this filter of type I measures the gray level distribution over all four neighbours, mean gray level value in only one neighbour contributes to the output of the filter. Therefore, it may be said that this type of filtering operation involves redundancy.

On the other hand, in type II, by taking weighted average of mean gray level values in all for neighbours, accute switching of the neighbours is prevented, and spike-like noise is less liable to be produced. Thus, this type of V-filter compensates the shortcomings of V-filter type I. However, its edge sharpening ability is inferior to that of type I.

4.4 Experiments of the V-filter

4.4.1 Simulation experiment

In order to evaluate the nonlinear filters proposed in the previous section, a simulation experiment using an artificially made test pattern was carried out. Fig.4-5 a shows the artifitial pattern (128 x 128)

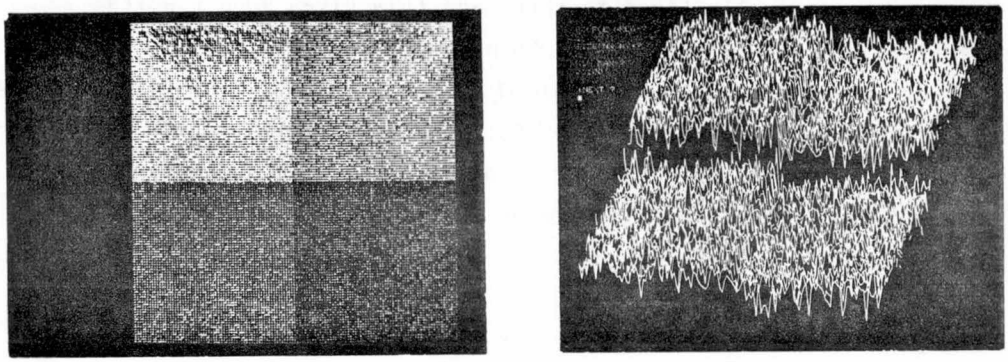

(a) (b)

Fig. 4-5 Normally distributed artifitial pattern

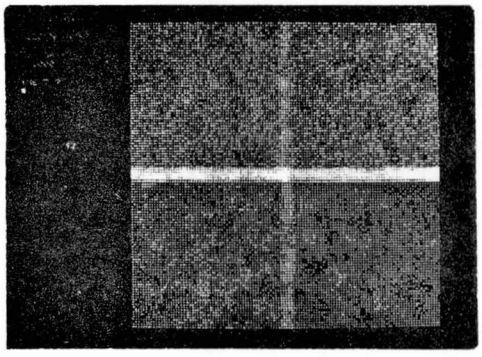

Fig. 4-6 Map of local variance obtained from the image of Fig. 4-5

which consists of four regions each having normally distributed gray level distribution with different mean gray levels and an identical standard deviation. Mean gray levels are, from top-left to bottom-right, 100, 80, 60 and 40, respectively, and the standard deviation is set to 10 in all regions. Figure 4-5b is a pseudo three-dimensional representation of Fig.4-5a. Figure 4-6 shows a map of local variance derived from the image of Fig.4-5 using a 7 x 7 mask. In this figure, it can be seen that the variance value exhibits higher value around the region boundaries.

Figures 4-7 and 4-8 are the results of applying V-filters type I and type II, respectively, to the image of Fig.4-5. In Fig.4-9, also the results of the usual simple moving average are presented for comparison purpose. In these figures several results are presented varing the size of the filters. In this occasion, the size of the V-filter is defined by the size k x k of the square neighbours R_l (see Fig.4-3), and the size of the simple moving average is defined by the size of the rectangular mask for averaging.

The difference in the ability of smoothing and edge sharpening can be clearly observed. In the results of simple moving average the edges are much blurred. On the other hand, in the results of V-filtering, quite sharp edges are obtained, while adequate smoothing being done within the regions. However, spike-like noise is a little conspicious in the results of V-filter, especially that of type I.

4.4.2 Application of V-filter to RI-angiocardiograms

Now, we will apply these V-filters to the actual RI-images, namely, RI-angiocardiograms. As mentioned earlier, in these images the number of radioactive counts which contribute to the image formation is considerably less than in usual static RI-images. The image is formed by the sparse cluster of dots and is very ambiguous. Adequate smoothing is required to smooth out this dot structure of the image, namely, the noise of the image. However, excessive smoothing will cause blur in region boundaries, which is undesirable since the boundaries in these image are originally indistinct. The V-filter is suitable for the

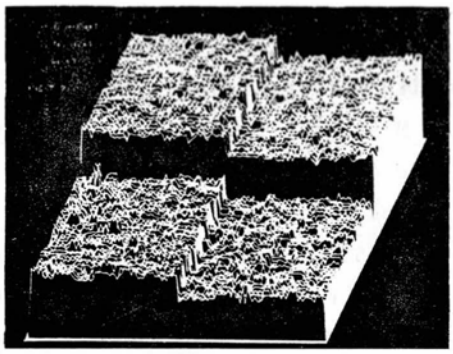

(a) 3 x 3

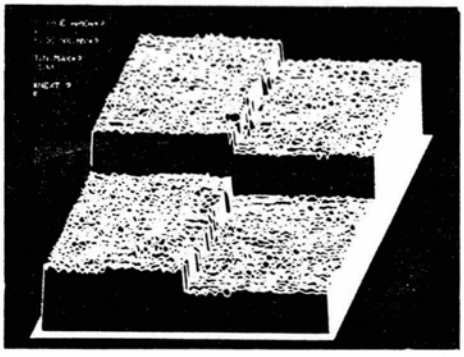

(b) 5 x 5

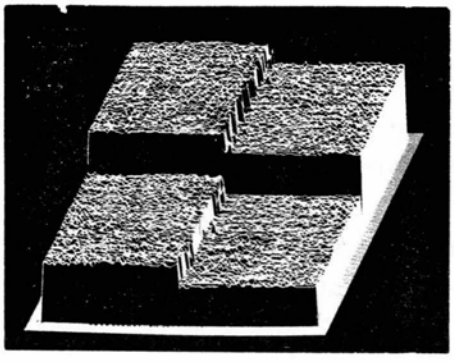

(c) 7 x 7

Fig. 4-7 Results of V-filter type I

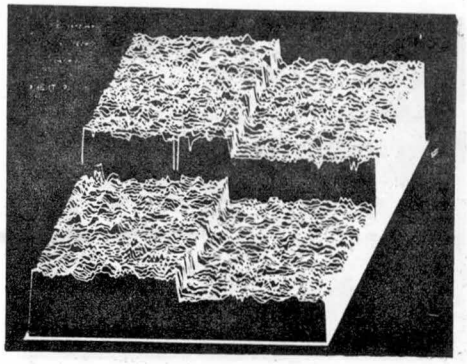

(a) 3 x 3

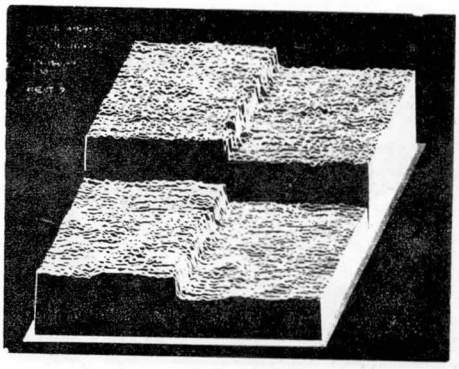

(b) 5 x 5

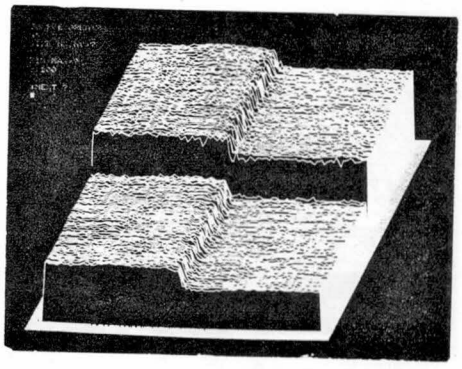

(c) 7 x 7

Fig. 4-8 Results of V-filter type II

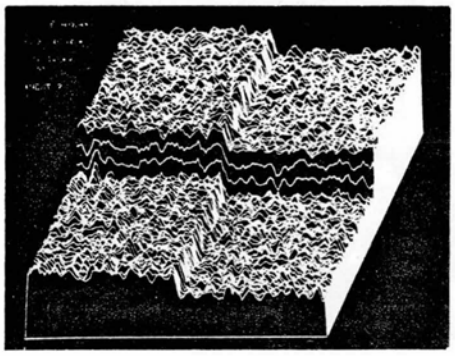

(a) 3 x 3

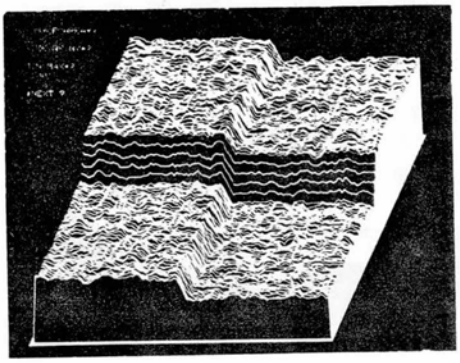

(b) 5 x 5

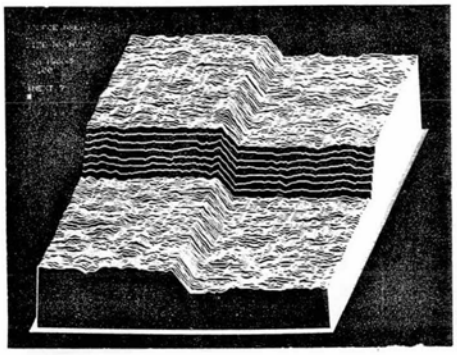

(c) 7 x 7

Fig. 4-9 Results of simple moving average

recovery of these images.

Figure 4-10 shows one of the RI-angiocardiograms obtained photographically, and digitized by the flying-spot-scanner in 128 x 128 pixel array of 256 gray levels†. Results of V-filtering are presented in Figs. 4-11 and 4-12, and result of simple moving average is also presented in Fig.4-13. The size of the filters used are all 7 x 7. All of these figures are accompanied with their gray level histograms (Fig.4-10c to 4-13c).

V-filtering results give better impression than the result of the simple moving average. Namely, in Fig.4-13, the degree of noise reduction is not so adequate considering the induced blur at the region boundary, and that the dot structure of the original image still remains. On the other hand, in the V-filtering results, the dot structure no more remains and each region in the image has become to possess almost constant gray level of its own, and edges at the boundaries of the regions show sharp step-like transition. Consequently, each image region can be distinguished much easier than in the original image.

Next, the resutls of the V-filtering and simple moving average are compared on the basis of the gray level histogram. The original image may be, roughly speaking, devided into two parts; a region of background and a region of object. The leftmost peak or mode of the histogram in Fig.4-10c corresponds to the gray level distribution of the region of background. However, the mode corresponding to the object region is quite broad due to the dot structure of the image, and, hence, these two modes are not so distinctly separated in this histogram.

By applying the averaging operation to this image, we can smooth the dot structured, rugged gray level distribution in the object region. Consequently, modes in the histogram will become apparent as in Figs. 4-11c to 4-13c. However, in the histogram of the simple moving averaged image, the valley between conspicious peaks are not so distinct as in the histogram of the V-filtered images. This is based on the fact that the simple moving average operation takes an average over the region boundary and produce a distribution of a mixture of two distributions,

†) Display of the image is done in 10 gray levels due to the restriction of the hardware used.

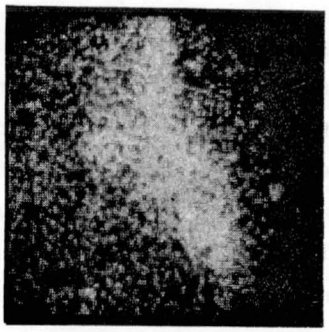

(a)

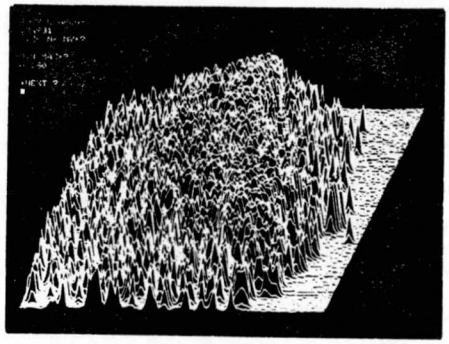

(b)

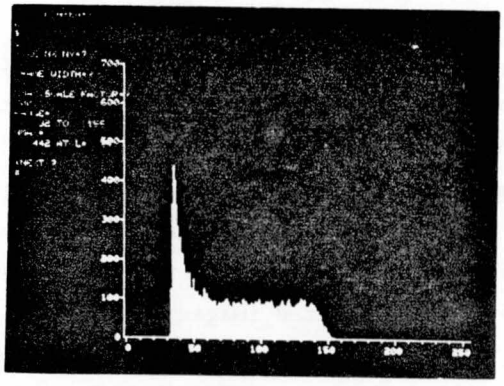

(c)

Fig. 4-10 Original RI-angiocardiogram

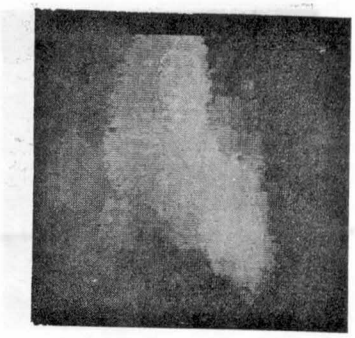

(a)

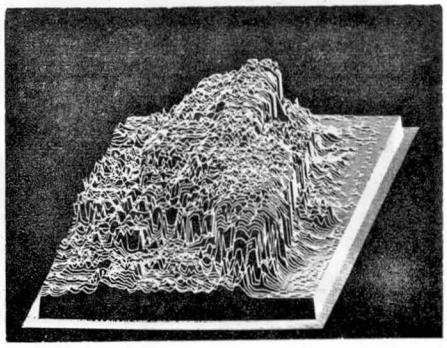

(b)

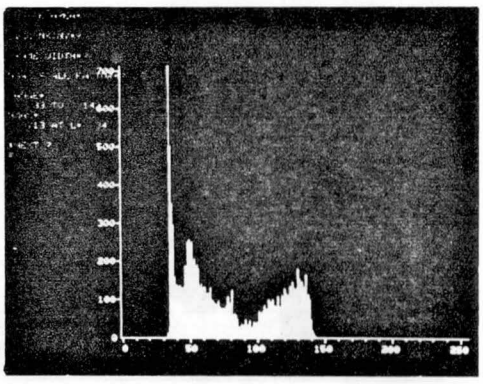

(c)

Fig. 4-11 V-filter result (type I)

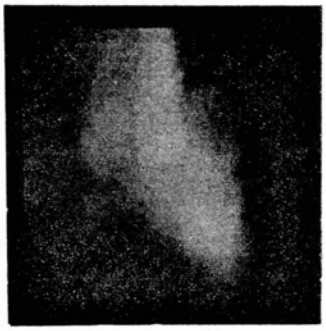

(a)

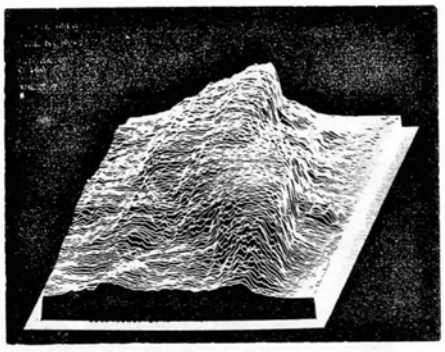

(b)

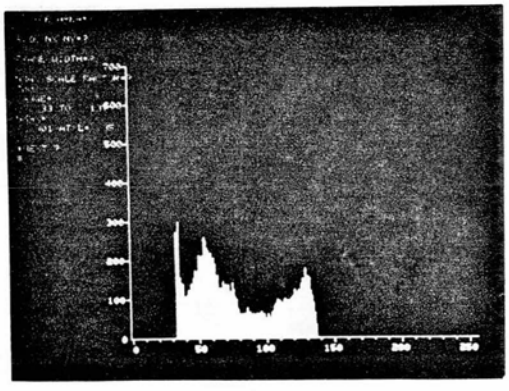

(c)

Fig. 4-12 V-filter result (type II)

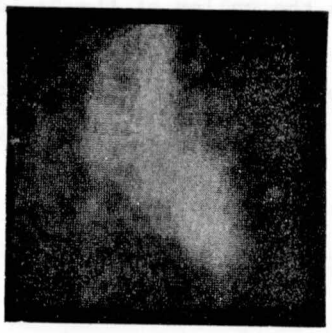

(a)

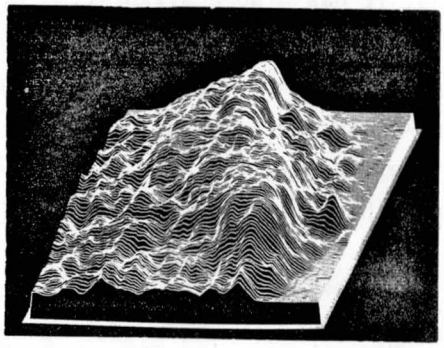

(b)

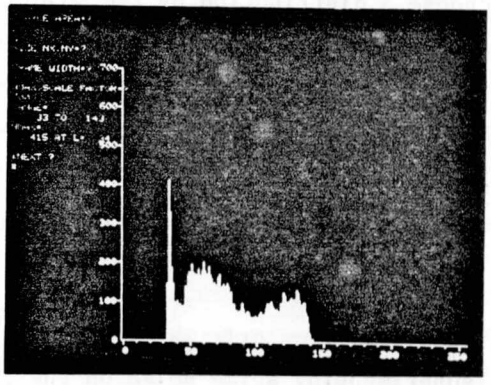

(c)

Fig. 4-13 Simple moving average result

and this mixture fills the valley of the histogram. On the contrary, the V-filter does not average over the region boundary and smooths the gray level distribution within each region, so it does not produce a mixtured distribution and a valley becomes apparent.

In Fig.4-14, another experimental result is shown. An original image in this case is an RI-angiocardiogram obtained by the method described in section 2.3.

4.5 Median filtering

Although the V-filter has a powerful function in noise reduction and edge sharpening, it has also a slight tendency to produce spike-like noise. The noise of this kind cannot be successfully removed by linear filtering techniques. A median filtering technique is hopeful for the removal of this spike-like noise [4-1].

The median filter is a filter that outputs a median of the gray level distribution within a local area, i.e. filter mask, which is laid around the pixel in consideration. Since the median is one of the statistics to represent the "center" of distribution, this filter has a function of smoothing. However, the median is an order statistic and is more affected by the frequency of occurrence than by the magnitude itself, then the effect of spike-like noise will hardly appear in the output of this median filter. Furthermore, since the median filter works as if it choose a distribution by the majority rule even when its filter mask is sited on the region boundaries, it will not produce the blurred image as the simple moving average filter does.

Thus, the median filter is a nonlinear smoothing filter which eliminates spike-like noise effectively, while retaining edge or boundary definition. It will be quite suitable for post processing of the V-filtered image.

Figure 4-15 demonstrates the function of the median filter above described. Figure 4-15a is an original test image and Fig.4-15b is an image formed by superimposing spike noise on the original image. The result of applying the median filter to Fig.4-15b is shown in Fig.4-15c.

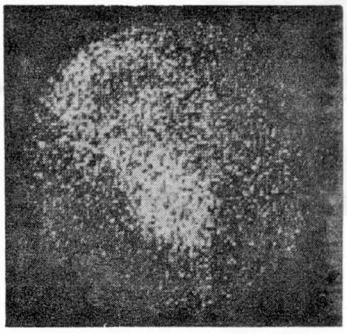

(a) Original

(b) V-filter type I

(c) V-filter type II

(d) Simple moving average

Fig. 4-14 Filtering results of digital RI-angiocardiogram

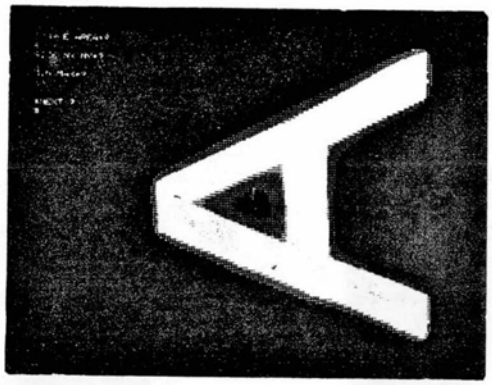

(a) Original

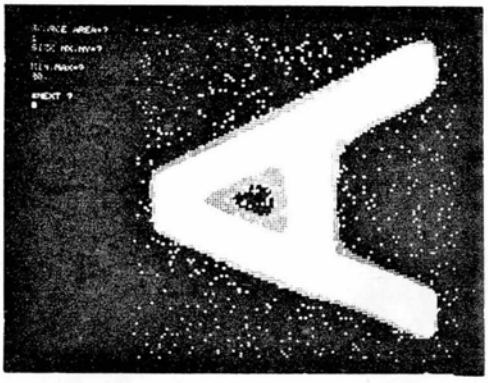

(b) Original + noise

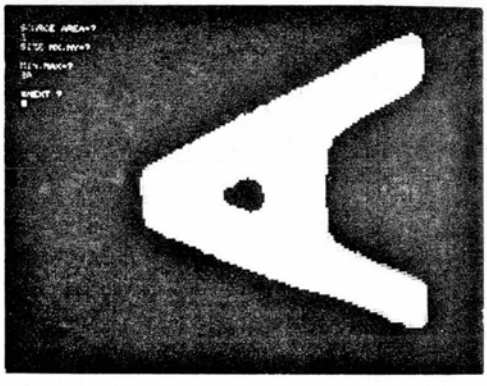

(c) Restored

Fig. 4-15 Median filtering for eliminating spike-noise

The filter mask used is a 5 x 5 square mask centered on the pixel in observation. Spike noise is eliminated almost completely while less blurring the original gray level distribution.

In Figs.4-16 and 4-17 are the results of applying the median filter to Fig.4-7c and 4-8c which are V-filtered images of artificially made test pattern. A 5 x 5 square filter mask was used for median filter. The notched ripples and spike-like noise are eliminated and quite desirable results are obtained.

Figures 4-18 and 4-19 present the results of median filtering applied to the V-filtered RI-angiocardiograms (Figs.4-11 and 4-12). In these figures spike-like noise is also eliminated. The dot structure of the original image no more remains and each image region has come to possess almost constant gray level value. The edges at the boundaries of the regions show sharp step-like transition. Consequently, each image region can be distinguished much clearly compared with the original image.

Thus, the combination of the V-filter and the median filter gives quite desirable results as the preprocessing or enhancement of the RI-angiocardiograms. The combined use of the median filter and the V-filter type I is rather preferable than that of the median filter and the V-filter type II. This is because the V-filter type II has an adequate smoothing power in itself and the application of the median filter gives us an impression of over smoothing.

4.6 Conclusions

A nonlinear digital filter (V-filter) was proposed, which was devised to enhance or recover the low-count RI-images for the further automated image processing. The assessment of the filter was made by a simulation experiment and by appling the filter to actual RI angiocardiographic images. Although the V-filter is based on rather simple idea which requires a simple calculations, it is proved that the filter has powerful function for smoothing and deblurring of low-count RI-images. Furthermore, it was shown that we could obtain much more desirable images by applying the median filter to the results of V-filter.

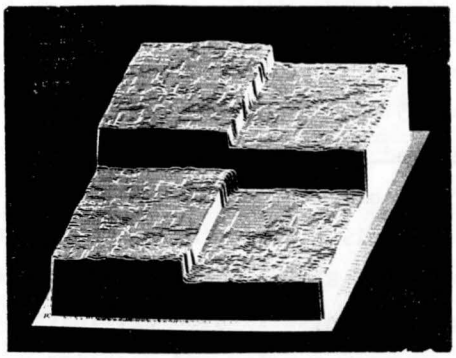

Fig. 4-16 Results of applying median filter to Fig. 4-7c

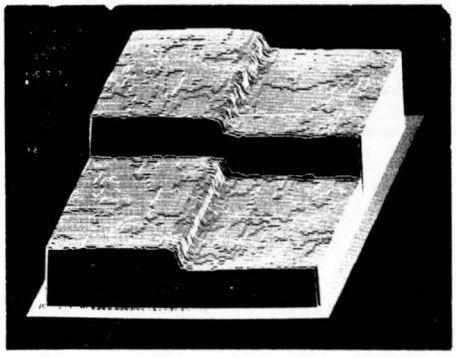

Fig. 4-17 Results of applying median filter to Fig. 4-8c

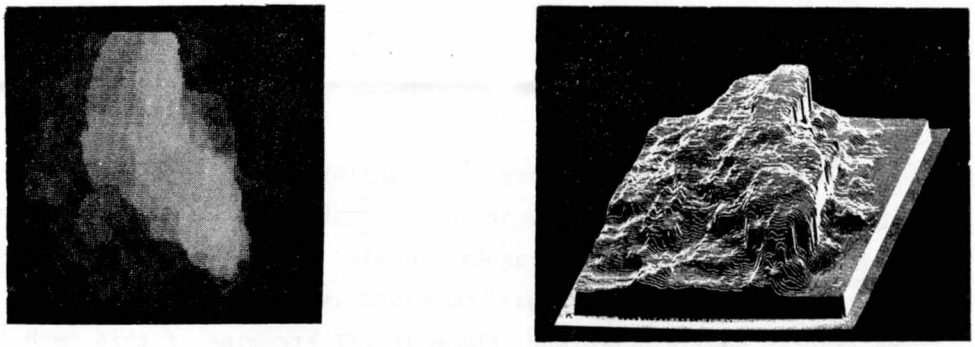

(a) (b)

Fig. 4-18 Results of applying median filter to Fig. 4-11

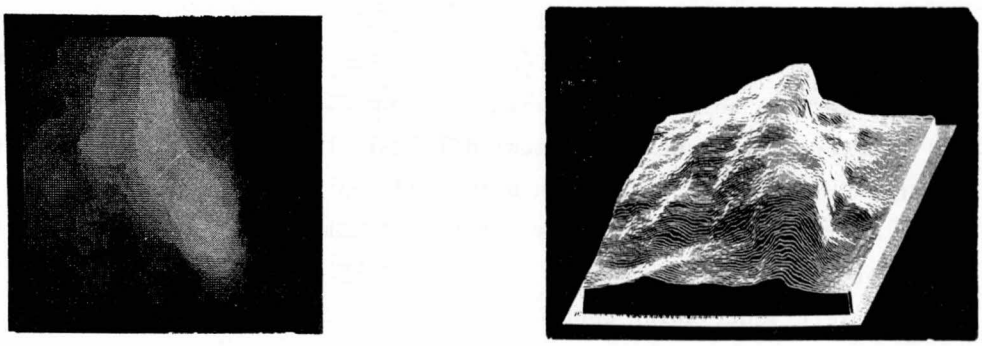

(a) (b)

Fig. 4-19 Results of applying median filter to Fig. 4-12

Chapter 5 Left Ventricular Contour Extraction and Volume Computation from RAO RI-Angiocardiograms

5.1 Introduction

One of the prime interests in cardiovascular research is to measure the function of the left ventricular chamber of the heart, in a non-invasive and quantitative manner. While, as previously stated, RI-angiocardiography is generally non-invasive to human body and can be relatively easily performed, the major shortcoming of this technique is that the obtained image is usually very noisy and ambiguous. This has been the obstacle for the quantitative measurements on this image, even if the measurements are made manually by the well-trained physicians. When the processing of the images are done by a computer, certain degree of objectiveness would be added to the measurement, but it may be difficult to fully automatize the processing due to the noisy gray level distribution of a raw image.

The most important quantity to represent the cardiac functions is the volume of left ventricle, especially the time course of the volume. The information about the function of the left ventricle, including the volume, can be derived largely from the figure of its contour or outline. However, it is one of the most difficult tasks to locate the contour of the object region in such a noisy and poorly defined RI image.

This chapter describes the method which will overcome the difficulty presented above. It is a consistent processing system to extract the left ventricular contour (LV-contour) and to compute the left ventricular volume (LV-volume) from the RI-angiocardiogram of RAO view. It is based upon the successive processing concept rather than the direct processing scheme described in Chapter 3.

5.2 Outline of the processing

Sample images which sholud be processed are the RAO view RI-angiocardiograms described in section 2.2. A flow chart of the whole processing is shown in Fig.5-1. Sample images obtained photographically are digitized by the FSS and stored in the disk storage of the computer system. Preceding to the LV-contour extraction, an image enhancement processing is performed as the preprocessing for recovering the image quality. Then, LV-contour is extracted from this enhanced image by using spatial derivative (differentiation) operation as well as thresholding. Some feature points are determined on the contour extracted and the original image plane in order to compute the LV-volume. Finally, the LV-volume is computed by making the assumption on the three dimensional shape of the left ventricular chamber.

By repeating this sequence of processing for the images at different cardiac phases, we can obtain the change of LV-volume. Usually, volumes at phases of end-diastole (ED) and end-systole (ES) are used to roughly evaluate the function of the left ventricle.

Processing softwares are implemented on the minicomputer system and are installed into the interactive software system "PIPS". The hardware configuration of the minicomputer system and the software system are described in Appendix B. Each processing step will be explained in order.

5.3 Preprocessing

An original ECG-gated RI-angiocardiogram obtained photographically by means of the scintillation camera is digitized by the flying-spot-scanner into a 128 x 128 pixel array. Figure 5-2a shows an example of digitized RI-angiocardiogram of right anterior oblique (RAO) view, and in Fig.5-2b an illustration of the corresponding anatomical regions and their boundaries are presented. Abbreviations used in this figure and in this chapter are listed in Table 5-1. We use this terminology only for the convenience of explanation. Hence, there may be included some

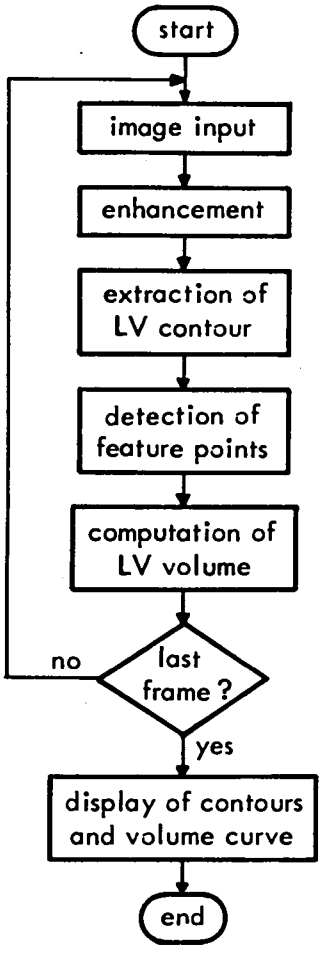

Fig. 5-1 Flow chart of the processing

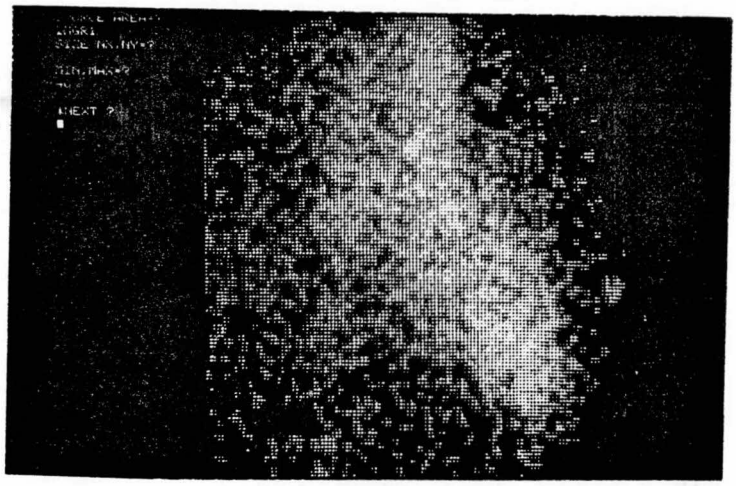

(a) Digitized image

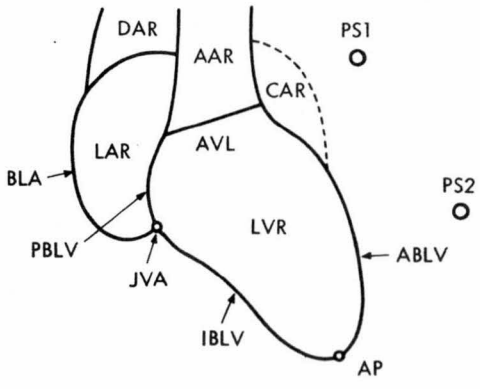

(b) Corresponding anatomical regions and boundaries

Fig. 5-2 RI-angiocardiogram of RAO view

Table 5-1 Abbreviations used for RI-angiocardiograms

LVR	Left ventricular (LV) region
LAR	Left atrial (LA) region
AAR	Ascending aortic region
DAR	Descending aortic region
ABLV	Anterior boundary of LV
IBLV	Inferior boundary of LV
PBLV	Posterior boundary of LV
BLA	Boundary of LA
AVL	Aortic valve line
AP	Apical point
JVA	Junction of ventricular and atrial boundary
CAR	Coronary arterial region
PS1	Point source marker No.1
PS2	Point source marker No.2

non-formal medical terms.

In this original image, objects are depicted by clusters of scattered dots and object regions are poorly defined and hardly recognizable. It is difficult to locate exact region boundaries on this raw image. It is desired to apply certain smoothing or recovering operations. In case of using the simple local averaging, the size of the averaging neighbourhood should be made large enough since the dot structure of the image is very prominent and, consequently, the region boundaries are inevitably blurred, which is usually objectionable for the boundary extraction.

We have already proposed the nonlinear adaptive filter, V-filters, for the enhancement of RI-images in Chapter 4. These filters were proved to possess the property that they smooth the noisy gray level distribution within the object region while retaining boundary or edge definition. Out of some types of V-filters we use V-filter type I. As stated in chapter 4, V-filter type I has the tendency to produce spike noise around the region boundaries and it is desirable to eliminate this noise by the median filter. Therefore, nonlinear filtering by the V-filter type I followed by the median filtering is used for the preprocessing. Figure 5-3 shows the resutls of this preprocessing applied to Fig.5-2a.

5.4 LV-contour extraction

To extract LV-contour from the preprocessed RI-angiocardiogram, we use two fundamental techniques commonly used, namely thresholding and derivative operation, according to a priori knowledge about the image. The anterior-inferior part of the LV-contour (ABLV and IBLV, c.f. Fig. 5-2) can be determined by thresholding without difficulty, owing to the abrupt change in gray level at the boundary caused by the preprocessing. However, the posterior part of the LV-contour (PBLV) will not be successfully determined by thresholding because the gray level difference between the left ventricular region (LVR) and the left atrial region (LAR) is usually very small. Then, considering that PBLV is an almost

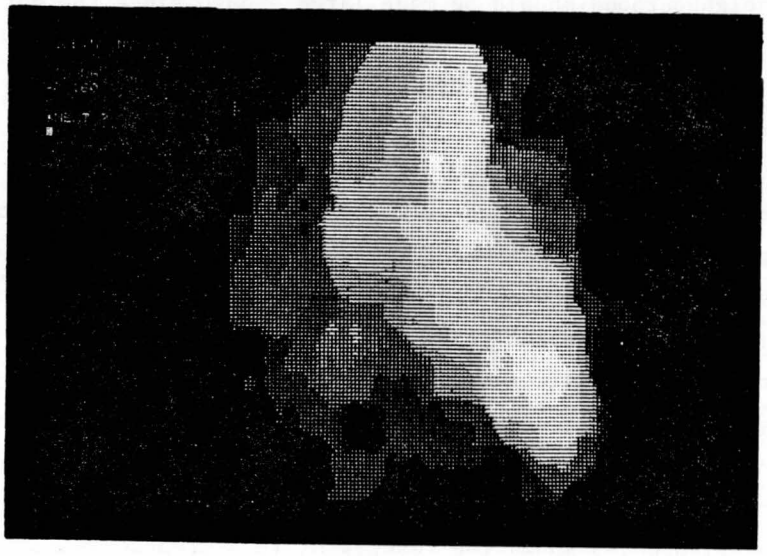

Fig. 5-3 Result of preprocessing

straight vertical line, PBLV is determined by making use of a differential vertical line detector. Thus, we determine the LV-contour dividing it into two parts, each of which is detected by different methods.

Consequently, the process of LV-contour extraction will be as shown in Fig.5-4. By thresholding the preprocessed image, a two-valued figure indicating the composite region of the left ventricular region (LVR) and the left atrial region (LAR) is obtained. This two-valued figure will be referred to as a VA-mask hereafter. A complex of ABLV and IBLV will be extracted from the contour of this VA-mask, and PBLV is determined from the preprocessed image by the differentiation as described above. Prior to the boundary detection, the rough position of the aortic boundary is located and it is used to determine the boundaries. In the following, each processing step will be described in order.

5.4.1 Extraction of the VA-mask

Figure 5-5 shows an example of the gray level histogram of the preprocessed sample image. In this histogram, an apparent valley can be observed almost at the middle of the gray level range. This is caused by the smoothing and edge enhancement effect of the nonlinear filter used in the preprocessing. If we threshold at a level located at the bottom of this valley for the purpose of extracting the VA-mask from background, the region of coronary artery (CAR), whose gray level value is slightly lower than the left ventricular region, may also be extracted connected to the desired ventricle-atrium region. An optimum threshold to successfully extract the VA-mask is hardly determined from the shape of the histogram alone. Considering the fact that the fraction of the area of the CAR to the area of the picture points above the level at the bottom of the valley is about 10%, we threshold the image so that just the 90% of the pixels above the bottom of the valley may be above the threshold level.

Since the gray level histogram of the preprocessed image is locally rugged, it is not so easy to locate reliably the bottom of the valley in a global sense. The histogram may be approximated by the mixture of two Gaussian distributions; The mixture function is fitted to the actual histogram curve in the sense of least squares, and the position of the

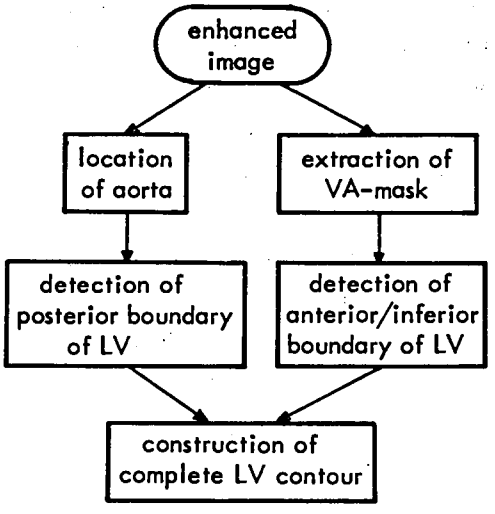

Fig. 5-4 Process of LV-contour extraction

valley bottom can be derived from the mixture function. In performing this procedure, direct optimization method may be used to minimize the sum of squares of errors. Although, by this method, we can approximate the histogram in a theoretically explicit form, this does not always give satisfactory results, since the actual component distributions are not necessarily normal. Moreover, it is quite time consuming, because the calculation of exponential function is involved in the optimization process and also the optimization must be done in five dimensional parameter space.

Let us consider a more simple way to decide the bottom of valley of the histogram. The histogram is approximated by a fourth-order polynomial curve. This can be done easily by the usual method of least squares. The bottom of the valley in a global sense is decided at the local minimum of this polynomial curve within the range of the histogram. An example of this approximation is shown in Fig.5-6.

The threshold level is, then, determined making use of this valley bottom level of the histogram by the method mentioned earlier. The resulting two-valued figure, i.e., the VA-mask is shown in Fig.5-7.

5.4.2 Location of the aorta

Rough position of the aorta can be determined from the averaged horizontal gray level profile, which is obtained within the horizontal strip window overlaid at approximately one third of the image height from the top of the image, in which the aortic region is considered to be present. Considering that, in this profile, the position of the maximum value corresponds to the point in the region of the aorta, positions where profile values are lower than the maximum by an appropriate constant are decided as the positions of the left and the right aortic boundaries. An example of the averaged horizontal profile and the positions of determined aortic boundaries are shown in Fig.5-8.

5.4.3 Extraction of the ABLV and IBLV

The contour of the VA-mask can be easily traced by the usual contour tracing method for two-valued figures [5-1]. ABLV and IBLV are extracted from this contour by locating, on this contour, the point (JVA)

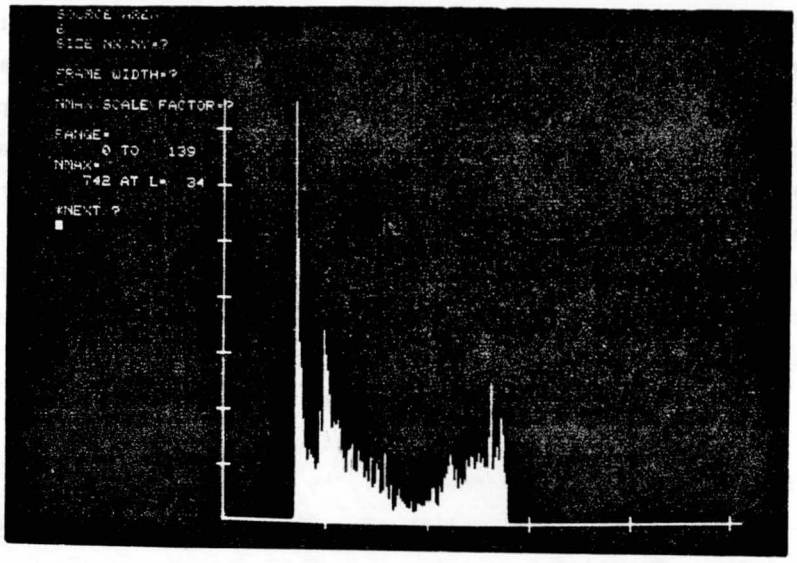

Fig. 5-5 Gray level histogram of the preprocessed image

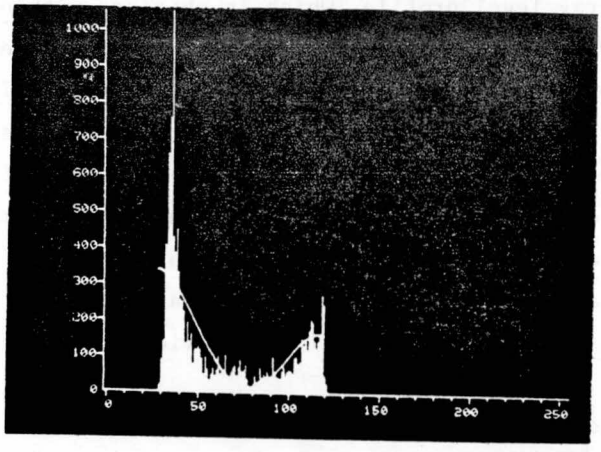

Fig. 5-6 Polynomial apploximation of the histogram

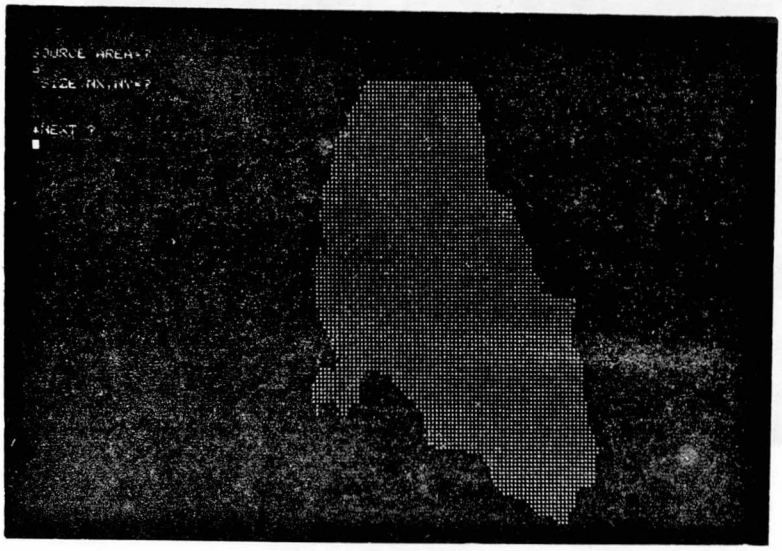

Fig. 5-7 Two-valued figure resulted by thresholding

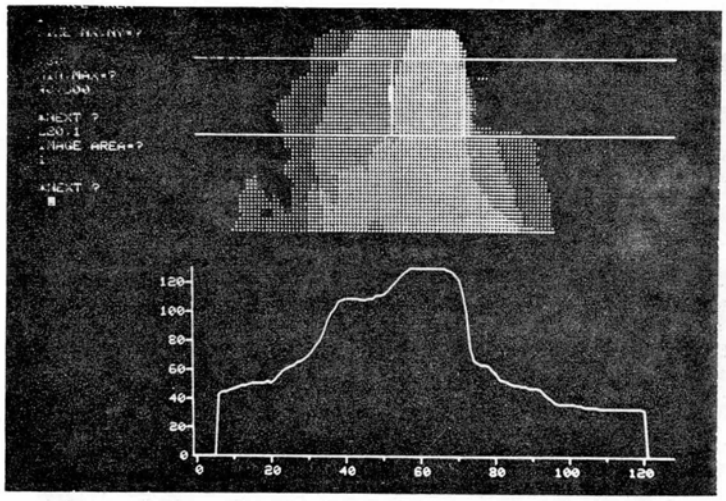

Fig. 5-8 Determination of the aortic boundary

which divides the whole contour into two parts, namely, the part of the left ventricle and that of the left atrium. As is seen in Fig.5-2b, JVA is located beyond the apical point (AP) as the contour is tracked clockwise, and at the neighbour of JVA the contour exhibits the concavity. Besides, AP is located at the head of the most marked prominence of the contour. Considering these properties, these points can be located on the basis of the curvature information of the contour.

The curvature at each point P_i on the contour is estimated, as in Fig.5-9, by the angle θ of the line segment connecting the points P_i and P_{i+k} with respect to the line segment connecting P_{i-k} and P_i. This measure is so called the k-curvature of the contour [5-2]. The sign of the curvature is decided so that a right turn may correspond to a positive θ while a left turn to a negative θ.

This curvature measure is rather a local measure and is liable to be affected by small variations of the contour. Therefore it may be undesirable to decide AP and JVA, which are rather global features, by this curvature measure alone. We should define some appropriate measures for a conspiciousness of the corner (which is either convex or concave) in order to detect corners in a relatively global sense. When we plot the curvature value versus the arc length along the contour from the starting point of the tracing, we can devide this plot into several (positive or negative) lobes according to the zero crossings of the plot. As shown in Fig.5-10, each lobe corresponds to the (convex or concave) corner of the contour, and an integral of the curvature within each lobe is equal to the total angular variation ϕ_i of the corresponding i-th corner. The "cornarity" of the corner is defined, reflecting the angular variation as well as the extent of the corner, as

$$c_i = l_i \phi_i \tag{5-1}$$

where l_i is the arc length of the corner. Positive c_i's correspond to convex corners and negative c_i's to concave ones.

The apex AP is located at the point corresponding to the peak of the lobe possessing the maximum positive c_i. Next, for all negative lobes which lie beyond this AP in the curvature plot, corresponding concave corners are examined according to their directions and positions.

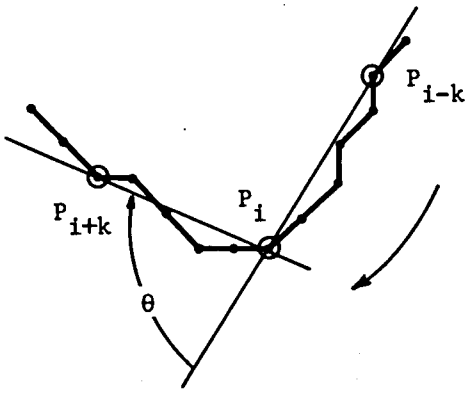

Fig. 5-9 Curvature of the contour

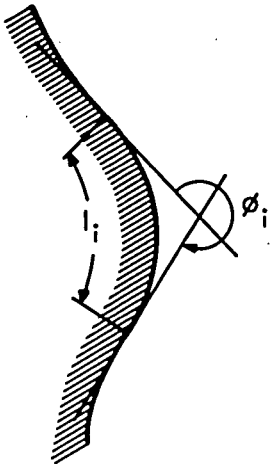

(a) Corner of the contour

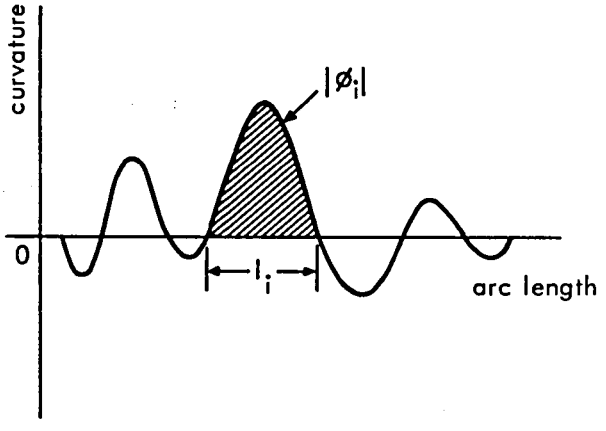

(b) Lobe in curvature plot

Fig. 5-10 Lobe in curvature plot and corresponding corner of the contour

The direction criterion is whether a corner is concave upward rather than horizontally, and the position criterion is whether a head of a corner lies within a certain horizontal distance from the left side boundary of the aorta and below the center of gravity of the VA-mask contour. JVA is located at the head of the corner having the minimum negative c_i, of all the lobes satisfying the above criterions. If there are no such corners satisfying the criterions, the position criterion is relaxed and search continues.

Figure 5-11 shows a contour of the VA-mask and its curvature plot. On the contour, AP and JVA decided are indicated by the mark □ . The cross represents the position of the center of gravity of the contour, and parallel vertical lines appeared in the upper side indicate the position of the aorta.

5.4.4 Extraction of the PBLV

We make use of a smoothed horizontal derivative (differentiation) to detect the edge point of the PBLV. The template for differentiation is shown in Fig.5-12. Since the gray level at the right side of the PBLV is higher than the left side, edge points can be detected by this template, at the peaks of the differential value above a predetermined positive threshold. In this occasion, some edge points are detected on each row and the concept of the raster tracking algorithm [5-2] is used so that edges can be extracted as connected and labelled line segments (edge elements).

Then, of all the edge elements extracted, possible elements to form the PBLV should be picked out. First of all, the edge element which corresponds to the aortic boundary is determined, since the edge of this part is usually well-defined and can be detected reliably. This is done by picking out the one possessing a length above an appropriate threshold and whose center is nearest to the rough position of the left side aortic boundary determined in section 5.4.2. If the selected edge element has adequate length to cross the contour of the VA-mask, this element itself becomes the PBLV, otherwise an appropriate element below this element is searched and connected. That is, as shown in Fig.5-13, a vertical rectangular window is laid downward from the lower end point

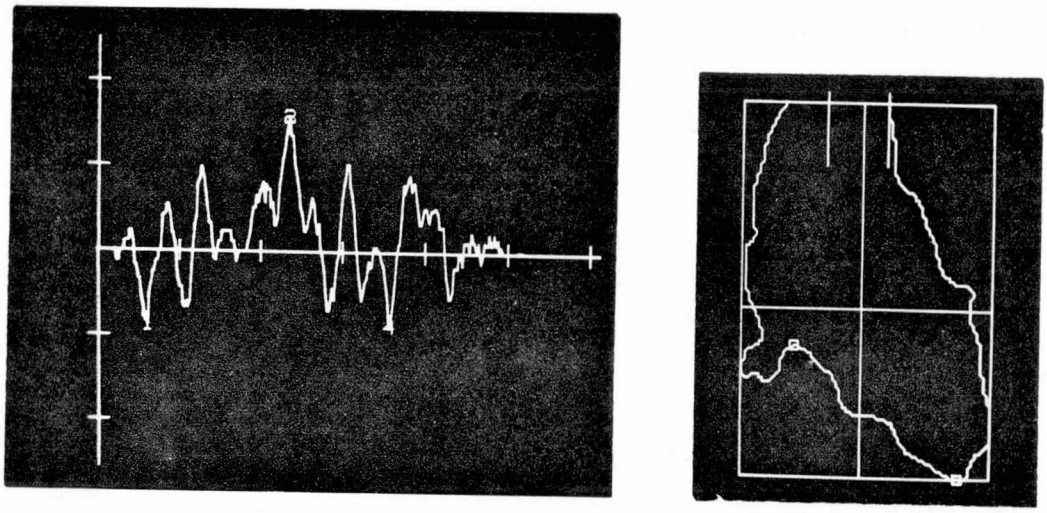

(a) (b)

Fig. 5-11 Curvature plot of VA-mask contour and AP and JVA decided

-1	-1	0	1	1
-1	-1	0	1	1
-1	-1	0	1	1
-1	-1	0	1	1
-1	-1	0	1	1

Fig. 5-12 Template for horizontal differentiation

of the element so far determined, and if the upper end point of the another edge element is present within this rectangle, these end points are connected by a straight line segment. This operation is iterated until the extended curve crosses the VA-mask contour or no segments can be found within the window. The resulting curve becomes the PBLV.

5.4.5 Construction of the complete LV-contour

In case where the obtained PBLV crosses the VA-mask contour, we can obtain the complete LV-contour by simply re-arranging the sequence of points. However, there may be some cases where significant edge elements cannot be found any more in the area where the left ventricle and the left atrium overlap each other. In this case, it is convenient to determine the boundary element by an interpolation method. This interpolating operation will be done by connecting the lower end point of PBLV and the end point of ABLV-IBLV complex, namely, JVA, by a third degree polynomial curve as shown in Fig.5-14. The explicit form of the polynomial can be given by specifying the coordinate values of the end-points (x_1,y_1) and (x_2,y_2), and the first derivatives at the end points $t_1 = dy/dx|_{x=x_1}$ and $t_2 = dy/dx|_{x=x_2}$. Namely,

$$y = p(x) = p_0 + p_1(x-x_1) + p_2(x-x_1)^2 + p_3(x-x_1)^3 \qquad (5\text{-}2)$$

where

$$p_0 = y_1$$

$$p_1 = t_1$$

$$p_2 = \frac{1}{x_2 - x_1}\left(3\,\frac{y_2 - y_1}{x_2 - x_1} - 2t_1 - t_2 \right)$$

$$p_3 = \frac{1}{(x_2 - x_1)^2}\left(t_1 + t_2 - 2\,\frac{y_2 - y_1}{x_2 - x_1} \right)$$

The values of derivatives at end points which will be used to determine the polynomial curve is estimated from the positions of end points and the positions of the several appropriate points which lie on the curve segments to be connected. This is done by the algorithm proposed by Akima [5-3].

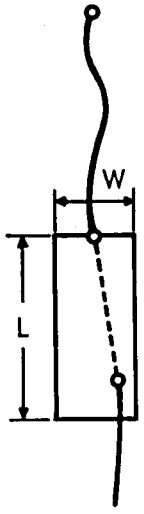

Fig. 5-13 Search and connection of edge elements

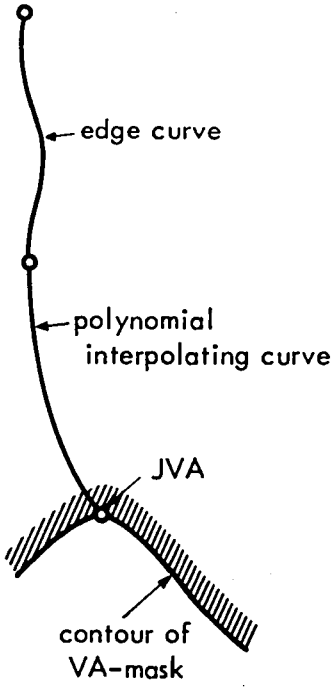

Fig. 5-14 Interpolation by third degree polynomial

5.4.6 Results

Examples of the result of the LV-contour extraction are shown in Fig.5-15. In this figure, the LV-contours determined are depicted by thick curves. Another solid thin curves represnt the part of the VA-mask contour. Line segments shown by dotted lines are edge elements detected by the horizontal differentiation and tracking. Numbers attached to the elements indicate their labels in modulo 10. In the case of Fig.5-15a the interpolation by the polynomial curve is not necessary, but this operation is required in another example.

5.5 Location of feature points

5.5.1 Location of the apex and the aortic valve line

When calculating the volume of the left ventricular chamber, we must make use of the information about the positions of the left ventricular apex and the aortic valve line. The position of the apex was already determined when we determined the position of JVA (cf. section 5.4.3). The aortic valve line (AVL) can be determined by locating the end points of AVL on the LV-contour, and connecting these end points by a straight line. Determination of end points is done by minimizing the cost function derived from a priori anatomical knowledge that the LV-contour compresses and narrows at the aortic valvular region and that the apex of the left ventricle locates nearly on the perpendicular bisector of the aortic valve line [5-4].

First, the curvature along the LV-contour is measured in the same manner described in section 5.4.3, and points corresponding to the position of the minimum in every negative lobes of this curvature plot are located on the LV-contour. These points serve as candidates for valve end points; points which lie on the right (left) half (with respect to the position of the apex) of the contour for the right (left) end point. For every pairs of left and right candidates, the cost function is evaluated and the pair which gives the minimum is decided to be the pair of the left and right valve end points. The cost function is formulated as

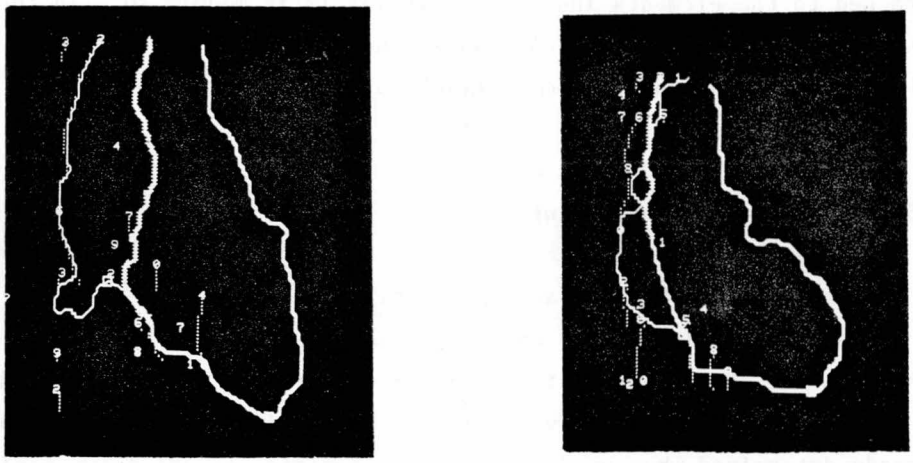

(a) (b)

Fig. 5-15 Results of LV-contour extraction

$$C = w_1 \mid d_1 - d_2 \mid + w_2 d_3 + w_3 a_1 + w_4 a_2 \qquad (5\text{-}3)$$

where d_1 and d_2 are distances from the apex to left and right candidates, respectively, d_3 is a distance between left and right candidates (Fig.5-16), a_1 and a_2 are values of curvature on left and right candidates, respectively, which are both negative, and w_i (i = 1,...,4) are positive weighting constants.

At the phases near end-systole, since the left ventricle contracts greatly, compression and narrowing of the LV-contour at the aortic valve are not so definite as on the end-diastolic contour, it becomes to be difficult to determine its location by the above cost function. However, since it is said that the location of the aortic valve does not shift too much during the contraction of the ventricle, the left and right end points of aortic valve on the contour at systolic phases may be determined as the nearest contour points to the left and right end points of the end-diastolic contour, respectively.

5.5.2 Location of the point source markers

Two point sources (PS1 and PS2) positioned at a known interval are imaged together with the object, so that they may serve as positional references for registration and so that we may get an actual scale of the object. Considering that these point sources are imaged as circular blobs with areas within a certain range, we can detect them by the following method: The original image is smoothed and then thresholded. The gray level at the valley bottom of the histogram of the preprocessed object image, which is determined in the section 5.4.1, is used as the threshold level. After labelling each connected component of the resulting two-valued image, area and perimeter of each component are measured, and each component is examined with respect to the area and the circularity index (area)/(perimeter)^2: Among the components having areas within the predetermined range, two with the largest and the second largest circularity index are picked out. The positions of the point source markers are decided at the centers of gravity of these components. Since these point source markers are included in the right half of the object image, the above processing is restricted to be

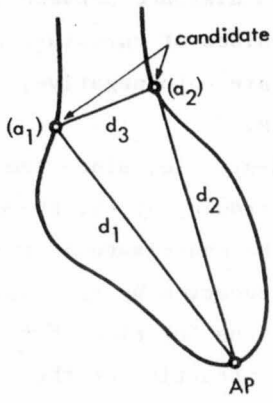

Fig. 5-16 Determination of the aortic valve line

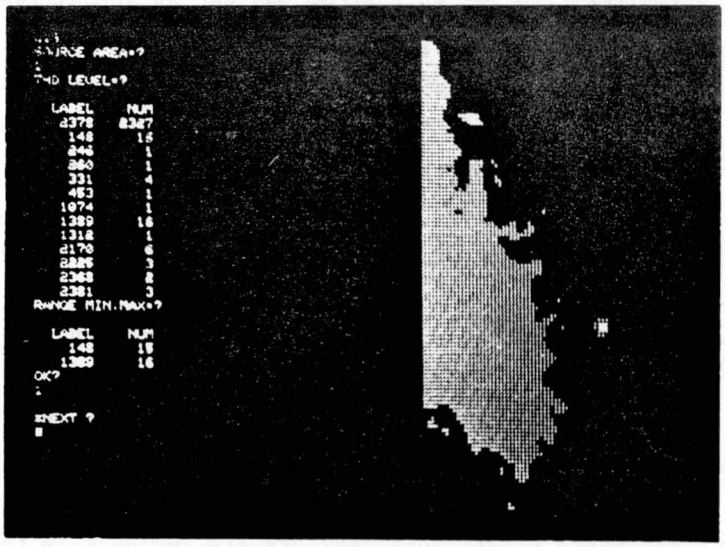

Fig. 5-17 Detection of point source markers

applied to this area. Figure 5-17 shows the result of the processing. Determined positions of the point source markers are plotted superimposed on the two-valued image obtained by thresholding.

5.6 Calculation of the LV-volume

With an appropriate assumption on a 3-dimensional configuration of the left ventricular chamber, we are able to calculate its volume from its two-dimensional projection. First, on the figure of the LV-contour, major axis of the left ventricle is determined by connecting the apex (AP) and the midpoint of the aortic valve line (AVL). Assuming that cross-sections perpendicular to the major axis are everywhere circular, we can derive sectional area from a diameter of each cross-section, which can be obtained from the LV-contour. The LV-volume can be calculated by numerically integrating the sectional area using Simpson's method.

Dividing the major axis of the left ventricle into $2N$ equal parts (where N is an integer), the sequence of diameters of cross-sections, d_i $(i = 0,\ldots,2N)$, are obtained as in Fig.5-18. Letting the spacing of division be h, the volume of the left ventricular chamber, V, is calculated by Simpson's method as

$$V = \frac{h}{3}\left[S_0 + S_{2N} + 2\sum_{k=1}^{N-1} S_{2k} + 4\sum_{k=1}^{N} S_{2k-1} \right]$$

$$= \frac{\pi h}{3}\left[\frac{1}{4}\left(d_0^{\,2} + d_{2N}^{\,2} \right) + \frac{1}{2}\sum_{k=1}^{N-1} d_{2k}^{\,2} + \sum_{k=1}^{N} d_{2k-1}^{\,2} \right] \qquad (5\text{-}4)$$

where S_i is sectional area of the i-th section, and $S_i = \pi(d_i/2)^2$ from the above assumption. The actual volume of the chamber can be derived from the relative volume represented in the unit of the image grid, using the conversion coefficient obtained from the interval of point source markers.

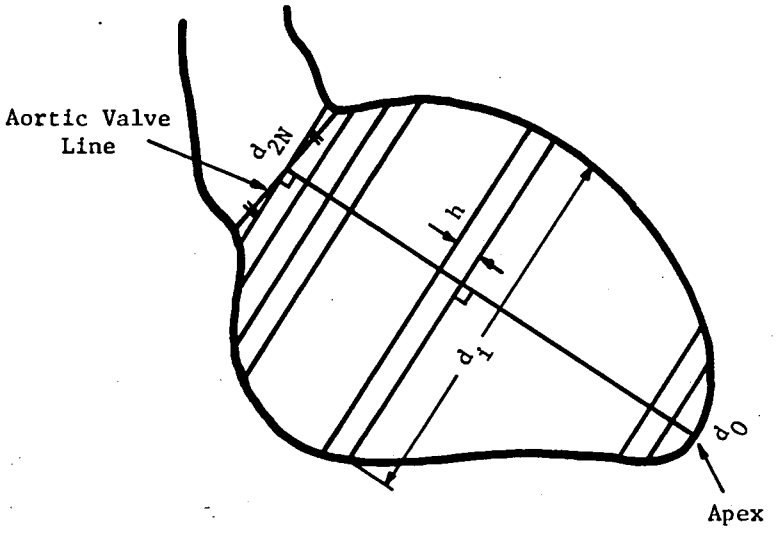

Fig. 5-18 Calculation of the left ventricular volume using Simpson's method

5.7 Results of the processing

Figure 5-19 shows the results of the left ventricular contour extraction and the feature points determination. The aortic valve line and the point source markers as well as the LV-contour are overlaid on the original image. Figure 5-19a corresponds to the phase of zero delay from the R-wave of the ECG-signal, namely the end-diastole, and Fig.5-19b to the phase of the end-systole.

Processing time required to obtain a result of each frame is 1.5 minutes for preprocessing (nonlinear filtering) and about 2 minutes for LV-contour extraction and feature points extraction. However, this includes time for inputting parameters and also for displaying intermediate results when the processing is implemented on the interactive image processing system described in Appendix B.

Contours extracted are chain coded [5-5] and stored in a disk file together with information about the positions of feature points and the volume computed. In Fig.5-20, the end-diastolic and the end-systolic LV-contours are superposed with respect to the position of point source markers. The form of contraction of the left ventricle can be observed. Since the actual distance between these two point sources is, in this case, 10 cm, a scale graduated in centimeters can be derived and displayed in the figure.

Figure 5-21 shows change of LV-volume versus time, which is obtained from nine images in one cardiac cycle obtained at an interval of 100 msec. The unit of the ordinate is in ml, and the leftmost position corresponds to the phase of the end-diastole. Decrease in volume by the contraction of the left ventricle can be observed.

Next, let us briefly examine the LV-volume determined by the method. Since the truths about the left ventricular contour and volume are unknown, examination based on the absolute evaluation criterion is at this time, by no means possible. Hence, the evaluation is made by comparing the volumes obtained automatically to the volumes derived from manually traced LV-contours.

Figures of LV-contours were depicted by tracing the contours on original RI-angiocardiograms by a cardiologist who was not shown results

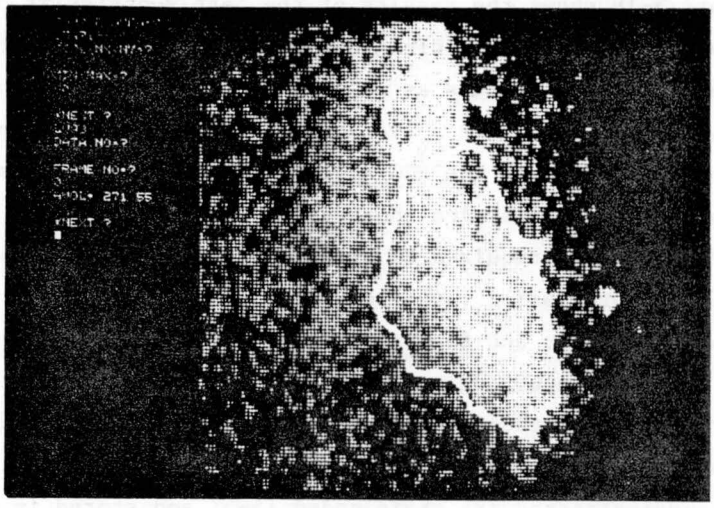

(a) End-diastole

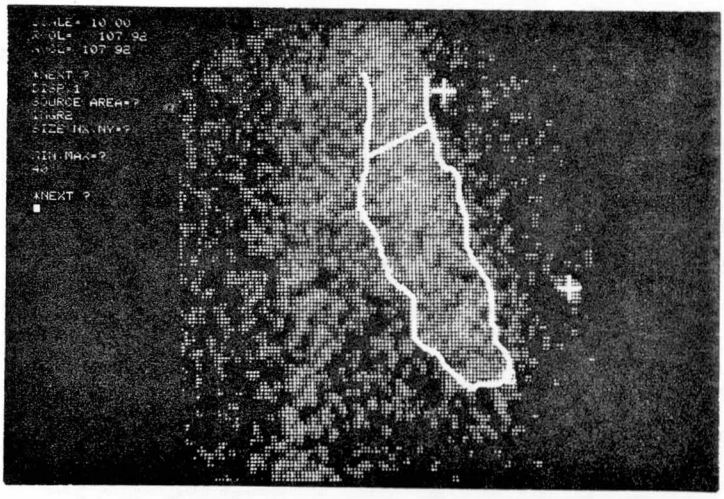

(b) End-systole

Fig. 5-19 Results of the processing

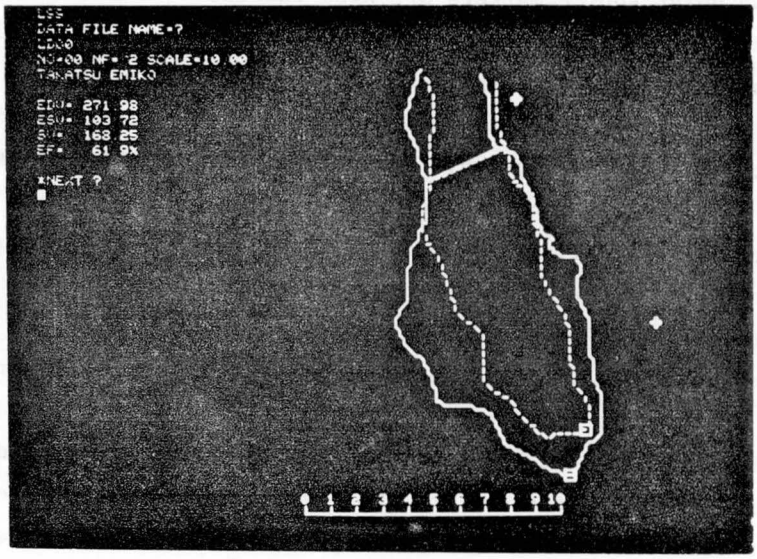

Fig. 5-20 Superposition of end-diastolic and end-systolic contours

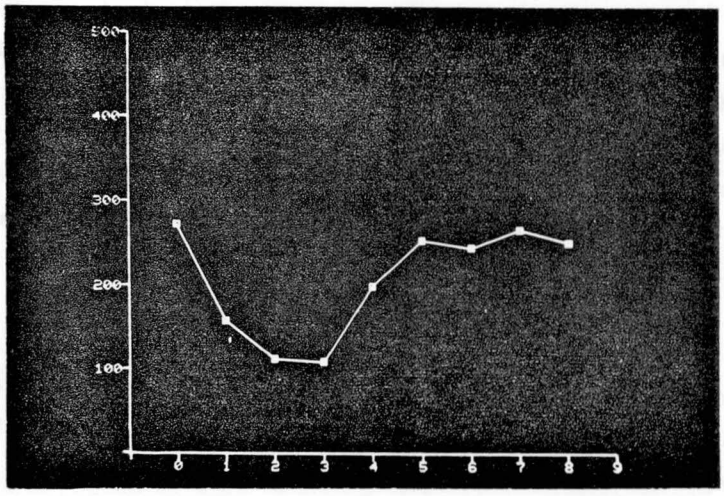

Fig. 5-21 Change of LV-volume v.s. time

of automatic processing. The positions of the aortic valve line, the apex and two point source markers are also indicated in the same figure of traced contour. These figures photographed on frames of a film were digitized by the flying spot scanner. After thresholding and thinning operations were performed on these digital images, the LV-contours were extracted by the curve following. Positions of feature points were given by a cross-hair cursor of the graphic display terminal and the volume of the left ventricle was calculated by using the same routine used for the contours automatically extracted. Thirty two cases of subjects were treated, each of which consisted of two images for end-diastole and end-systole. Thus, a total of sixty four images were processed. The result of this experiment is shown in Fig.5-22. As is shown in the figure, these two sets of values, volumes determined from automatically extracted contour and those from manually traced contour, do not correlate each other tightly enough. It may not always be said that the values derived from figures of manual trace reflect truth. However, we should admit a fact that the difference between these two values are fairly great. Several causes for the difference may be considered as follows.

First of all, in cases where the number of counts, i.e. dots, to form the image is fairly small the left ventricular contours extracted are apt to be smaller than the contours recognized by the human eyes. This is considered to be caused partially by the nature of the filter which was used for the preprocessing and the way of determining threshold value, and this may be improved, to a certain extent, by adjusting the parameters for these processings. However, this is rather a common trend and cannot completely be avoided. We should normalize the number of counts of the images to be processed or we should select and discard the images of which number of counts is excessively small.

Next, in contrast with this case of underestimation, there are cases of overestimation. This is due to the fact that there are cases where the coronary arterial region cannot be completely excluded by the thresholding operation. In these cases, generally, the aortic valve lines are mislocated so that the coronary arterial region is included in the left ventricular region, and consequently volumes are overestimated.

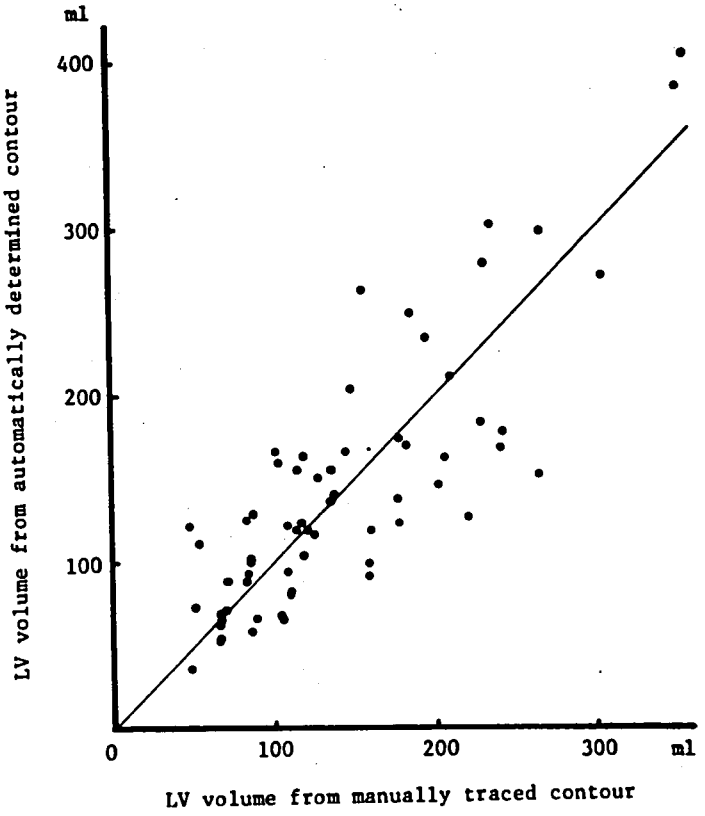

Fig. 5-22 Comparison of LV-volumes determined from manually derived contour with those determined from automatically derived contour

Finally, the error involved in determining the scale of the image from two point sources cannot be ignored. Because these point sources have spatial extent, their positions decided by automatic and manual methods may differ in several digital grid units.

Since, as previously stated, it cannot be said that the results obtained from manually traced contour are correct, it is difficult to strictly identify the sources of errors. It is desired to evaluate results by using also the results for the same subject obtained by other techniques such as a X-ray angiocardiography.

5.8 Conclusions

In this chapter, the method to delineate the left ventricular contour from RI-angiocardiogram and to determine the left ventricular volume by sequentially processing the original image was described. The interactive picture processing system was used. Since the original image has a dot structure and quite noisy, contour extraction form the original image by directly applying the usual derivative or thresholding operation may be impossible. In the method described in this chapter, we employed the preprocessing by nonlinear filtering techniques to recover the quality of the images and convert them to more smooth and definite images. Through this preprocessing we were able to extract reliable left ventricular contours by applying usual thresholding and derivative operation. Processing was conducted by arranging these operation and applying gap filling operation according to the information about the structure of the object image.

Feature points, namely the apex and the aortic valve end points, were located on the LV contour extracted according to the curvature information of the contour. Moreover, the positions of two point source markers inserted in the original image were determined. These feature points were used to calculate the left ventricular volume, and markers were used to obtain the actual scale and for registration purpose.

In order to evaluate the resutls obtained by the method described, LV volumes were compared to the volumes obtained from the manually

traced LV contours. Correlation between these two variables were not so distinct. This might be because errors are involved in each variable independently to each other. Future subject is to examine and improve the accuracy of the measurement by comparing them to the results of other methods of measurement.

Chapter 6 Classification of the Left Ventricular Wall Motion

6.1 Introduction

Important information derived from the ECG-gated RI-angiocardiography other than the volume of the left ventricle is the motion of the left ventricular wall. The abnormalities in the left ventricular wall motion indicates the defect of the heart muscle. In some ischemic heart diseases, which are caused by the partial lack of blood supply in heart muscle, the muscle of the heart is spoiled and dose not function well, and consequently, the left ventricular wall exhibits abnormal motions. The left ventricular wall motion will be represented by the change of the shape of the LV-contour, which is extracted from the ECG-gated RI-angiocardiogram by the method described in the previous chapter.

In this chapter, the function of the left ventricle is evaluated from the view point of the left ventricular wall motion. The wall motions will be classified into normal and abnormal classes.

Contours extracted form the images at end-diastole and end-systole are consolidated into a pattern indicating the LV wall motion and this pattern is represented by means of Fourier descriptors. A set of vectors, whose elements are composed of Fourier descriptors, is extracted from a set of samples including abnormal as well as normal samples. This set of vectors is subjected to the principal component analysis so that the dimensionality reduction may be realized. The classification by means of the minimun distance classifier is conducted and the set of samples are classified into two categories of normal and abnormal LV wall motions.

6.2 LV contraction pattern and its Fourier descriptors

The motion of the left ventricular wall can be evaluated by examining the change of shape of LV contour versus time. However, it may be

considered that the information concerning the left ventricular wall motion can be derived from the figure of superposition of LV-contours only at the phases of end-diastole and end-systole, such as in Fig.5-20. When the contraction of the left ventricle is normal, the every portion of the left ventricular wall moves toward the inside of the left ventricular chamber in nearly equal speed, and a spacing between two contours is almost uniform. However, in case of the myocardial infarction, this figure of superposition may exhibit narrowing between two contours or even touch of contours, as shown in Fig.6-1a, at the infarcted part, namely, the area of dying or dead muscle tissue. Occasionally, it may exhibit a paradoxical motion that the end-systolic contour projects, in part, out of the end-diastolic contour as in Fig.6-1b.

How can we extract features concerning the LV wall motion so that we may extract each of the samples objectively and may classify samples according to normal or abnormal motion? Generally there are two ways for doing this. One of them is an intuitive method to extract some appropriate geometrical features from the figure of superposition, such as area enclosed by two contours, distance between two corresponding points and so on. In this method, however, there is generally no answer to a question what features are adequate to classify the set of samples. By contrast, to represent a figure in a mathematical manner such as by polynomial approximation or orthogonal expansion of the contour is usually more general and is considered to convey almost all information contained in the original figure. The disadvantages of the latter are that the number of parameters used are liable to increase and that parameters which are closely correlated each other may be involved. However, since the method of the principal component analysis or Karhunen-Loeve expansion can be used for information compression and dimensionality reduction of the parameters extracted, the disadvantages described above may not be so serious. Hence we will employ the latter way, that is, the mathematical method.

First of all, we consolidate the end-diastolic and the end-systolic LV-contours into a closed curve pattern by connecting the corresponding aortic valve end points of each contour as indicated in Fig.6-2 and the ordered list of points is obtained by tracking along the direction

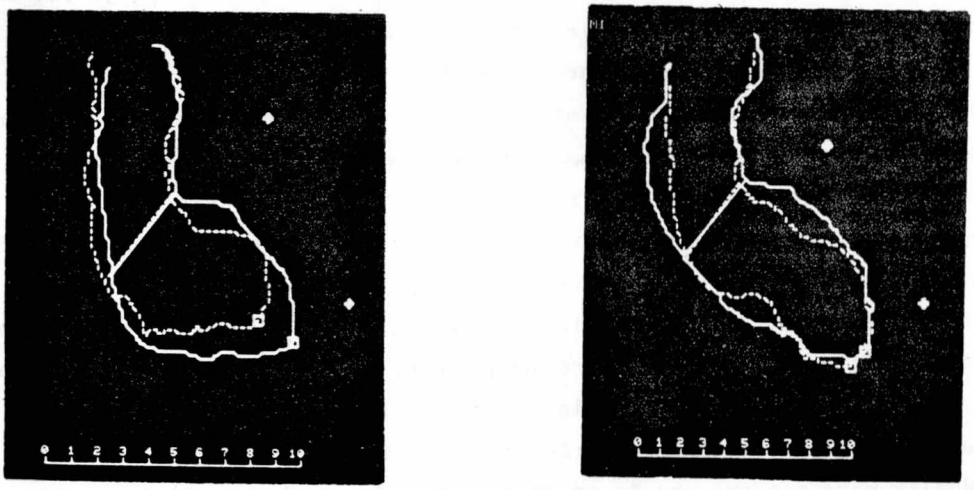

(a) (b)

Fig. 6-1 Superposition of end-diastolic and end-systolic contours (cases of myocardial infarction)

indicated by arrows. This pattern will be referred to as the LV contraction pattern hereafter. This pattern is then described in terms of the Fourier descriptors. There are several different ways for defining the Fourier descriptors of the closed curves [6-1, 6-2, 6-3]. Here we will introduce another definition described below, referencing the materials published by other authors.

As shown in Fig.6-3, the contraction pattern is assumed to be in the complex plane [6-1] and is represented by a mapping from the unit interval onto the set of complex numbers given by

$$z(t) = x(t) + iy(t) \; ; \; t \in [0,1], \quad z(0) = z(1) \tag{6-1}$$

where x and y are real valued functions on the interval [0,1]. The parameter t will be chosen to be proportional to arc length from an appropriate starting point. The function z for $t\varepsilon(-\infty,\infty)$ shall be considered to be the periodic extension of z for t in the basic interval [0,1].

This periodic function $z(t)$ can be represented by a Fourier series

$$z(t) = \sum_{k=-\infty}^{\infty} c_k \exp(i2\pi kt) \tag{6-2}$$

where

$$c_k = \int_0^1 z(t) \exp(-i2\pi kt)dt \tag{6-3}$$

Expressing the complex coefficient $c_k = a_k \exp(i\alpha_k)$, the real numbers a_k and α_k are the k-th harmonic amplitude and phase angle, respectively. The set $\{a_k\}$, which is referred to as amplitude spectrum, is invariant under rotations, reflections and shift in starting point of the tracing.

The zero-th harmonic

$$c_0 = \int_0^1 z(t)dt = \mu \tag{6-4}$$

represents the center of gravity of the curve and reflects the position of the curve. Since the absolute scale of the contraction pattern is not so important to assess the LV wall motion, one may use normalized version z^* instead of z;

$$z^* = \frac{z(t) - \mu}{\| z(t) - \mu \|} \tag{6-5}$$

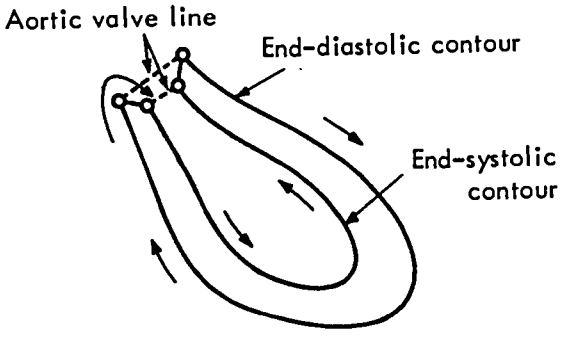

Fig. 6-2 LV contraction pattern

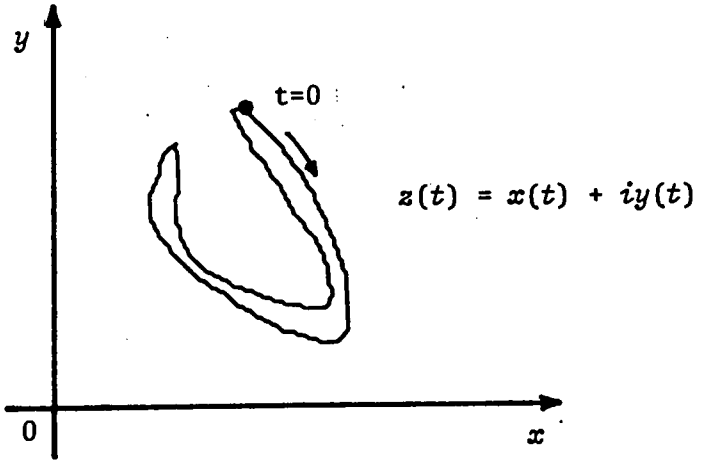

Fig. 6-3 Contraction pattern laid in complex plane

where

$$\| z(t) - \mu \|^2 = \int_0^1 | z(t) - \mu |^2 dt \qquad (6\text{-}6)$$

The Fourier coefficients of this normalized curve becomes invariant with respect to the position and the size of the curve.

If we restrict ourselves to analysis based solely on amplitude spectra, some of the information involved in the pattern may be missed and certain kinds of patterns may not be discernible to each other. However, since we are concerned only with the LV contraction patterns which are involved in a specific class of the closed curves, the loss of the information by ignoring the phase angle information are not so serious for the classification. Consequently we may use only the amplitude spectrum for describing the contraction patterns. Further, in the Fourier spectrum, most of the information about the global shape of the curve are contained in the lower order harmonics and the higher order harmonics are considered to reflect mainly the irrelevant ripple of the curve.

Considering the above mentioned, we define the Fourier descriptors of the contraction pattern as the truncated amplitude spectrum of the normalized curve z^*;

$$\{a_k^* \; ; \; -K \le k \le K, \; k \neq 0\} \qquad (6\text{-}7)$$

The choice for K is done experimentally: Truncated complex Fourier coefficients are inversely transformed and the reconstructed patterns are compared to the originals. Figure 6-4 shows the results of this experiment. This experiment indicates that K=7 is sufficient to preserve the overall shape of the contraction pattern.

A $2K$-dimensional column vector (feature vector) is formed in terms of the Fourier descriptors such that

$$x = (a_{-K}^*, \ldots, a_{-1}^*, a_1^*, \ldots, a_K^*)' \qquad (6\text{-}8)$$

where the prime denotes transpose of the matrix or vector. Consequently, a set of 14-dimensional feature vectors is obtained.

(a) K = 3

(b) K = 5

(c) K = 7

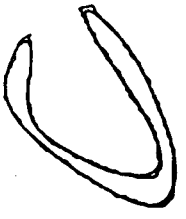

(d) K = 9

Fig. 6-4 Effect of truncation of Fourier coefficients

6.3 Principal component analysis for dimensionality reduction

The principal component analysis or the Karhnen-Loeve expansion may be used to summarize a number of measurements which may be correlated one another into the fewer uncorrelated parameters. Thus the dimensionality reduction of feature vectors may be realized. The outline of this method is as follows [6-4].

We assume that N samples of p-dimensional feature vector x_i, $i=1,\ldots,N$, are given. An estimate of the covariance matrix of the set of these samples is

$$C = \frac{1}{N-1} \sum_{i=1}^{N} (x_i-\bar{x})(x_i-\bar{x})' \tag{6-9}$$

where

$$\bar{x} = \frac{1}{N} \sum_{i=1}^{N} x_i \tag{6-10}$$

Let q x p matrix

$$R = (e_1, e_2, \ldots, e_q)' \tag{6-11}$$

where e_j, $j=1,\ldots,q$ $(q \leq p)$ are eigen vectors of C corresponding to eigen values λ_j, $j=1,\ldots,q$ of C such that $\lambda_1 \geq \lambda_2 \geq \ldots \geq \lambda_q$. The feature vector x_i is transformed to a vector y_i by means of a linear transformation

$$y_i = R\,(x_i - \bar{x}) \tag{6-12}$$

The vector y_i is a q-dimensional vector and its j-th element is referred to as the j-th principal component. The transformed vector y_i will be used as the feature vector of the sample in the classification experiment later described.

The principal component analysis was carried out with the set of feature vectors extracted from 39 contraction patterns, which are obtained by the method described in Chapter 5, including 14 normal and 25 abnormal subjects. Table 6-1 shows the result of the analysis. In this table, eigen values, coefficients of determination, cumulative coefficients

Table 6-1 Result of principal component analysis

Principal component	1	2	3	4	5	6
Eigen value	8.38	4.40	1.09	0.72	0.35	0.26
Coefficient of determination	0.526	0.276	0.068	0.045	0.022	0.016
Cumulative coefficient of determination	0.526	0.802	0.870	0.915	0.937	0.953

of determination corresponding to each principal component are tabulated up to the 6th component. From this result, it is found that four principal components are sufficient to describe more than 90% of the total variance of the data set. Here, we might use from the first up to the fifth principal components for caution's sake. Consequently, the dimensionality of the parameter (feature) space is reduced from 14 to 5.

6.4 Classification

Classification of the contraction patterns are made by employing the minimum distance classifying algorithm in the five-dimensional feature space obtained by the principal component analysis. Since we have not yet gathered sufficient number of samples to be devided into a training set and a test set, the classification experiment is conducted by minimum distance classifying algorithm using multiple prototypes. Prototype patterns are drawn manually for each of the normal and the abnormal wall motions. Figure 6-5 shows the prototype patterns used. Let ϑ_k be feature vector of prototypes. Given an unknown vector y_i, Euclidian distances to each of ϑ_k are calculated and y_i is classified to the class (normal or abnormal) of the prototype giving the minimum distance. This classification problem is a multi-prototype, two-class problem, and the decision surface will be piecewise linear.

The data set subjected to the principal component analysis were processed and the classification results are given in Table 6-2. The total correct classification rate is 79.5%. Figure 6-6 shows the distribution of the samples projected onto the subspace spanned by the 1st and the 2nd eigen vectors and the intersection of the decision boundary to this subspace.

6.5 Conclusions

The motion of the left ventricular wall was classified into normal and abnormal classes by examining the pattern of the end-diastolic and

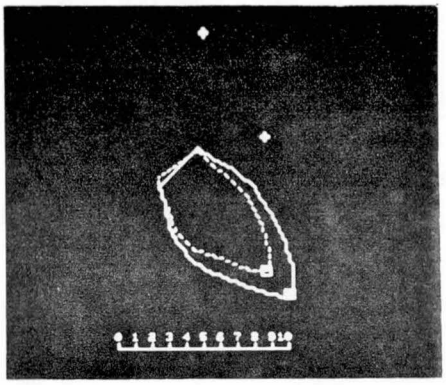

(a) Normal

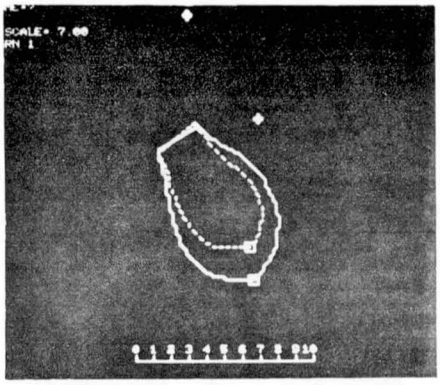

(b) Normal

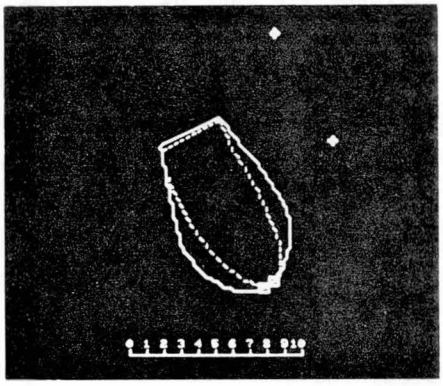

(c) Abnormal
(apical akinesis)

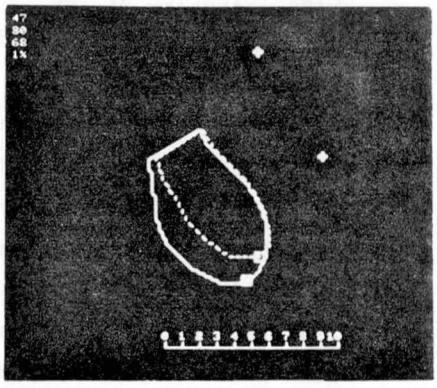

(d) Abnormal
(anterior akinesis)

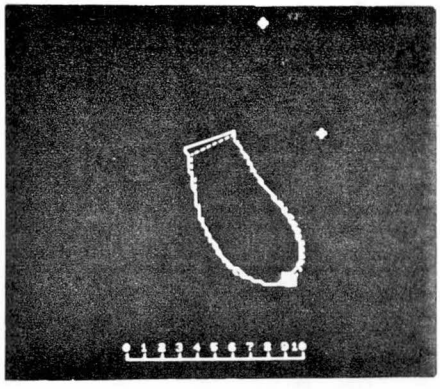

(e) Abnormal
(diffuse hypokinesis)

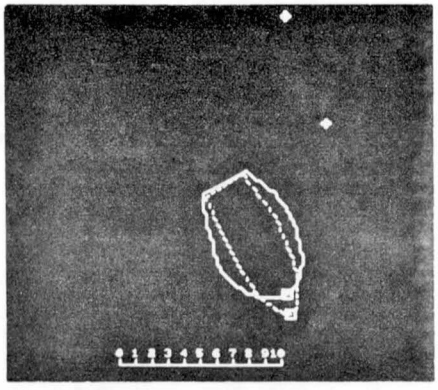

(f) Abnormal
(diskinesis)

Fig. 6-5 Prototype contraction patterns

Table 6-2 Classification result

		Doctor's diagnosis	
		Normal	Abnormal
Computer's Diagnosis	Normal	6	0
	Abnormal	8	25
	Total	14	25

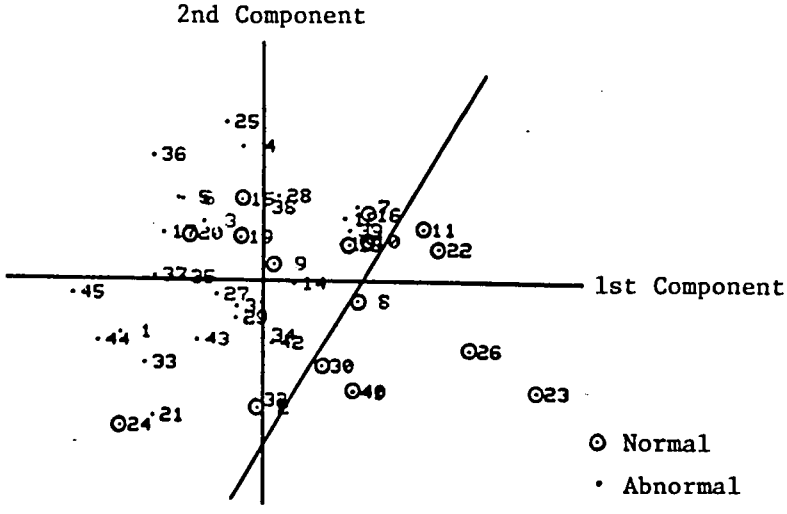

Fig. 6-6 Distribution of samples

the end-systolic contours of the left ventricular chamber. Since the diagnostics of the left ventricular wall motion has not yet been established, no one can tell what kinds of measurement will be suffice to the classification. In this thesis, however, the motion of the left ventricle was represented by the contraction pattern, which was formed only the end-diastolic and the end-systolic left ventricular contours, and the difference in wall motions were appreciated as the difference in shapes of contraction patterns. Namely, the contraction patterns were numerically described by the Fourier descriptors; blindly, disregarding what parameters were important for classification. After that, the principal component analysis was carried out so that the parameters which were composed of the Fourier descriptors and which might be correlated each other or some of which might be meaningless for the classification might be summarized into fewer parameters. By this we can extract only the parameters necessary for classification disregarding what kind of information is meaningful in medical sense.

Since the number of samples gathered so far is insufficient, it may be too hasty to fully conclude the possibility of the processing. However, the results of the initial experiment have shown the applicability of this pattern recognition technique to the diagnosis of the LV wall motion abnormalities.

Chapter 7 Concluding Remarks

This thesis has been devoted to the descriptions of the image processing of nuclear medicine images, especially radioisotope angiocardiograms.

In Chapter 2, the method of obtaining the image of the heart by means of radionuclides, namely the radioisotope angiocardiography, was described. Though poor in quality, since object image can be obtained non-invasively, the method of radionuclide imaging has come to be applied in various fields of medicine. However, depicting the image of the moving object like heart in real time is difficult, because accumulation of the scintillation counts for some appropriate duration is necessary. The method described utilizes the periodicity of the heart motion and the electrocardiogram to obtain the image of the heart at a certain phase of a period of heart motion. This technique greatly facilitates the diagnosis of heart diseases.

In Chapter 3, methods of outlining the left ventricle in the radioisotope angiocardiogram by using the prototype image processing system was persented. The principal components of the system were a minicomputer and a flying spot scanner. The fundamental idea of the processing was to regard the raw object image as the storage of the image, and the access to the raw image data was done whenever the demand for specific area arose. So the image processing, which has generally been considered to require a large computing facility with sufficient amount of storage, has become to be performed on minicomputer system with small storage space.

The methods of boundary detection incorporated in the system were successful for finding boundary points in dot-structured, noisy image. However, there left some problems concerning to that the boundary at the ventricle-atrium overlap area cannot always be successfuly determined.

A nonlinear filtering technique called V-filtering was suitable for recovering or restoring the image quality of dot-structured image like RI-angiocardiogram. The V-filter smooths out the dot structure of the

image while retaining the edge or boundary definition. Limitation of the linear restoration technique in application to the low-count RI-image was first reviewed. The V-filter was evaluated on the artifitial pattern and actual RI-images and results had proved the marked ability of the filter for recovering the RI-image.

In Chapter 5, the method of left ventricular contour extraction and volume computation was presented. The contour extraction was done in a different manner than in the methods described in Chapter 3. The original image digitized was first preprocessed by the V-filter and the median filter. Consequently, the image was converted to a smooth and well-natured image. Thresholding and derivative operations were then applied according to a priori knowledge about the structure of the object image to extract the left ventricular contour. This technique overcomes the limitations of the methods described in Chapter 3. After some feature points were located, the volume of the left ventricle was calculated by using the Simpson's numerical integration.

The analysis of left ventricular wall motion on the basis of left ventricular contours extracted at the end-diastolic and the end-systolic phases was performed in Chapter 6. Since the methodologies of diagnosing the left ventricular wall motion abnormalities from these contours had not yet been established, the contraction pattern, which was made from these contours, was expressed mathematically by means of the Fourier descriptors, without taking the medical correspondence into account.

The dimensionality of the feature space was reduced by applying the principal component analysis to the set of feature vectors, whose elements were composed of Fourier descriptors, and patterns were classified into normal and abnormal wall motion patterns by means of the minimal distance classifying algorithm. Detection of abnormal wall motion patterns was successful.

As described above, the RI-angiocardiography is a powerful tool for noninvasive diagnoses of cardiac diseases. The inferiority of the picture quality, however, has prevented us to apply the quantitative processing. The research described in this thesis may be the first consistent processing, within the scope of the author's investigation, of the RI-angiocardiograms, which makes the automated and quantitative

approacch possible. Success of this processing may be mainly due to the preprocessing by the V-filtering.

Thus, we have successfully started to develope a clinically useful diagnostic technique by the combination of non-invasiveness of RI-angiocardiography and objectiveness of the computer processing. Principal remaining problems are to examine classification of the LV-wall motion on a larger data base, and to incorporate the processing into the routine inspection of the hospital. It is considered that solving these problems can make the method more and more firm and reliable.

Acknowledgements

The author wishes to express his gratitude for the continuing guidance and encouragement received from Professor Michiyoshi Kuwahara during the course of this study. The author also would like to express his appreciation to Dr. Shigeru Eiho, Dr. Takehiko Mori, Mr. Hisao Kitagawa and his colleagues at Professor Kuwahara's laboratory of Kyoto University.

The author is also deeply indebted to Dr. Masahiko Kinoshita of Shiga University of Medical Science, Dr. Kanji Torizuka, Dr. Yasushi Ishii and Dr. Yoshiharu Yonekura of Kyoto University School of Medicine for kindly permitting him to use their clinical data and also for their guidance and suggestions from the medical standpoint.

Thanks are also due to the staff of National Museum of Ethnology for their heartiest support in preparing the manuscript.

References

[1-1] C.K.Chow and T.Kaneko, "Automatic Boundary Detection of the Left Ventricle from Cineangiograms", Computers and Biomedical Research, 5, pp.388-410 (1972)

[1-2] E.S.Beckenbach and D.T.Desilets, "The Computerization of High Speed Cineangiocardiographic Left Ventricular Volume Determination", SPIE Pattern Recognition Studies Seminor Proceeding, pp.173-192 (1969)

[1-3] M.Tasto, "Guided Boundary Detection for Left Ventricular Volume Measurement", Proc. of the 1st Intern. Joint Conf. on Pattern Recognition, pp.119-124 (1973)

[1-4] --, "Motion Extraction for Left-Ventricular Volume Measurement", IEEE Trans. on BME, BME-21, pp.207-213 (1974)

[1-5] P.D.Clayton, L.D.Harris, S.R.Rumel and H.R.Waner, "Left Ventricular Videometry", Computers and Biomedical Research, 7, pp.369-379 (1974)

[1-6] P.H.Heintzen, V.Malerczyk, J.Pilarczyk and K.W.Scheel, "On-Line Processing of the Video-Image for Left Ventricular Volume Deter mination", Computers and Biomedical Research, 4, pp.474-485 (1971)

[1-7] T.F.Budinger and J.Harpootlian, "Developments in Digital Computer Implementation in Nuclear Medicine Imaging", Computers and Biomedical Research, 8, pp.26-52 (1975)

[1-8] M.A.Douglas, H.G.Ostrow, M.V.Green, J.J.Bailey and G.S.Johnston, "A Computer Processing System for ECG-Gated Radioisotope Angiography of the Human Heart", Computers and Biomedical Research, 9, pp.133-142 (1976)

[1-9] S.M.Pizer and H.G.Vetter, "Processing Quantum Limited Images", in Picture Processing and Psychopictorics (Lipkin and Rosenfeld eds.) pp.165-176, Academic Press (1970)

[1-10] P.P.Varoutas, L.R.Nardizzi and E.M.Stokely, "Digital Image Processing Applied to Scintillation Images from Biomedical Systems", IEEE Trans. on BME, BME-24, pp.337-347 (1977)

[1-11] F.M.Wahl, J.Hofer, L.Abele and U.Schmierer, "Processing of Static Scintigrams with Adaptive Digital Optimum Filters", MEDINFO 77 (Shires and Wolf eds.), pp.1039-1042, North-Holland (1977)

[1-12] T.Iinuma, "Application of Digital Technique to Radioisotope Imaging" (in Japanese), Jap. Jour. of Med. Elec. and Bio. Eng., 7, pp.269-280 (1969)

[1-13] N.Sezaki and K.Ukena, "Automatic Computation of the Cardiothoracic Ratio with Application to Mass Screening", IEEE Trans. on BME, BME-20, pp.248-253 (1973)

[1-14] F.X.Roellinger,Jr., A.E.Kahveci, J.K.Chang, C.A.Harlow, S.J.Dwyer,III and G.S.Lodwick, "Computer Analysis of Chest Radiographs", Computer Graphics and Image Processing, 2, pp.232-251 (1973)

[1-15] A.Ueyama, M.Saito, I.Yamaguchi and E.Kimura, "Automatic Diagnosis of Cardiac Shadow in X-ray Films Using Polynomial Model" (in Japanese), Jap. Jour. of Med. Elec. and Bio. Eng., 13, pp.16-22 (1975)

[2-1] H.W.Strauss, B.L.Zaret, P.J.Hurley, T.K.Natarajan and B.Pitt, "A Scintiphotographic Method for Measuring Left Ventricular Ejection Fraction in Man without Cardiac Catheterization", American Jour. of Cardiology, 28, pp.575-580 (1971)

[3-1] A.Rosenfeld, "A Nonlinear Edge Detection Technique", Proc. IEEE 58, pp.814-816 (1970)

[4-1] W.K.Pratt, "Median Filtering", Semi-annual Technical Report, Image Processing Institute, USC, USCIPI Report 620, pp.116-123 (1975)

[4-2] A.V.Oppenheim, R.W.Shafer and T.G.Stockham, Jr., "Nonlinear Filtering of Multiplied and Convolved Signals", Proc. IEEE, 56, pp.1264-1291 (1968)

[4-3] D.J.H.Moore and D.J.Parker, "On Nonlinear Filters Involving Transformation of the Time Variable", IEEE Trans. on IT, IT-19, pp.415-422 (1973)

[4-4] T.G.Newman and H.Dirilten, "A Nonlinear Transformation for Digital Picture Processing", IEEE Trans. on Comp., C-22, pp.869-873 (1973)

[4-5] F.Tomita, M.Yachida and S.Tsuji, "A Non-Linear Filter for Detection of Textures (in Japanes), Trans. Inst. Elec. Com. Eng. Japan, 58-D, pp.102-103 (1975)

[5-1] A.Rosenfeld, Picture Processing by Computer, Academic Press (1969)

[5-2] A.Rosenfeld and A.C.Kak, Digital Picture Processing, Academic Press (1976)

[5-3] H.Akima, "A New Method of Interpolation and Smooth Curve Fitting Based on Local Procedures", Jour. Ass. Comput. Mach., 17, pp.589-602 (1970)

[5-4] R.L.Griffith, C.Grant and H.Kaufman, "An Algorithm for Locating the Aortic Valve and the Apex in Left-Ventricular Angiocardio grams", IEEE Trans. on BME, BME-21, pp.345-349 (1974)

[5-5] H.Freeman, "On the Encoding of Arbitrary Geometric Configurations", IRE Trans. on EC, EC-10, pp.260-268 (1961)

[6-1] G.H.Granlund, "Fourier Preprocessing for Hand Print Character Recognition", IEEE Trans on C, C-21, pp.195-201 (1972)

[6-2] C.T.Zahn and R.Z.Roskies, "Fourier Descriptors for Plane Closed Curves", IEEE Trans. on C, C-21, pp.269-281 (1972)

[6-3] C.W.Richard and H.Hemami, "Identification of Three-Dimensional Objects Using Fourier Descriptors of the Boundary Curve", IEEE Trans. on SMC, SMC-4, pp.371-378 (1974)

[6-4] T.Okuno, H.Kume, T.Haga and T.Yoshizawa, Tahenryo-Kaisekiho (Multivariate Analysis), Nikka-Giren Shuppan, Tokyo (1971) (in Japanese)

List of Publications

1. M.Kuwahara, K.Hachimura, S.Eiho, T.Manabe and Krisada Visavateeranon, "Picture Processing System and Its Application to RI-Angiocardiograms" (in Japanese), Technical Report of the Professional Group on Image Engineering of Inst. Elec. Comm. Engrs. Japan, IE74-62 (1974)
2. K.Hachimura, H.Taneno, H.Kitagawa, M.Kuwahara, M.Kinoshita and R.Kusukawa, "Computer Analysis of the Left Ventricular Volume Using RI-Angiocardiography", Proc. of the 1st World Congress of Nuclear Medicine, pp.768-770 (1974)
3. M.Kinoshita, T.Hoshino, G.Tomonaga, I.Mashiro, Y.Shimono, R.Kusukawa, K.Sato, M.Kuwahara, K.Hachimura and H.Kitagawa, "Measurement of Left Ventricular Volume and Ejection Fraction by ECG-Gated RI Angiocardiography - The Comparison with X-ray Cineangiographic Measurement -" (in Japanese), Japanese Jour. of Nuclear Medicine, 12, pp.393-403 (1975)
4. K.Hachimura, S.Eiho, M.Kuwahara and M.Kinoshita, "Processing of RI-Angiocardiographic Left Ventricular Images - Image Enhancement and Extraction of Left Ventricular Boundary" (in Japanese), Technical Report of the Professional Group on Image Engineering of Inst. Elec. Comm. Engrs. Japan, IE76-65 (1976)
5. --, "Extraction of the Left Ventricular Boundary from RI-Angiocardiogram" (in Japanese), Japanese Jour. of Medical Electronics and Biological Engineering, 14, pp.452-458 (1976)
6. --, "Nonlinear Digital Filtering of Medical RI-Images" (in Japanese), ibid., 15, pp.327-333 (1977)
7. M.Kuwahara, K.Hachimura, S.Eiho and M.Kinoshita, "Processing of RI-Angiocardiographic Images", in Digital Processing of Biomedical Images, (K.Preston,Jr. and M.Onoe eds.), pp.187-202, Plenum (1976)
8. K.Hachimura, M.Kuwahara and M.Kinoshita, "Left Vintricular Contour Extraction from Radioisotope Angiocardiograms and Classification of Left Ventricular Wall Motion", Proc. of the 4th Intern. Joint Conf. on Pattern Recognition, pp.911-913 (1978)
9. K.Hachimura, S.Eiho, M.Kuwahara and M.Kinoshita, "Left Ventricular Contour Extraction and Volume Computation from RI-Angiocardiographic Images" (in Japanese), Japanese Jour. of Medical Electronics and Biological Engineering, 17, to be published (1979)

Appendix A Flying Spot Scanner

The flying spot scanner (FSS) system was designed and built as an image input device which is capable of computer controlled random scanning. This FSS system was used throughout the course of this study. Some detailed descriptions of this FSS system will be given in this appendix.

Although various image input facilities have been devised and used, the FSS is superior to others in its fast random scanning capability and position and gray level accuracy.

The FSS system built consists of two major subsystems, namely the scanner subsystem and the scanner controller. The scanner subsystem, which is the most principal part of the system, includes the deflection system, the optical system, the video signal system and the film transport. On the other hand, the scanner controller subsystem is an electric circuitricity which controls the scanner and facilitates the interface between a computer. Figure A-1 shows the overall view of the FSS system.

A.1 Scanner

In Fig.A-2 the block diagram of the scanner subsystem is shown.

A.1.1 Deflection system

An electromagnetic focusing and deflection high resolution cathode ray tube (133 mm in diameter) is used as the flying spot tube. In order to realize a fast random scanning, a deflection coil with low inductance is used and driven by a deflection amplifier with large current output capability. Consequently, the rate of deflection is such that the movement of the maximum amplitude on the CRT face is done in approximately 12 μsec. View around the CRT is shown in Fig.A-3.

Although the deflection angle of the electron beam is proportional to the deflection current applied to the deflection coil, the deflection amplitude on the CRT face is not proportional to the deflection current

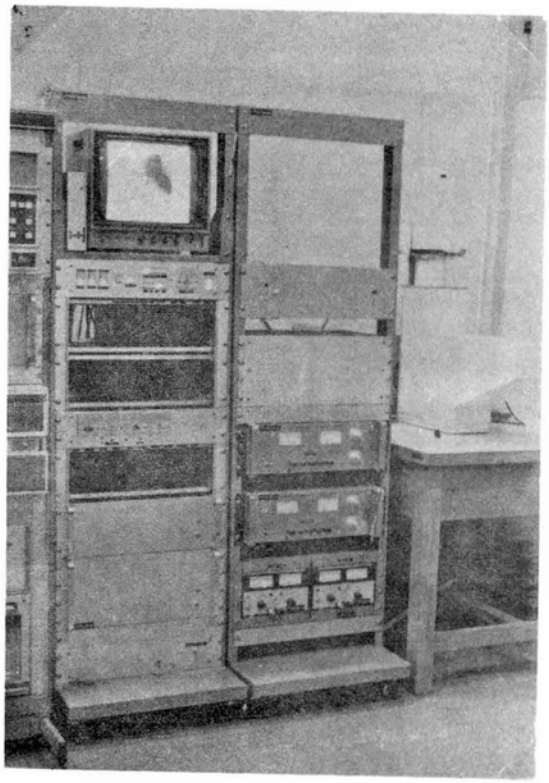

Fig. A-1 View of the FSS system

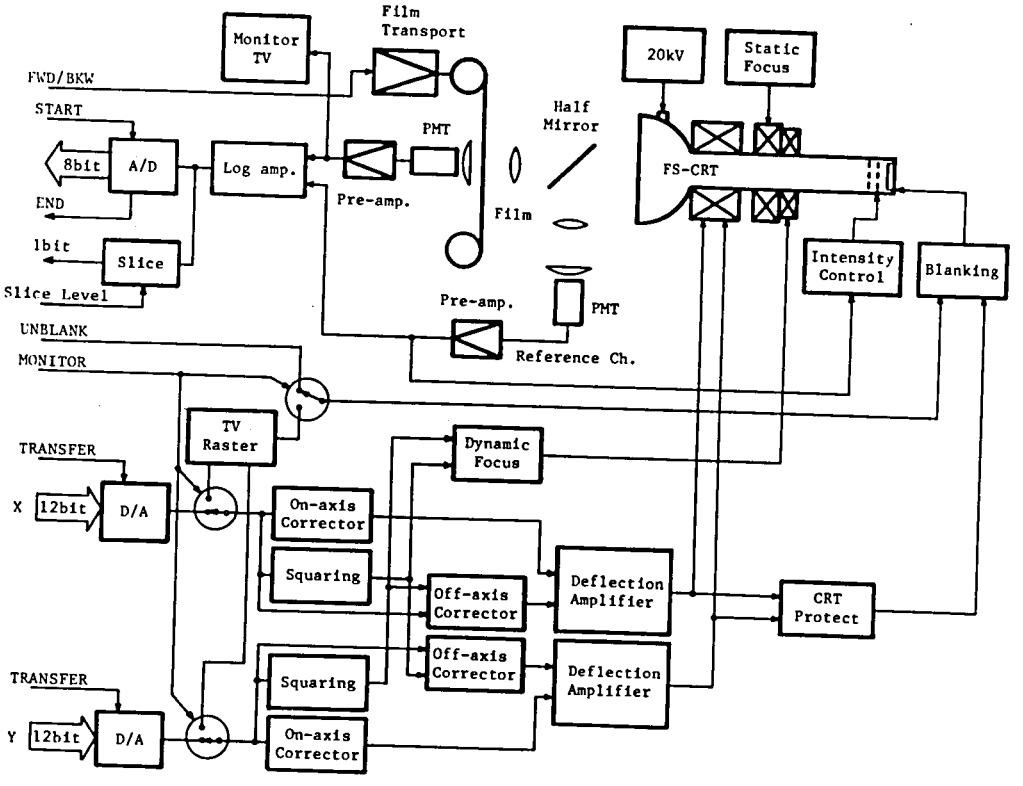

Fig. A-2 Block diagram of the scanner subsystem

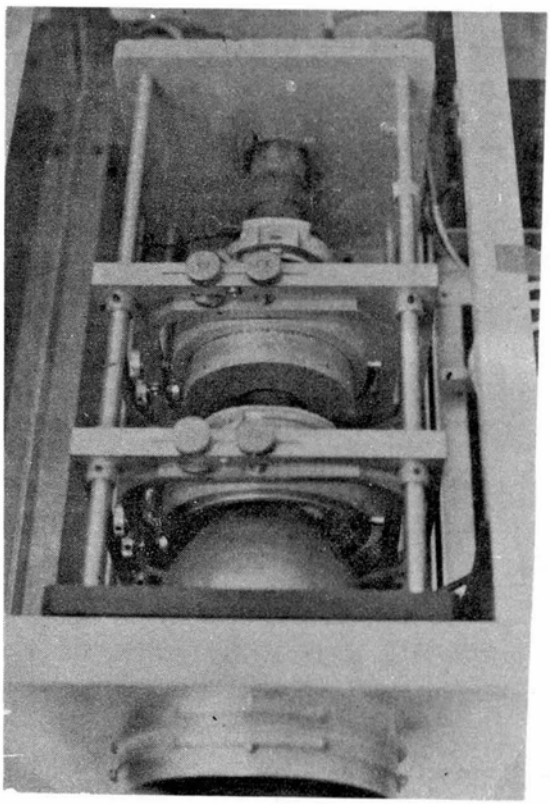

Fig. A-3 CRT and deflection coil

since a flat faced CRT is used. This deflection distortion is corrected by superimposing the correction signals on the deflection signal. These correction signals are generated by the on-axis corrector, the squaring circuit and the off-axis corrector.

In addition to the focusing by the static magnetic field, a dynamic focusing technique is used, which corrects the defocusing caused by deflection. This is done by applying, to the dynamic focus coil, the focus current which is proportional to the sum of squares of the x and y deflection signals.

Twelve-bit digital signals from the scanner controller are digtal-to-analog converted and fed into the deflection circuit of the scanner. On the other hand, the scanner provides a raster signal generator of the standard television rate. This raster signal is used for monitoring purpose. Namely, since this television raster signal and the digitally applied positional signals can be switched each other either manually or by the control signal from the scanner controller, the object image can be monitored by the conventional television monitor when a digital scanning and reading of data is disactivated. Thus, no special hardware for monitoring is needed.

Blanking and unblanking of the spot of the beam on the CRT face is made by the unblanking signal applied to the cathode of the CRT. This unblanking signal can be applied from the controller and controlled by the program. Protecting circuit for CRT phosphor is equipped so that the phosphor of the CRT may not be burnt when the deflection signal ceases for some reasons. This protection is done by generating the blanking signal when the rate of change of the deflection current decreases below the predetermined threshold.

A.1.2 Optical and video signal system

Figure A-4 shows the exterior view of the optical system of the scanner. Two optical and video channels are provided in the scanner. One of them, which is principal, is a data channel to read the gray level information of the object photo film. The other is a channel for monitoring the light intensity incident to the object film, which is called the reference channel. The light flux emitted from the bright

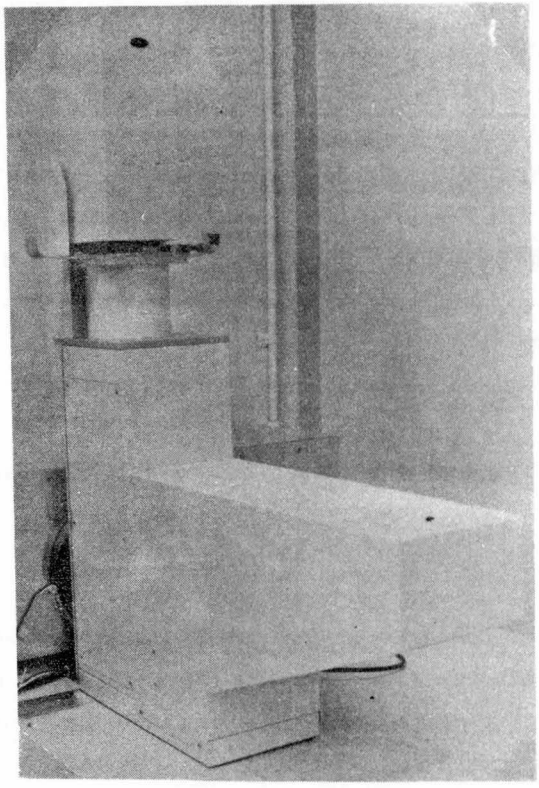

Fig. A-4 Optical system of the scanner

spot on the CRT phosphor is splitted by a half mirror mounted in front of the CRT screen, and the half of the light flux is introduced to the data channel and the rest to the reference channel. The configuration of the optical system of these two channels are made to be identical. The reference channel is used to form a negative feed back loop. By this, the light intensity incident to the object film plane can be kept nearly constant compensating the irregularity of the CRT phosphor and the shading characteristics of the CRT-optical systm. Besides, taking the logarithm of the ratio of the signals obtained from data and reference channels, by a logarithmic amplifier, we can obtain the signal proportional to the optical density of the object film, being unaffected by the unevenness of the optical system. Thus, this scanner system provides two different mechanisms for compensating the shading and the irregularities, and accurate density information is obtainable. By performing the logarithmic transformation we can obtain the value of optical density which corresponds to the human visual perseption characteristics, and density value is effective particularly in treating the under-exposed low contrast negative film. Density transformation is usually applied, but the linear scale gray level signal can be obtained either.

These image signals are sampled and quantized into 8-bit signal by an analog to digital converter. Conversion time required is 6.3 μsec. One bit signal is also obtained simultaneously by using the high speed comparator. The range of the density value to be digitized and the slice level for the comparator can be set by the control signal from the controller.

A.1.3 Film transport

The film transport mechanism advances or reverses 35mm perforated photo film by a stepping motor. This transport provides the supply and take-up reels which act synchronously with the sprocket wheel driving the film. Hence, it can handle the long cine film. Time required to transport the film for a perforation interval is about 0.5 sec. Figure A-5 shows the view of the film transport.

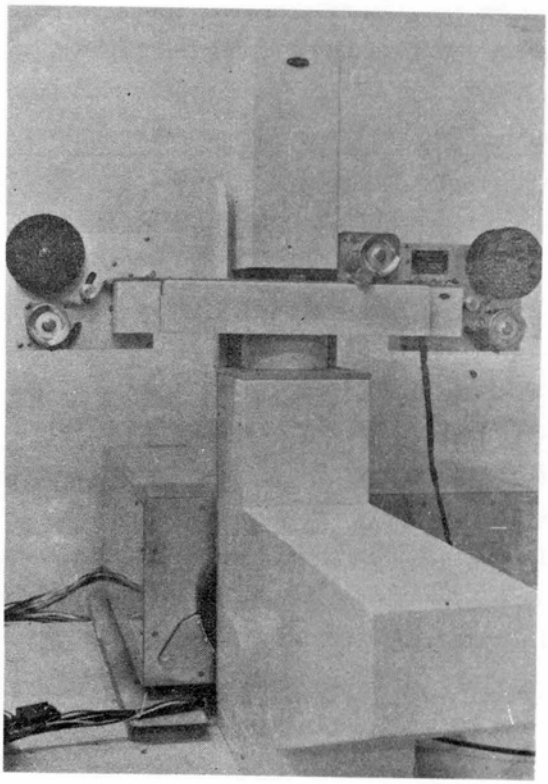

Fig. A-5 Film transport

A.2 Scanner controller

The scanner controller controls the scanner and acts as an interface between a computer. Figure A-6 shows the block diagram of the scanner controller. The controller receives the command and coordinate signals from the computer and returns image data to the computer. The principal role of the controller is to arrange the timing for scanning and data transfer.

The actual interface between the scanner controller and the cpu (YHP 2100A) is supported by the general purpose input/output interface card which is supplied by the manufacturer of the cpu. This card is designed for transferring one word (16 bits) data to or from the cpu, and it provides the encode command line to the external device and the flag response line from the external devices. One can transfer data by the input/output instructions specifying the device address attached to the slot to which the card is installed.

The most significant four bits of the output word from the computer are used for command code. The rest of the word, that is, the least significant twelve bits, owns different meanings according to the codes used in the command field. Table A-1 shows the command codes and their functions. In Fig.A-7, the bit pattern of each command word and the meanings of the fields in the twelve least significant bits are shown. In this figure, bits in the blank area are ignored and irrelevant.

There are scanning mode and monitoring mode. In monitoring mode, as described previously, the standard television raster signal is applied to the scanner and the object image can be monitored via a conventional television monitor. This mode is activated and disactivated by the command codes MON and MOF respectively, and whenever the monitor mode is disactivated the scanning mode is set and the beam of the CRT is deflected to the point corresponding to the coordinate signals applied to the D/A converters of the scanner. The scanning mode consists of two different modes. One of them is a random mode in which the scan is made so that the coordinate signals are generated by the computer program and applied to the scanner point by point. The other is a raster mode in

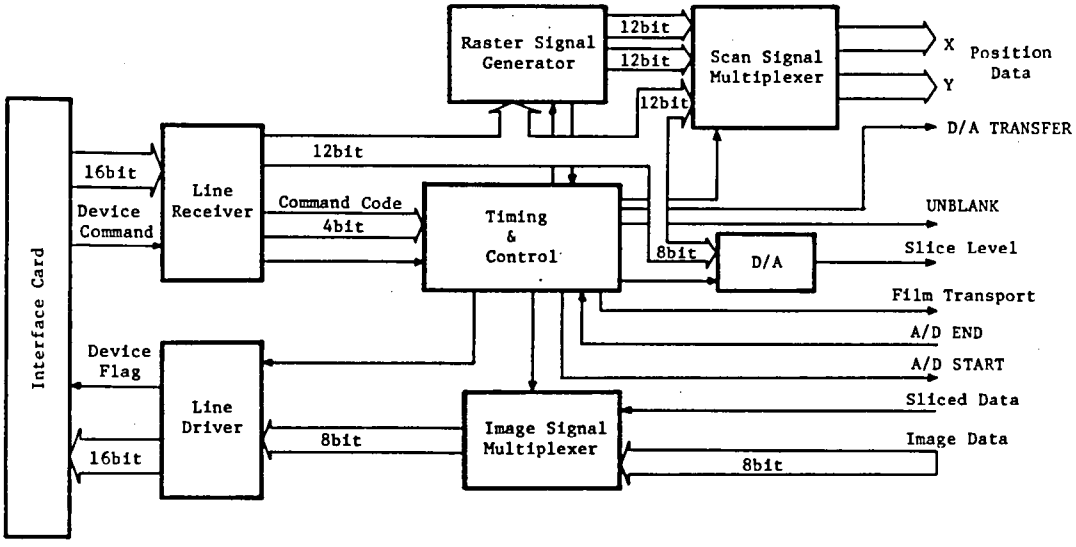

Fig. A-6 Block diagram of the scanner controller

Table A-1 Command codes

Command Code (in octal)	Abbreviation	Function
00	UBK	Unblank beam
10	RST	Start raster scan
01	MOD	Mode set
11	FIL	Move film
02	SLV	Set slice level
12		Spare
03	MON	Turn on monitor mode
13	MOF	Turn off monitor mode
04	XCO	Set x-coordinate of random scan
14	YCO	Set y-coordinate of random scan
05	XST	Set start x of raster scan
15	YST	Set start y of raster scan
06	XNM	Set number of points (in x) of raster scan
16	YNM	Set number of points (in y) of raster scan
07	XSP	Set x step of raster scan
17	YSP	Set y step of raster scan

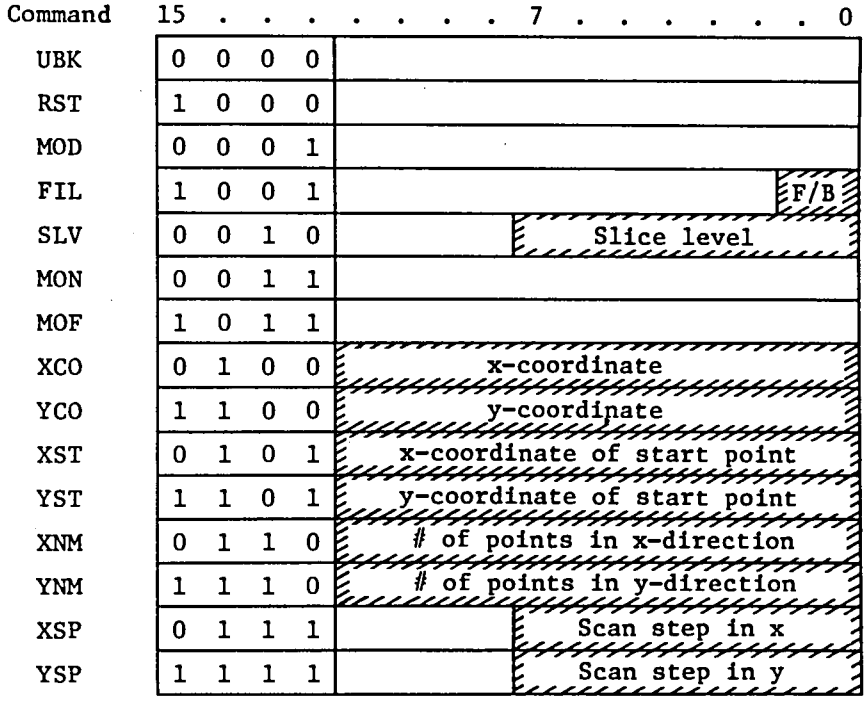

Fig. A-7 Bit pattern of command words

which the coordinate signals to perform the rectangular raster scan are internally generated by the hardware. In the random scanning mode, since coordinate data are transferred by the codes XCO and YCO point by point, arbitrary random scanning can be performed by the program. Operation timing in the random mode is illustrated in Fig.A-8: After the coordinate values are set, unblanking command UBK is issued by the computer program. The scanner controller generates the start pulse for analog-to-digital conversion signal after a 10 μsec delay from the unblanking command. This delay is for beam settling. When analog-to-digital conversion is completed, the scanner controller sets the flag and consequently the computer starts reading of image data. Thus, in the random mode, the scan is made in about 40 μsec maximum per one pixel.

In the raster mode, as shown in Fig.A-9, the coordinates (X_s, Y_s) of the starting point of the raster, number of points in x and y direction N_x, N_y, and steps in x and y direction K_x, K_y are specified by the corresponding command codes. These values are set to the registers in the raster signal generator. After these settings were made, unblanking commands are issued from the computer point by point, and by this the coordinate values are up-dated successively. In this mode, since the coordinate data need not be generated by the computer program, the time required to read a point becomes shorter than the ramdom mode, actually about 25 μsec per a point.

Command MOD sets the mode of the scanner. Twelve least significant bits of the output word is divided into 5 fields as shown in Fig.A-10. Each field is used to determine the density range, the resolution of the scanner, scanning mode, operation mode and mode of digitization. Each field provides an enable/disable bit in the head of the field and only when this bit is 1, the field is activated and the state of the scanner is changed according to the information in the rest of the field. Thus, the setting of mode can be made independently. The field of density range determines the range of optical density to be digitized into 256 levels. The field of resolution specifies the coarseness of the fundamental grid system of the scanner. Although the scanner provides two 12-bit digital-to-analog converters for coordinate data, there are only

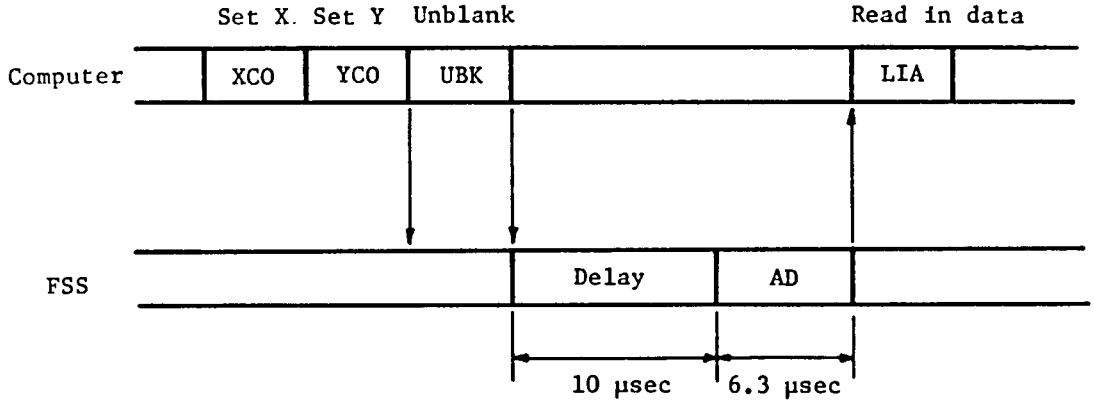

Fig. A-8 Operation timing in the random mode

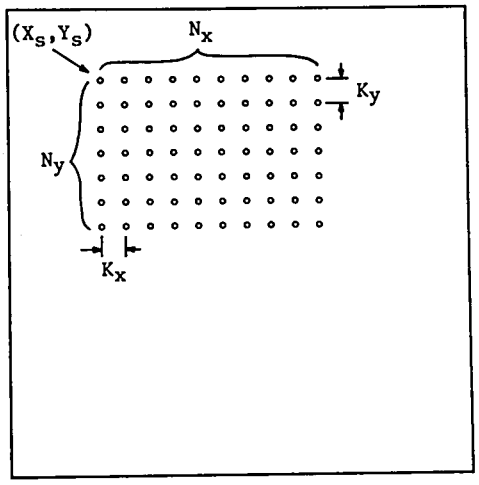

Fig. A-9 Raster mode

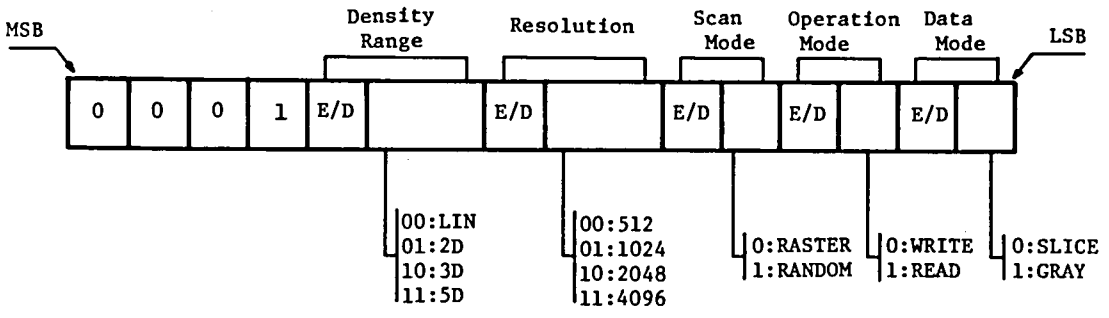

Fig. A-10 Interpretation of output word coupled with the command MOD

few cases in which such a high resolution is required. Hence, it is convenient that the coarseness of spatial digitization can be varied according to the resolution required by the problem. When the code in the bit 7 and bit 6 of the resolution field is 11, the full 12 bits are used and 4096 points in both x and y directions can be accessible, and so on. The scan mode field swithes the modes of scanning, namely, random mode and raster mode.

The operation mode field determines the operation mode of the scanner, i.e. the read mode and write mode. The FSS system was designed to be used not only as an image input device but also as an output device. Namely, by controlling the duration of stay of the spot at each point according to the image data, one can generate gray level of the point. In this case, the optical system and the video signal system of the scanner should be detached and the camera should be attached facing to the screen of the CRT. The shutter of the camera should be opend until all the image data are transferred.

Finally, the digitization field determines the mode for digitizing the image data. Eight-bit gray level mode or one bit slice mode can be selected.

A.3 Fundamental subroutines for FSS

Several fundamental subroutines were written to facilitate the control of the FSS. Some of the principal subroutines are listed in Table A-2. All of them are written in the assembler language and are callable from FORTRAN programs. The subroutine SCAN operates in the random scan mode. The coordinate values of the points to be scanned are transferred through arguments of array IX and IY, and resulting image data are returned to the array IDATA. Number of points to be accessed is specified by NUM. The subroutine RASTR performs the scanning in the raster scan mode. The upper left corner point of the raster is specified by the arguments IXS and IYS. The arguments NX and NY specify number of columns and rows, respectively, and ISTEP spacing of rows and columns. Scanned image data are returned to the array IDATA. The subroutine

Table A-2 Fundamental subroutines for FSS

```
SCAN (IX,IY,IDATA,NUM)
RASTR (IXS,IYS,NX,ISTEP,IDATA)
SSPOT (IX,IY,KX,KY,IDATA,NUM)
TVON
TVOFF
RESLN (IR)
RANGE (ID)
FEED (NUM)
```

SSPOT realizes the KX x KY rectangular smoothing spot centered at the point (IX,IY). Gray level values of the grid points within this rectangle are averaged and returned to the IDATA.

Subroutines TVON and TVOFF activates and disactivates the monitor mode respectively. RESLN sets the resolution of the FSS system. When IR=1, 4096 x 4096 points can be accesible and when IR=2, 2048 x 2048 and so on. RANGE is used to determine the range of the optical density to be digitized. When ID=3, optical density range from 0 to 3D is digitized into 256 levels, and when ID=2, from 0 to 2D is digitized. When ID=0 is specified, logarithmic (density) transformation is disactivated and the image data in a linear scale are transferred.

Finally, the subroutine FEED is used to control the film transport. Argument NUM specifies the number of perforations to be advanced or reversed. Postitive value means the forward direction and negative the reverse direction.

Appendix B Interactive Image Processing System

In this appendix, an interactive image processing hardware and software system used throughout the text, except Chapter 3, will be described.

B.1 Hardware

A block diagram depicting the hardware configuration of the system is illustrated in Fig.B-1, and overall view of the system is shown in Fig.B-2.

A minicomputer used as a central processing unit is YHP 2100A with 32 kword memory. This minicomputer is furnished with a paper tape reader and a puncher as well as a teletypewriter as fundamental peripheral devices. The flying spot scanner described in detail in Appendix A is used as an image input device. By this, one can digitize the 35 mm photo film in 4096 x 4096 maximun resolution and in 256 levels of gray scale.

A storage type graphic display terminal Tektronix 4012 is used as not only an operating console but an image display device. An image of 170 x 128 pixels can be displayed on this display terminal in 10 levels of gray scale. Since this display terminal can take only two levels of brightness, we have to use 3 x 3 dot matrix per a pixel in order to express 10 gray levels. The gray level (brightness) of a pixel is expressed by a number of bright dots in the 3 x 3 dot matrix.

Two magnetic disk drive are provided. Each drive has one non-removable disk and one removable cartrige disk, each having 2.5 Mbyte capacity. With these disk drives the computer system can be operated under the disk operating system (DOS), which facilitates the job control, file management and input/output of data. The system is also furnished with a 9-track, 800 bpi magnetic tape handler.

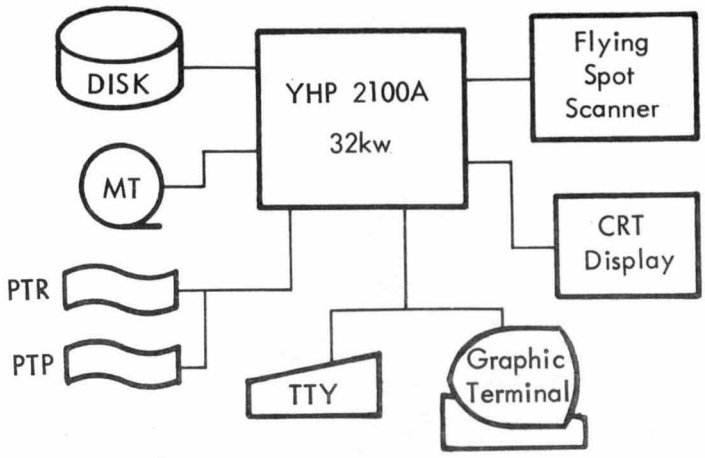

Fig. B-1 Hardware configuration of the interactive image processing system

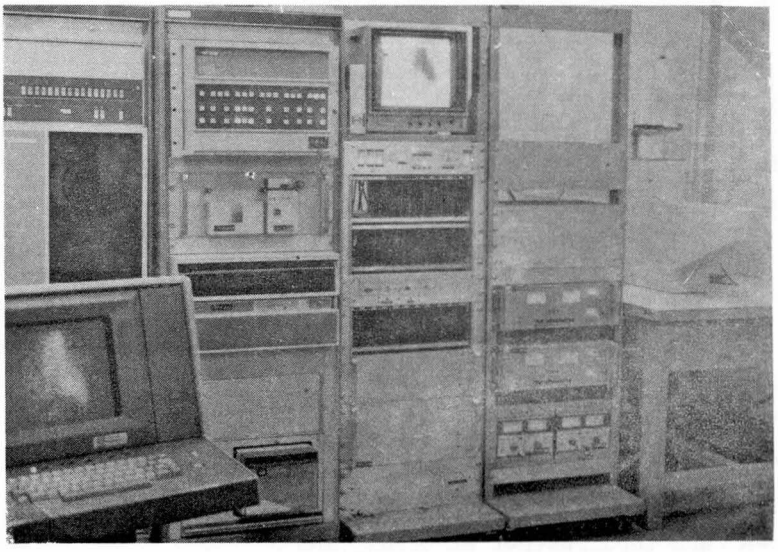

Fig. B-2 View of the system

B.2 Software

A command type conversational software system for image processing was constructed on the hardware facility described in the previous section.

Since the disk operating system supplied by the manufacturer of the minicomputer has a powerful function for data transfer and file management, we may fully make use of the disk operating system to construct the processing system and can avoid to spend our labour in developing the management part of the system. Furthermore, this disk operating system has also the function of program overlay called segment load. Consequently, the processing system was constructed and operated under the control of the disk operating system, and it was designed as the command type system which has its processing units in the form of overlay segments and loads and executes the segment on acceptance of the corresponding command. This software system is named *PIPS* (Pictorial Information Processing System). The organization of the system is illustrated in Fig.B-3. The system PIPS consists of a main program and various processing segments. The main program resides in the memory of the minicomputer and manages the loading of segments stored in the disk file. The memory map of the minicomputer is shown in Fig.B-4. The main program and segment programs share a common area, which consists of 26 words for system parameters and 16 kwords for a data buffer. The system parameter area is used for processing parameters to be transferred to processing segments, timer and the information concerning the work are tracks which will be described later.

When the image processing is done in a interactive and succesive fashion, it is desired to keep the raw image unchanged so that one may readily retry the processing modifying the parameters of the processing. Temporal storage area for several images are required for this purpose. However, because of the limitation of the capacity of the computer memory available, we cannot keep sufficient storage space in the computer memory. Hence, the temporary storage areas are decided to be provided in the work area of the DOS disk. These are referred to as the work areas

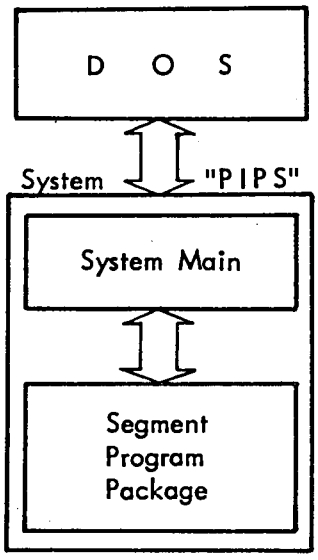

Fig. B-3 Organization of the software system

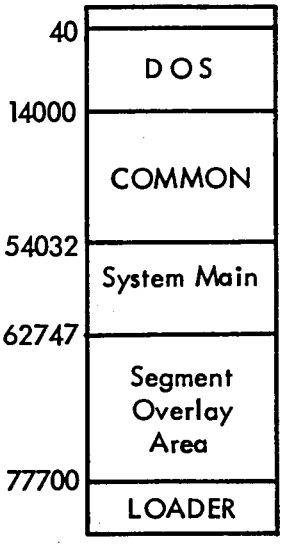

Fig. B-4 Memory map

of system PIPS. The number and the size of each work area are decided as follows: The size of the image to be treated in the system is decided to be normally 128 x 128 pixels, and the gray level at each pixel is expressed in the form of 16 bit fixed point value. Images smaller in size than this size can also be treated. Six areas will be sufficient for storing the original, intermediate and resulting images. Consequently, as shown in Fig.B-5, six 128 x 128 image data areas called work areas of PIPS are allocated in the DOS disk. These areas are numbered 1 through 6 from the head, and each work area is referenced by the number of its own. Each work area is considered to be the operand of the image processing operations, such as data transfer, measurement, numerical operation and geometrical manipulation. Figure B-6 illustrates the data flow of the processing in this system. Image data files for permanent storage are organized on the DOS disk in the standard file format of DOS. By this the transfer of image data between other stand-alone programs becomes possible.

General purpose processing program segments so far programmed and available are tabulated in Table B-1. In addition to the segments listed in this table, various segments for problem oriented processing are also included in the system. The main program and all of the segments are written in FORTRAN.

These segments can be called by the commands, which are the abbreviated names of the function of the segments, via the keyboard of the terminal. After the segment is loaded, the parameters necessary for the processing is acquired conversationally. Figure B-7 shows the example of the record of the dialog between an operator and the system.

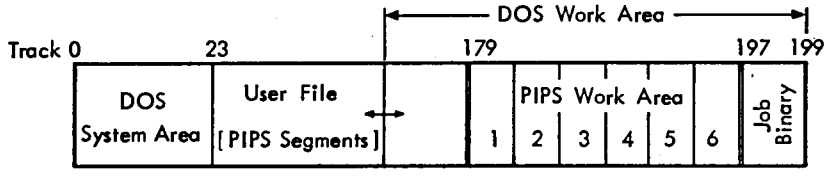

Fig. B-5 Format of the PIPS disk

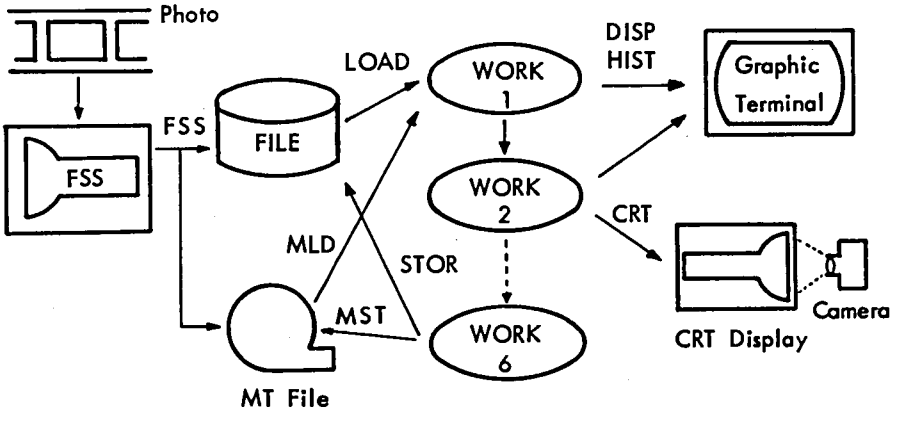

Fig. B-6 Data flow of the processing

Table B-1 General purpose processing segments in PIPS

Segment name	Function
PIPS	System main program
END	Terminate PIPS
MENU	List system program segments
LIST	List system picture files
RNAM	Rename picture files
PURG	Purge picture files
BACH	Switch to BATCH mode
TYPE	Return to KEYBOARD mode
TIME	Turn timer option ON/OFF
WAIT	Wait until keying
ERAS	Erase graphic display screen
MT	Position magnetic tape
FSS	Input picture from FSS
LOAD	Load picture from file to work area
STOR	Store picture from work into file
MOVE	Transfer picture between work areas
MLD	Load picture from MT-file to work area
MST	Store into MT-file
DISP	Display gray picture
DSB	Display two-valued picture
DS3	Psuedo three-dimensional display
DSN	Display picture by alpha-numeric characters
DSM	Display four 64 x 64 gray pictures
DSR	Display specified density range
DSA	Display specified area
HIST	Get gray level histogram
AHIS	Histogram in a specified rectangular area
DHIS	Differential histogram (type 1)
GHIS	Differential histogram (type 2)
HIS2	Two-dimensional histogram
MHIS	Histogram in masked area
SECT	Get section of picture
PROJ	Get horizontal or vertical projection
COOR	Get x,y coordinates of specified pixel
VAL	Measure gray level value of specified pixel
CLR	Clear work areas
RND	Generate randomly distributed pattern
GAU	Generate Gaussian random pattern
LINE	Draw line pattern
PAT	Attach gray level value to pixel
CIR	Draw circular pattern
PHA	Generate phantom RI image

Table B-1 General purpose processing segments in PIPS (cont'd)

Segment name	Function
UPR	Upright picture matrix
REV	Reverse picture matrix
SFT	Shift picture matrix
TR	Transpose picture matrix
ROT	Rotate picture matrix
RDUC	Reduce picture size
EXPD	Expand picture size
BIN	Convert to two-valued picture (thresholding)
INV	Invert polarity
CUT	Analog thresholding
CAD	Add constant to each pixel
MAG	Magnify by constant
ABS	Take absolute value
ADD	Add two pictures
SUB	Subtraction
IOR	Inclusive logical OR
AND	Logical AND
XOR	Exclusive OR
CONV	Convolution by arbitrary weight matrix
SMT	Smoothing by simple moving average
RSMT	Smoothing by oblique rectangular mask
GRD	Gradient operator (type 0)
GRD1	Gradient operator (type 1)
GRD2	Gradient operator (type 2)
LAP	Laplacian operator
NONM	Nonmaxima supression
MED	Median filtering
VF1	V-filtering (type 1)
VF2	V-filtering (type 2)
LBL	Connected component labelling
DST	Distance transformation
SKT	Skelton transformation
RSK	Reverse skelton transformation
CNCT	Connected component counting
BND	Boundary tracing
THIN	Thinning
PROP	Propagation
SRNK	Shrinking

Table B-1 General purpose processing segments in PIPS (cont'd)

Segment name	Function
FT	Fourier transformation
RFT	Reverse Fourier transformation
FSPC	Fourier spectrum display
FLT	Convert to floating point data
FIX	Convert to fixed point data
FWM	Construct weight matrix
FMPY	Multiplication of two Fourier domain data
FDIV	Division (inverse filtering)

```
:PR,PIPS

*NEXT ?
LOAD
SOURCE FILE=?
IMG5
WORK AREA #=?
1
SIZE NX,NY=?
128,128

*NEXT ?
SMT
SOURCE AREA #= ?
1
DESTINATION AREA #= ?
2
SIZE NX,NY= ?
,
SMT SIZE KX,KY= ?
3,3

*NEXT ?
LAP
SOURCE AREA=?
2
DESTINATION AREA=?
3
SIZE NX,NY=?
,

*NEXT ?
STOR
WORK AREA NO=?
3
SIZE NX,NY=?
128,128
FILE NAME=?
RESUT

*NEXT ?
END
  PIPS  : STOP     7777
```

Fig. B-7 Example of the dialog